AN EVALUATION OF ANTHROPOGENIC TRACE METALS IN THE WESTERN BASIN OF LAKE SUPERIOR

A THESIS

SUBMITTED TO THE FACULTY OF THE GRADUATE SCHOOL

OF THE UNIVERSITY OF MINNESOTA

BY

CHRISTOPHER RONALD NIENDORF

IN PARTIAL FULFILLMENT OF THE REQUIREMENTS

FOR THE DEGREE OF

MASTER OF SCIENCE

JANUARY, 1998

ABSTRACT

Lake Superior sediment cores were collected and analyzed for a suite of trace metals in the solid and aqueous phase. There have been few prior studies of redox chemistry of trace metals and the effects of early diagenesis on metal in Lake Superior. In this study, redox chemistry of Fe, Mn and Co is examined, in addition to the sediment profiles of Cu, Pb, Zn and Ba. The interaction between the solid and aqueous phase redox elements is consistent with those found in other studies. The redox elements show a classic distribution, a distinct solid phase peak with a corresponding rapid increase in aqueous phase concentration. Historical events are discerned in the sediment record: the beginning of Cu mining in Michigan; and the rise and fall of alkyl lead consumption in the U.S. A mathematical model is used to predict early diagenetic concentrations of the redox elements (Fe, Mn and Co) in solid and aqueous phase assuming simple one-dimensional diffusion. The results of the model are compared to the actual vertical profiles of these metals. Trace metal fluxes of Cu and Zn into and out of the sediments are calculated. The net flux of Zn shows significant regeneration and release into the water column. Sedimentation rates and core chronologies are based on ^{210}Pb analyses. The 100-year average sedimentation rates range between 0.011 and 0.018 g/cm^2/yr (0.046 to 0.059 cm/yr), and are compared to others reported for Lake Superior. X-ray diffractometry is used to identify the presence or absence of taconite tailings and the general clay lithology at each site. Three of seven sites are affected by taconite mining. Taconite tailings were discharged into the lake beginning in 1956, therefore the first appearance of tailings in the sediment column can be used to calculate a rudimentary sedimentation rate, which ranged between 0.085 and 0.098 cm/yr.

DEDICATION

This thesis is dedicated to the memory of my grandfather, Don F. Goodrich. I miss him terribly. I will always remember what a good man he was and try to use his example on how to live my life, with compassion and caring for others.

ACKNOWLEDGMENTS

Projects like this one are not completed in a vacuum; there is always a cast of supporting characters without whose help the outcome would have been less successful. I would like to thank the people that helped me along with this thesis. I thank my advisor, Dr. Erik Brown, for the help he gave me all along the way, ensuring the success of this work. I would also like to thank the members of my committee, Drs. Tom Johnson and Howard Mooers, for their input and suggestions. I appreciate the assistance of Keri Anderson and Christie Haupert in the sampling and analysis stages of this work, respectively, and for keeping things light and fun this summer during the initial writing period.

I used the laboratory facilities at the Geology Department on the Twin Cities campus and those at the Great Lakes Research Facility in Milwaukee. I would like to thank Rick Knurr in the Twin Cities and Dr. David Edgington in Milwaukee, I am grateful for their help and support in my research. I also thank the EPA for the use of their floating laboratory, the R/V Lake Explorer, whose officers and crew helped in sample collection.

I thank Minnesota Sea Grant and University of Minnesota Grant-in-aid for their financial support of this project.

And finally I want to thank the most important people to the completion of this study, my parents and sisters, without whose help and support I never would have been able to complete my goal of earning a Master's degree.

TABLE OF CONTENTS

LIST OF FIGURES

LIST OF TABLES

1. INTRODUCTION

1.1 General Background

Trace metals introduced to lakes tend to be rapidly scavenged from the water column and sequestered in sediments. Increased anthropogenic loading can lead to an increase in concentration in surface sediments. However, enrichment near the sediment-water interface may also result from diagenetic processes that can assemble high concentrations of elements over a narrow depth interval. Studies of early diagenesis are necessary for evaluation of the long term impact of anthropogenic trace metals, as they can address questions about bioavailability of trace metals after deposition and their remobilization from the sediments back into the water column. This study examines the concentrations, mobility and possible sources of trace metals in lake sediments and their impact in the western basin of Lake Superior.

Lake Superior's distance from major population and industrial centers means that most pollutants arrive primarily from the atmosphere rather than from point sources. This allows the lake to be considered as a large-scale collector for monitoring effects of changes in heavy metal inputs on a regional rather than local scale.

1.2 Diagenetic Reactions

Early diagenetic processes can change the physical and chemical

characteristics of sediment during burial (Berner, 1980). One of the most important consequences of early diagenesis is the control it exerts upon the chemical composition of natural waters. Pore waters are very sensitive indicators of initial diagenetic changes in the solid phases. In lake sediments, many diagenetic reactions are driven by changes in oxygen availability and redox state.

1.2a Redox Chemistry

The water column of Lake Superior is saturated in oxygen after turnover, and is rarely depleted by more than 10% between turnovers. Oxygen is present down to the sediment-water interface, oxygenating the upper level of sediment and being consumed by organisms on the lake floor. The amount of oxygen decreases with depth in the sediment due to respiration and decomposition of organic matter, causing a gradual shift from oxic to sub-oxic conditions. The conditions determining the rate of this shift are the sedimentation rate, the initial availability of oxygen, and organic carbon content of the sediments.

The redox state of sediments can affect the mobility and reactivity of metallic elements. There are general zones of burial depth associated with the diagenetic changes in distributions of redox sensitive metals between the solid and aqueous phases. Klinkhammer (1980) defined zones of diagenesis for Mn, which can be applied to other redox sensitive transition metals that form insoluble oxides (Figure 1). Below the sediment-water interface is the oxidized zone, where there is a steady supply of solid phase Mn (in the Mn^{+4} valence

state) and no aqueous Mn (in the Mn^{+2} valence state). An increase in concentration of Mn^{+2} indicates the beginning of the oxidation zone (L1), where Mn^{+2} is diffusing up from below. The aqueous Mn is subsequently oxidized and precipitates as MnO_2, resulting in an increase in the solid phase concentration. The solid phase concentration builds via the process of diffusion and oxidation to a peak, which is defined as the redox boundary (L2). In a given sediment profile the position of the redox boundary can occur at different depths for elements with differing redox potentials. Manganese has a higher redox potential than Fe, therefore the Mn peak will be closer to sediment-water interface than Fe. Below the redox boundary is the reduction zone, where Mn oxides are reduced and dissolved into aqueous Mn; the solid phase concentration decreases to zero in this zone. Dissolved Mn increases to a constant concentration, below which is the equilibrium zone. As sediments accumulate over time, the position of the different zones shift upward in order to remain in sediments of the same redox potential. This keeps the redox boundary at a constant depth from the sediment-water interface, assuming a constant rate of availability of oxygen.

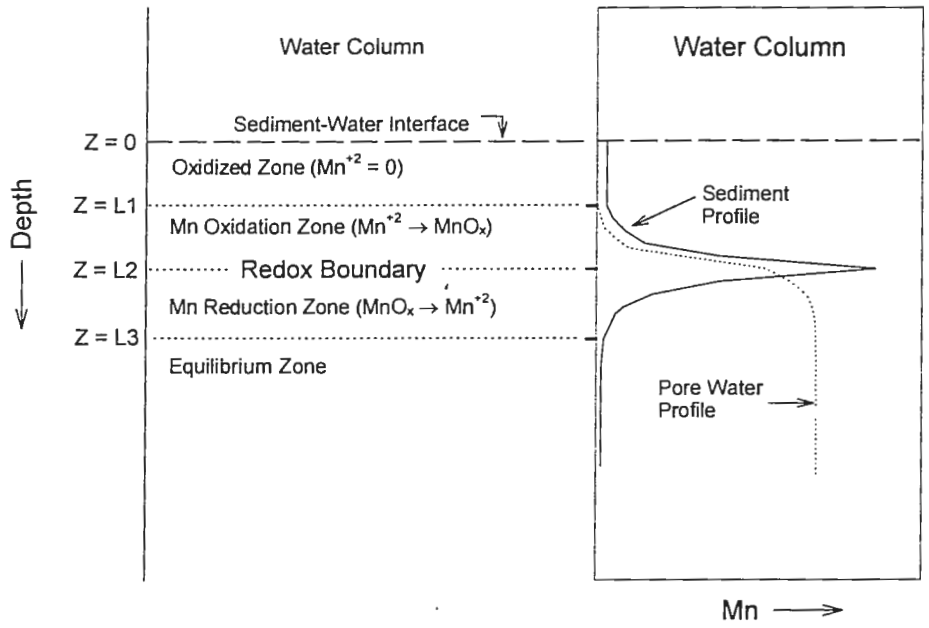

Figure 1. General zones of Mn diagenesis after McKee et al., 1989.

1.2b Trace Metal Fluxes

Diagenetic remobilization of a trace metal can create a concentration gradient between the interstitial water and lake water, resulting in a significant flux of the metal into the water column. Fluxes out of the sediment can affect the chemical composition of overlying waters. Such fluxes occur primarily due to the effects of diffusion and, if sedimentation rates are high, compaction and subsequent advection. This study follows the equations outlined in Berner (1980) to calculate fluxes of Cu, and Zn. It also follows Callender and Bowser (1980) who calculated fluxes of Mn and Cu from marine sediment pore waters into the overlying ocean.

1.2c Models Of Diagenesis

A number of approaches have been employed for numerical modeling of diagenetic processes. Burdige and Gieskes (1986) developed a mathematical model to describe distributions of Mn in pore waters and solid phase in a sediment column. Their model assumes that in the short-term, sediment profiles of Mn are at a steady-state balance between mobilization and reprecipitation. It is based on the distributions shown in figure 1, with a solid phase Mn peak at the redox boundary, the concentration of which decreases to zero lower in the core. The concentration of Mn in the pore waters is zero above the redox boundary. It increases near the boundary and goes to a maximum directly below the redox boundary.

1.3 Prior Studies

1.3a Marine Settings

Many studies (e.g., Klinkhammer, 1980; Heggie and Lewis, 1984; Schultz et al., 1994; Shaw et al., 1990) have examined the interaction between solid and aqueous phase trace metals in ocean sediments, studying the diagenetic mobilization of Fe and Mn at depth in suboxic conditions. In a classic study, Klinkhammer (1980) showed pore water Mn gradients reflecting dissolution at depth, upward diffusion and precipitation, with similar gradients of dissolved iron below the manganese oxidation zones.

Heggie and Lewis (1984) analyzed pore waters from marine sediments for

Co. They found that Co has profiles similar to Mn in both solid and aqueous phases. They concluded that cobalt was being recycled during dissolution and reprecipitation of sedimentary Mn oxides between suboxic and oxic sediments. They observed that the maximum Co concentration appeared at shallower depths than that of Mn. They could not explain this occurrence, since they linked Co concentration with the Mn oxides, not allowing Co a redox chemistry of its own.

More recently, Shaw et al. (1990) examined several depositional environments in order to compare the importance of parameters such as sedimentation rate and distance from the coast on trace metal cycling. At most of the shallow water Pacific ocean sites the redox boundary was at the sediment-water interface, causing an enriched layer of Mn near the surface. At the deeper water sites, with lower inputs of organic matter, the redox boundary was present deeper in the sediments.

1.3b Laurentian Great Lakes

Robbins and Callender (1975) investigated the diagenesis of Mn in Lake Michigan sediments. The study centered on the vertical distributions of total, acid-extractable, and dissolved Mn. They concluded that an enrichment of Mn in the surficial sediments was due to remobilization of Mn at the redox boundary. This was followed by diffusion and precipitation in the oxidation zone, near the sediment-water interface, and thus was the result of natural processes rather than increased anthropogenic loading.

Work of McKee et al. (1989a, b) examined geochemical partitioning across the sediment-water interface in cores from Lake Superior. McKee et al. (1989a), employed a selective chemical attack on sediment that was designed to sequentially remove specific fractions of elements. They concentrated on retrieving the interfacial sediments that occur close to the sediment-water interface to aid in development of a model for the early diagenesis of trace metals in the sediments since high concentrations of trace metals are often assembled there. The study of Mn, Cu and Pb in a single sediment core suggests that the Mn enrichments can be attributed to mobilization during early diagenesis, while Cu and Pb distributions reflect the interplay between diagenetic effects and changing fluxes from anthropogenic sources. McKee et al. (1989b) detail the collection and use of the trace metal pore water profiles for the same site. Their application of the Burdige and Gieskes diagenetic model led them to conclude that exchange between solid and aqueous phases was not at a steady state.

A study examining water column trace metal concentrations in three of the Great Lakes was completed by Nriagu et al. (1996). They noted the importance of atmospheric loading in the concentration of trace metals in the Great Lakes. They reported an increase in concentration of Zn with depth in Lake Superior, suggesting that there is some regeneration of Zn from the sediments.

1.4 OBJECTIVES

This thesis has the following objectives, which will lead to a better understanding of trace element modeling in Lake Superior's western basin.

- Examination of the effects of diagenesis on redox-sensitive elements by examining their depth profiles in sediment and associated pore waters.
- Determination of sedimentation rates and sediment chronologies at coring sites using ^{210}Pb-dating and other approaches.
- Use of those chronologies to examine the history of anthropogenic loading of Cu and Pb in the basin.

2. COLLECTION METHODS

Seven cores were collected from Lake Superior's western basin during three cruises in the summer of 1996 (Figure 2). Cores were collected using the Large Lakes Observatory's Ocean Instruments Multicorer and processed on the RV Lake Explorer, operated by the U.S. Environmental Protection Agency (Figure 3). Sampling was coincident with seismic and side-scan sonar profiling by Anderson (1997). Potential sampling sites were selected in advance, and cores were taken if seismic profiling confirmed the presence of post glacial sediment. An onboard Global Positioning System and echo sounder were used to locate each site, and determine depth. Every core acquired contained both an oxic and suboxic portion. Prior to processing, site locations (Table 1) and sample descriptions (Table 2) were recorded.

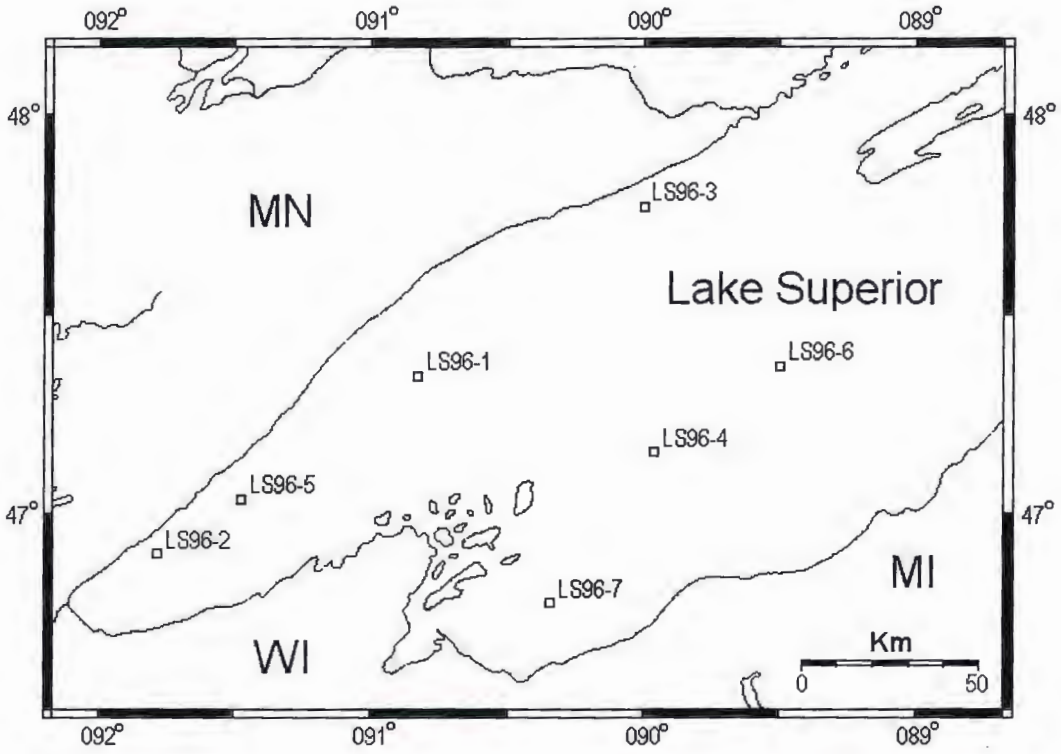

Figure 2. Lake Superior base map with coring locations.

Figure 3. EPA Research Vessel Lake Explorer.

Table 1. Lake Superior Core Locations.

Core	Latitude	Longitude	Water Depth (m)	Date and Time Recovered
LS96-1	47° 20.74' N	90° 50.18' W	191	7/15/96, 4:30 PM
LS96-2	46° 53.63' N	91° 46.98' W	143	7/29/96, 12:00 PM
LS96-3	47° 46.33' N	89° 60.00' W	241	7/30/96, 9:00 AM
LS96-4	47° 09.46' N	89° 58.29' W	174	7/31/96, 12:45 PM
LS96-5	47° 02.36' N	91° 28.91' W	251	8/28/96, 12:00 PM
LS96-6	47° 22.20' N	89° 30.00' W	211	9/6/96, 4:15 PM
LS96-7	46° 46.56' N	90° 21.23' W	94	9/7/96, 2:00 PM

Table 2. Lake Superior Core Descriptions.

Core LS96-1: This core is approximately 32 cm long. Between 10 cm and 11 cm there is a thin (~ 0.5 cm) iron rich layer. Above that the sediment is tan in color, below the layer the sediment is gray. There is a second thin (~ 3 cm) layer of dark material about 26 cm down.
Core LS96-2: This core is approximately 36 cm long. A slight gray discoloration appears at the top. Below that the sediment is tan in color. Around 15 cm down there is a dark gray layer. It appears to be ~4 cm thick. Below that layer the sediment turns back to the same tan color as before.
Core LS96-3: This core is approximately 34 cm long. It is tan in color for the top 5 cm. Then there is a thin, ~ 2 mm orange layer. The next 10 cm is dark gray. The rest of the core is a light to medium gray. There is no layer separating these two.
Core LS96-4: The cores retrieved vary in length meaning the multicorer must have gone in at an angle. Two cores are 30 cm and two are 33 cm. A tan color appears at the top with a gradational change into a darker tan over the next 7 cm. The next 3 cm is dark orange, and the 2 cm after that is orange. The rest of the core is medium dark gray.
Core LS96-5: Two of the cores retrieved are 30 -32 cm long, one is 22 cm long and the last is 8 cm long. The top 4 cm is tan in color, then there is the orange layer which is ~ 2 mm thick. The color changes to light gray for 4 cm and the next 3 cm is black or very dark gray. The remaining core is dark brownish gray.
Core LS96-6: The cores are 35 cm long. The top 9 cm are tan in color, and then ~ 2 mm of bright orange layer. The next 22 cm are light tannish gray, gradationally darkening as it gets deeper. Then there is a ~ 1 cm layer of black. The rest of the core is light gray.
Core LS96-7: The cores are 37 cm in length. This is the only set of cores that are heterogeneous on a one meter scale. The top is the same for all cores. The top 8 cm are brown in color, the next 7 cm are orangish tan, and then there is a ~ 2 mm orange layer. It is then light gray for 5 cm, and medium gray for 14 cm. Then the variation occurs, at the bottom of 2 of the cores is a bright orange blob from 2 to 4 cm thick which is not present in the third core.

2.1 MULTICORER

The Ocean Instruments Multicorer collects four replicate 10 cm diameter sediment cores of 30 to 36 cm in length (Figure 4). The cores were high quality samples of lake sediment with virtually undisturbed sediment-water interfaces (Figure 5), allowing precise subsampling of the sediment. In addition to the four cores, the multicorer also took a bottom water sample with a Niskin bottle. The sample bottle closed before the cores were taken to avoid entrapment of resuspended sediment.

The multicorer consists of four polycarbonate core tubes attached to a hydraulically damped center column supported by four legs (Figure 6). The whole assembly is deployed and lowered to the bottom by the ship's crane. When the legs touch the lake bottom, they stop, and the center column continues downward, at which point the Niskin bottle closes. The center column continues down, driving the core liners into the sediment. The multicorer remains on the bottom for approximately 20 seconds to allow the core liners to penetrate the sediments before being brought up. When the multicorer begins its ascent, large rubber stoppers hermetically seal the top of each tube. As the cores are pulled clear of the sediment, a trigger releases rubber lined plates that close the bottom of each core liner. The core holders are self contained units which can be removed individually from the multicorer frame for on shipboard processing.

There are many advantages to using the multicorer. Large quantities of

Figure 4. Ocean Instruments Multicorer being lowered overboard.

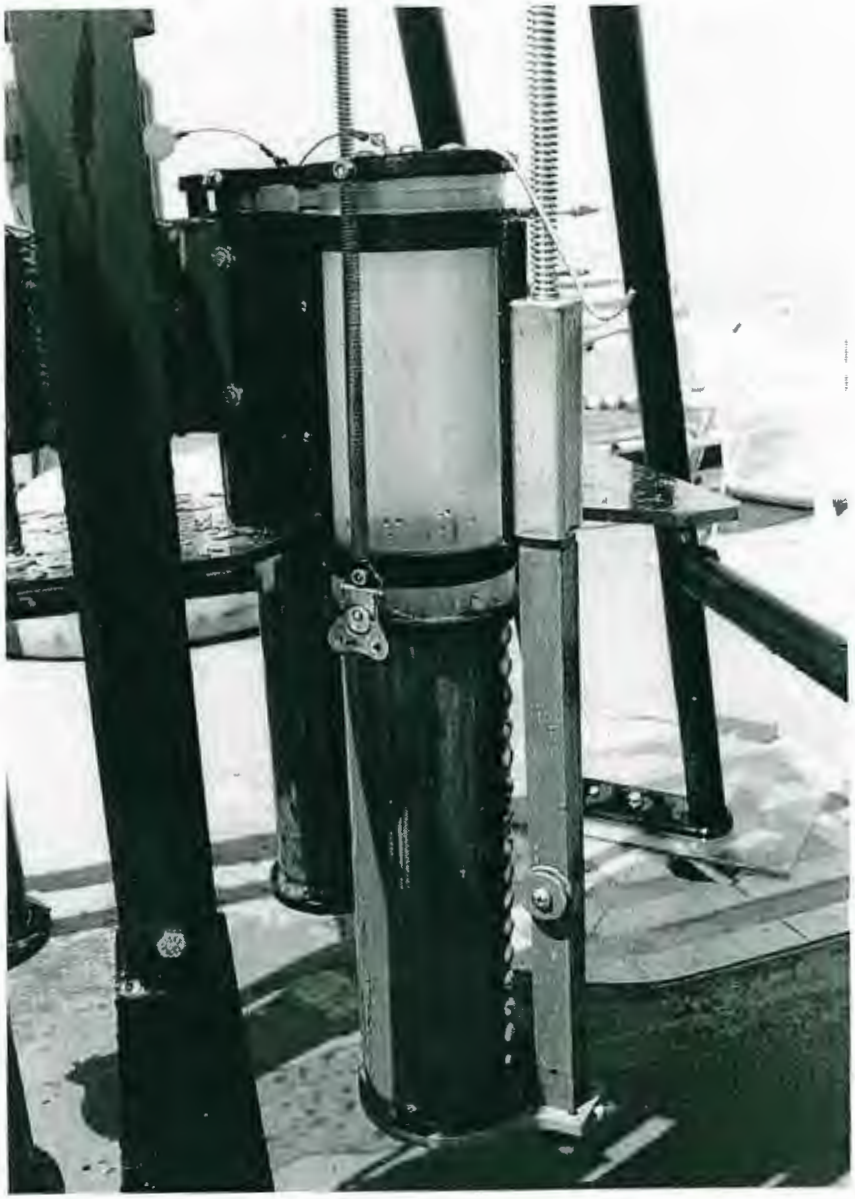

Figure 5. Multicorer tube with sediment.

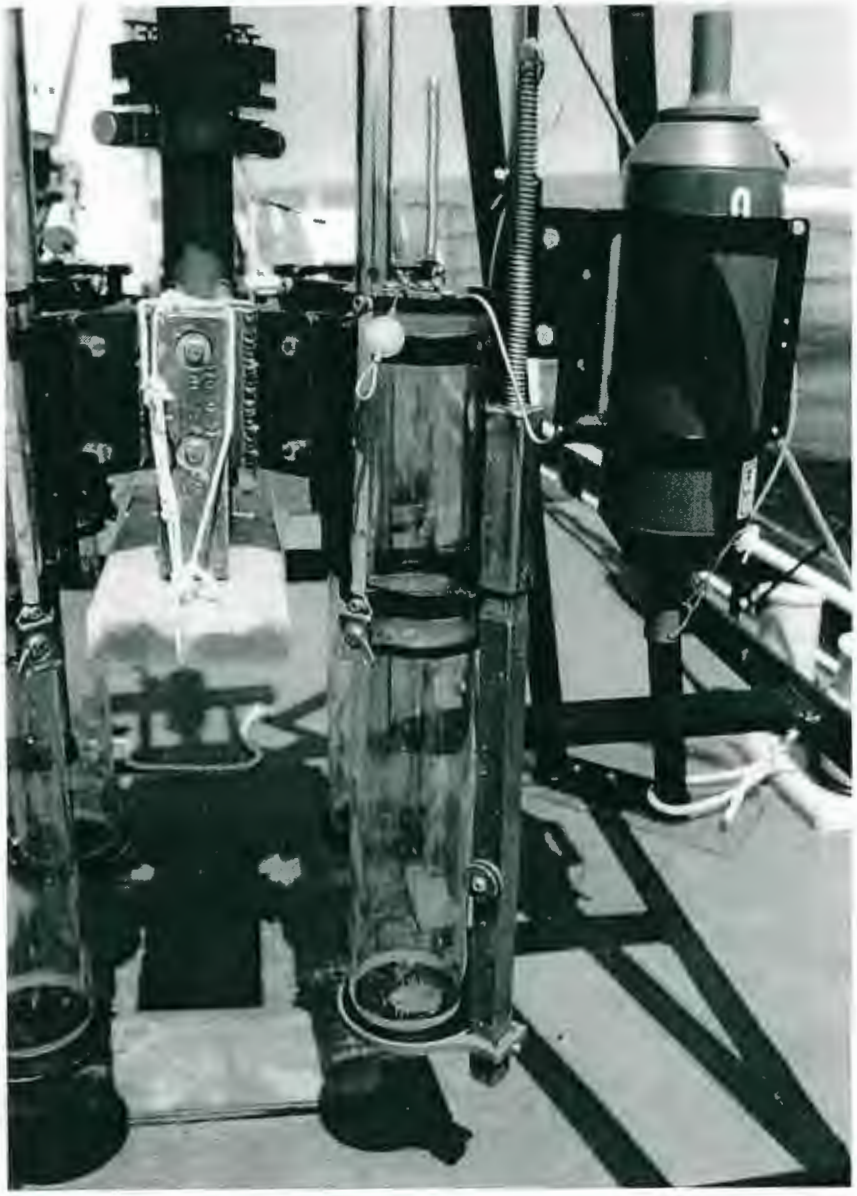

Figure 6. Close-up of empty core liner tubes and Niskin bottle.

sediment with undisturbed sediment-water interfaces are recovered. Sediment can be extruded directly out of the tube, it is unnecessary to transfer the sediment to another container to extrude as is the case with a box corer. The tubes can also be used directly with the pore water press, with minimal exposure to the atmosphere so the redox potential of the sediments is not significantly altered.

2.2 Sediment Sampling

The replicate cores were processed in different ways for various analyses: One (sub-core A) was used to extract sediment pore waters and was then discarded. Two cores were extruded (sub-cores B and C) and sub-sampled in 0.5 to 1.0 cm increments. The final core (sub-core D) was archived for possible later examination. Archiving involved removing the overlying water, capping the top, then cutting off the empty part of tubing and capping the bottom.

After shipboard processing, the water, sediment, and archive samples were stored in the onboard refrigerator. After docking, the samples were transferred to the LLO core repository.

2.2a Extrusion

Extrusion was employed to physically subsample sediment into smaller increments so that it could be later analyzed. The strategy of subsampling depended on the position of the Fe redox boundary, which appeared in the sediment as a orange clayey crust. The upper part of the core was sampled at

0.5 cm increments, to 2 cm below the iron crust, which had an average depth of 8 cm. The remainder of the core was sampled using increments of 1 cm. This strategy allowed precise examination of the distributions of solid phase trace metals, ^{210}Pb activities and mineralogical assemblages of each core.

The extruder was designed and built for this study (Figure 7). It was constructed with a stainless steel threaded rod and fittings, a polycarbonate piston with a rubber o-ring (used to force sediment through core tube), two polycarbonate disks, and a plastic and brass knurled knob. The threaded rod used for the backbone of the device has 13 turns per inch. This is convenient for rough conversion to the metric system since each turn corresponds to 0.195 cm.

The first step of sample extrusion was removal of the rubber-lined foot and insertion of a piston, with an o-ring seal, into the bottom of the core liner. With the bottom opening of the core tube secured by this piston, the rubber stopper sealing the top of the core tube can be opened and the water overlying the sediment removed by siphoning. The sediment was brought to the top of the core tube by sliding the piston up from the bottom of the liner (Figure 8). When the knurled knob was rotated downward the plastic disk supporting the core tube and the core tube itself were pushed down, leaving a layer of sediment raised above the top polycarbonate disk. A plastic scraper and rubber spatula were used to scrape the sediment into plastic bags, which were labeled prior to sampling. There was no other preparation to the bags. In most cases one-pint Ziplock freezer bags were used, but for three cores Whirlpak bags were used.

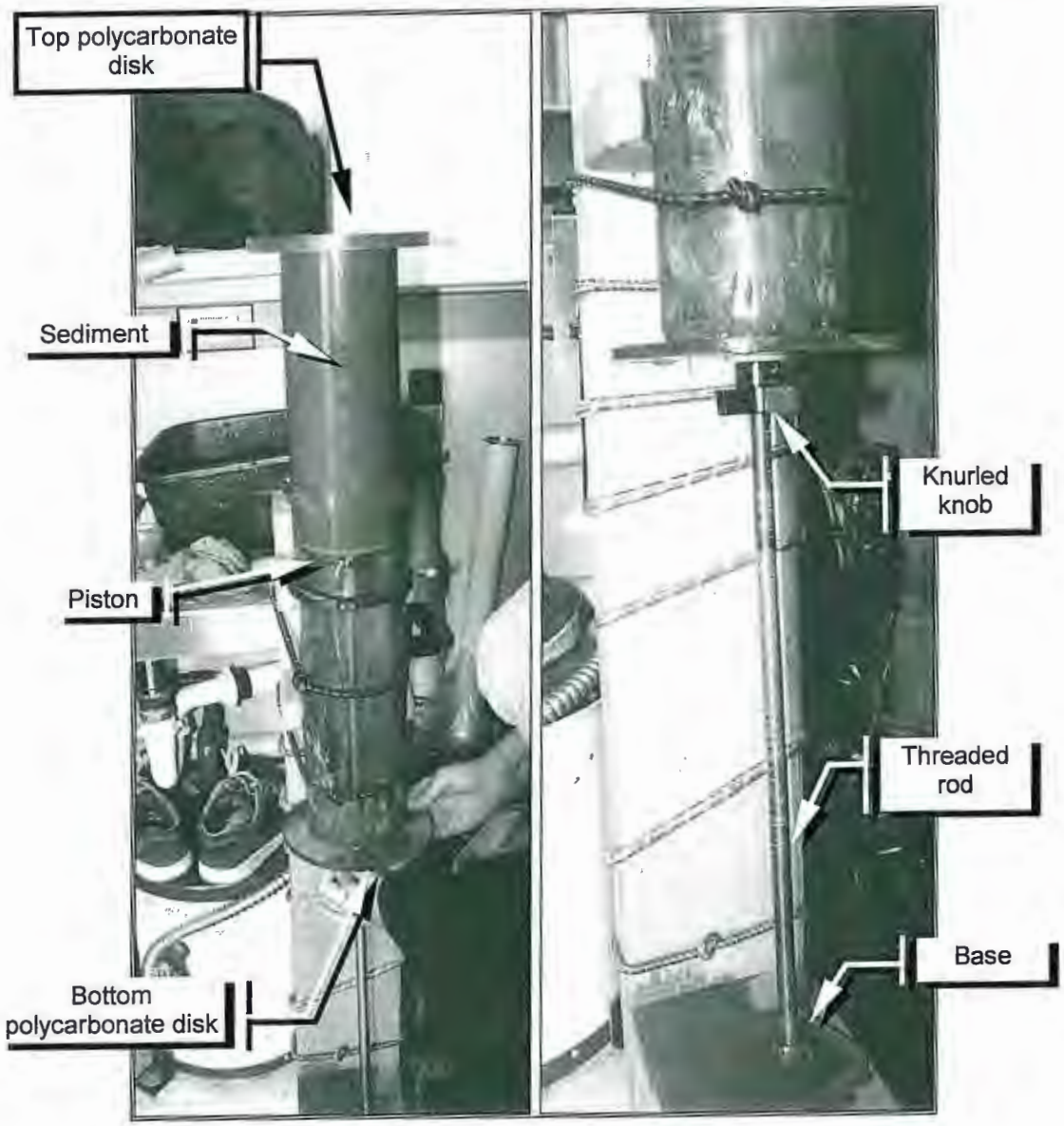

Figure 7. Schematic diagram of sediment extruder.

Figure 8. Extrusion process: Sediment flush with top, then raised and scraped into a bag.

2.2b Pore Water Press

A pore water press was used to extract interstitial waters from the sediment cores (Manheim, 1966). The core liner that was used for pore water extraction had a series of threaded sampling ports at 1 to 2 cm intervals. During multicorer deployment these ports were sealed with nylon screws and rubber o-rings. After retrieval of the core, pistons with o-ring seals were set in place, at the top and the bottom of the core liner (Figure 9). Once the pistons were in position, the nylon screws were removed from the sampling ports and replaced by filtration assemblies (Figure 10). These consisted of a filter and syringe attached to each other and to the core liner with threaded and luer-lock fittings. With the filtration assembly attached, the sediment was placed under pressure by forcing the pistons into the liner by rotating the knurled knobs along the threaded rods to build up the pressure against the frame of the press. The pressure squeezed sediment through the ports and forced the pore waters through the filters and into the syringes. After collection, pore waters were transferred from the syringes into bottles. The filters were replaced two to three times during squeezing since they quickly became plugged with sediment.

The pore water press required a number of expendable items, including filters, syringes, and sample bottles, all needed preparation before use. The filters used were Gelman Acrodisc PF 25 mm syringe filters with a 0.8 micron pore-size prefilter over a 0.2 micron pore-size final filter. The filters were cleaned by pumping filtered 1% HCl through them for 10 minutes and by rinsing with

filtered MilliQ water for 10 minutes. They were dried at 70 °C for approximately two days and packaged in individual Whirlpak bags. The 15 ml HDPE Nalgene bottles and syringes were prepared using an acid bath. They were submerged in a 1% HCl acid solution for 24 hours and then rinsed in MilliQ water and air-dried in a laminar flow bench. At all stages, clean polyethylene gloves were worn when handling the filters, bottles and syringes.

The pore water press is one of two common ways to extract pore waters from sediment cores. The other method involves extruding the sediment, either squeezing or centrifuging it, and filtering the resulting pore water (e.g., Klinkhammer, 1980; Callender and Bowser, 1980). The extrusion process and subsequent pore water extraction should be undertaken under a nitrogen atmosphere at lake floor temperature (in the Great Lakes, mean 4 °C). This method is expensive and labor intensive.

The pore water press method compares well with the extrusion and centrifugation method. One of the advantages of the pore water press is minimization of contact with atmospheric oxygen. It is also an inexpensive and quick method of pore water extraction. There are drawbacks to the use of a pore water press. It sometimes yields low sample volumes since filters clog rapidly. Another concern is that as the pore waters are extracted, the sediments column becomes compressed. This potentially distorts the sediment and can prevent the collection of pore waters from discreet layers. In this study, a core 30 cm in length was not compressed more than 3 cm suggesting that such effects are

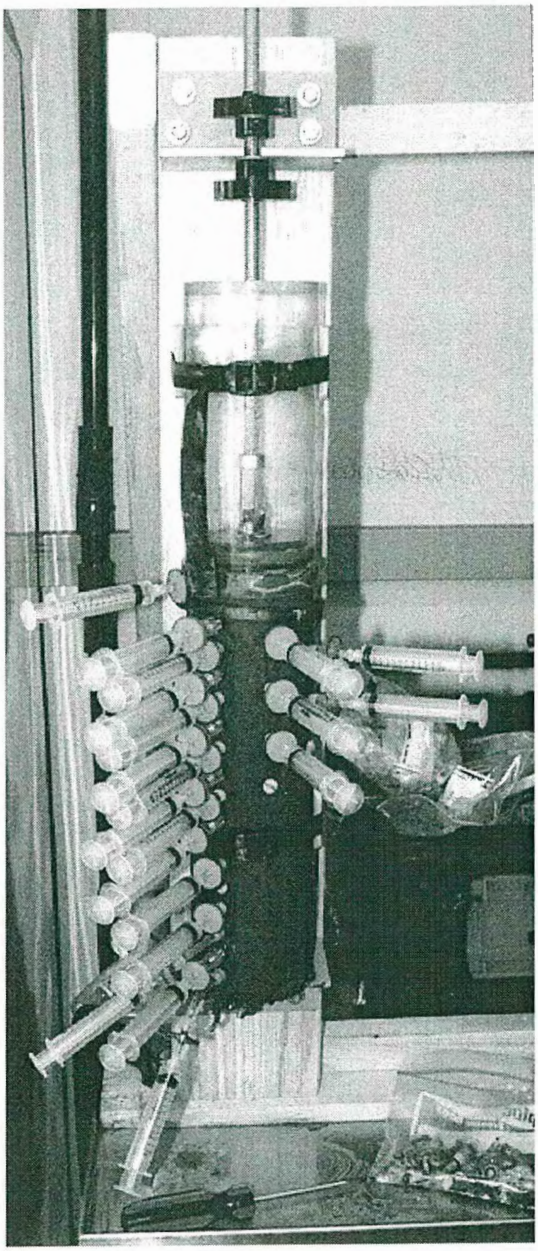

Figure 9. Pore water press with sediment sample.

Figure 10. Close-up of syringe/filter assembly.

minimal relative to these sediments. Finally, sediment may pull away from the wall of the core liner, allowing vertical migration of pore waters and any remaining overlying water. Examination of pore water chemical data indicates that such vertical migration was not significant.

3. LAB METHODS

3.1 SEDIMENT LEACHING

Iron and manganese oxides exist in sediments as nodules, cement between particles or simply as a coating on particles; these oxides are excellent scavengers for trace metals and are thermodynamically unstable under anoxic conditions (Tessier et al. 1979). The sediment leaching technique used in this study outlined by Tessier et al. (1979) and also applied by McKee et al. (1989), uses a moderately reducing attack to release trace metals scavenged by Fe and Mn oxides, as well as those loosely adsorbed onto clays. Iron, manganese and other trace metals are reduced to aqueous form by the hydroxylamine hydrochloride, and the high concentrations of liberated metals are able to remain in solution due to the acetic acid.

A subset of samples were selected for chemical analysis. The typical sampling increment was every centimeter for the top 10 cm of the core. The remainder of the core was mostly sampled at two or three cm increments. The sampling interval across the redox boundary was 0.5 cm, to ensure definition of the Fe and Mn peaks.

A weighed amount of dried sediment, typically 0.2 g, was placed in a centrifuge tube with 25 ml of a leaching solution of 25 % Glacial acetic acid (trace metal grade) and 0.04 M $NH_2O{\bullet}HCl$ (hydroxylamine hydrochloride) and a teflon-coated stir bar. This was heated on a stirring hot plate between 90 °C and

95 °C for 8 hours. The stir bar was then rinsed with MilliQ water and removed. The sample was then centrifuged at 3200 rpm for 3 minutes and decanted into bottles. Another 5 ml of MilliQ water was used to rinse the sample, which was then centrifuged, and decanted a second time. The resulting leachate was weighed and ready to be analyzed.

The samples were analyzed with a Direct Current Plasma (DCP) Emission Spectrometer, (a Spectrajet III). The DCP produces an argon plasma into which the sample is introduced. At the high temperature conditions of the plasma, the analytes are ionized and emit light of characteristic wavelengths. The intensities of these emissions, when compared to those of known concentrations of elements in the standard, are used to determine concentrations of elements in the sample. A set of three SPEX-certified standards and a blank prepared with the same reducing solution that was used to leach the samples, to match the matrices of the blanks and standards to those of the samples, were used to calibrate the DCP (Table 3). The instrument was re-calibrated after every five samples to minimize the effects of instrumental drift. Detection limits and instrument drift were calculated from the DCP standard data (Table 4). The detection limit for the DCP was calculated as three times the standard deviation (3σ) of the measurement of the blank. Instrument drift was calculated as the percent change in the number of counts for an element in the standard from one standardization to another. When drift was considered too high (over 15 %) the data were discarded and the samples re-analyzed.

The DCP could not be used to determine Pb concentrations in sediment leachate. Initial Pb profiles were exactly like those of Mn, indicating that the DCP was measuring interference from a Mn peak adjacent to the Pb peak. It was determined that the Pb levels were below detection limits due to interference from the 25% acetic acid matrix. A subset of sediment leaches that were critical to this study were analyzed by ICP-MS at the Department of Geology and Geophysics on the campus of the University of Minnesota. This allowed the precise determination of the Pb concentrations as well as Cu, Co, Ni and Zn, the concentrations of which were below the detection limit of the DCP.

Table 3. Concentration of elements in the DCP standards.

Elements	Blank (ppm)	LS-96-1 (ppm)	LS-96-2 (ppm)	LS-96-3 (ppm)
Mn	0	20	50	100
Fe	0	20	150	350
Al	0	20	35	70
Mg	0	14	40	
Ba	0	2		
Cu	0	4		
Ni	0	4		
Pb	0	4		
Sr	0	2		
V	0	4		
Zn	0	4		

Table 4. Detection limits and instrument drift of the DCP.

Element	Detection limit: (ppm)	(μmole/g)	Drift: 75% below	Not above
Al	4.0	40.0	6.3%	14%
Ba	0.3	0.60	5.1%	8.1%
Cu	0.4	1.70	5.1%	7.4%
Fe	0.7	3.50	3.9%	6.9%
Mn	0.2	0.80	3.9%	6.6%
Ni	2.5	11.0	3.1%	5.7%
Zn	0.5	2.00	2.2%	6.2%

3.2 Pore Waters

The collected pore water samples needed to be acidified and diluted prior to analysis. Since the pore waters came into contact with atmospheric oxygen after bottling, the redox chemistry could have been changed. This could cause Fe and Mn to oxidize and precipitate, altering their concentrations along with others, such as Ba. In order to keep the Fe and Mn and other elements in solution, each pore water sample was acidified to 0.5 %, by volume, with ultra-pure HCl (Fisher Optima). This retained metals in solution and dissolved any oxy-hydroxides that might have formed. The samples were diluted to increase the sample volume available for analysis. The dilutions ranged from 5 to 7.5 times to achieve a total sample volume of 5 ml. All of the acidification and dilution was completed on a laminar flow bench, while wearing polyethylene gloves, with care taken to maintain the purity of the acid and MilliQ water, and to minimize the potential for sample contamination.

The pore water samples were analyzed for trace element content on a Perkin-Elmer SCIEX ELAN 5000 Inductively Coupled Plasma-Mass Spectrometer (ICP-MS) at the Department of Geology and Geophysics on the Twin Cities Campus. ICP-Mass Spectrometry has detection limits of much less than a part per billion, often in the range of a part per trillion. The suite of elements examined in this study of pore water geochemistry included the following: Fe, Mn, Ba, Cu, Pb, Zn, Ni, Co, Al, Ca, and Mg.

The ICP-MS performs rapid multielement quantitative determinations of trace and ultra trace elements and isotopes. It uses an argon plasma torch coupled with a quadrupole mass spectrometer. The instrument is calibrated against external standards of the elements of interest with concentrations across the range expected in the samples.

To compensate for drift in ICP-MS response, internal standards were added to each sample. The elements used as internal standards were in the mass range of the elements of interest and were not naturally occurring in the samples. In this study ^{45}Sc was used to normalize Mg, Al, Ca, Fe, Mn, Co, Ni, Cu, and Zn, which have atomic masses ranging from 26 to 66. For the heavier elements, Ba and Pb, ^{103}Rh was used as the internal standard. The internal standard was pipetted into the samples, blanks, and standards to yield a final concentrations of 50 ppb of Rh and Sc. The standard set for the pore waters used a procedural blank that underwent the same treatment as the samples (filtration through an acid washed syringe filter and acidification using 0.5% of

ultra pure HCl).

Only a two point standardization (blank and standard) (Table 5) was required because the ICP-MS response curve is linear well beyond the concentrations of these samples.

Table 5. Concentration of elements in the ICP-MS standard.

Element	Blank (ppb)	96LS-ICP (ppb)
Al	0	88.3
Ba	0	43.16
Ca	0	2686
Co	0	45.81
Cu	0	46.01
Fe	0	44.79
Mg	0	449.9
Mn	0	47.15
Ni	0	44.6
Pb	0	43.46
Zn	0	46.51

The detection limit for the ICP-MS was calculated as three times the standard deviation (3σ) of the measured blank (Table 6).

Table 6. Detection limits of the ICP-MS.

Element	Detection limits: (ppb)	ηmole/g
Al	0.39	1.4E-02
Ba	0.007	4.9E-05
Co	0.14	2.3E-03
Cu	0.05	2.2E-03
Fe	1.1	8.0E-04
Mn	0.07	2.1E-02
Ni	0.73	1.2E-03
Pb	0.017	8.0E-05
Zn	0.089	1.1E-02

3.3 ^{210}Pb Dating

Dating was completed to quantify the sedimentation rate at four of the seven coring sites, LS96-3B, 4C, 5B and 6C. These cores had the most complete assemblage of pore waters, and showed the most promising trace metal profiles. Analyses were completed at the Sedimentary Analyses Laboratory in the Great Lakes Research Facility on the University of Wisconsin-Milwaukee campus under the guidance of Dr. David Edgington.

The decay series of ^{238}U includes ^{222}Rn, a radioactive, but chemically inert gas that escapes into the atmosphere at a global average rate of 42 atoms per minute per square centimeter of land surface (Faure,1986). Atmospheric ^{222}Rn has a half-life of 3.8 days and then decays to form a series of short lived, chemically-reactive daughter products. The daughter products are ^{218}Po ($t_{1/2}$ = 3.1 minutes), ^{214}Pb ($t_{1/2}$ = 26.8 minutes), ^{214}Bi ($t_{1/2}$ = 19.7 minutes), ^{214}Po ($t_{1/2}$ = 10^{-4} seconds), and ^{210}Pb ($t_{1/2}$ = 22.26 years). Due to the short half-lives of the

intermediate daughter products it is reasonable to treat ^{210}Pb as the primary daughter product of ^{222}Rn.

The technique of using excess ^{210}Pb activity precipitated from the atmosphere to date lake sediments less than 100 years in age was first used by Krishnaswamy et al. (1971). The ^{210}Pb is rapidly removed from the atmosphere by rain and snow; the residence time in the atmosphere is only about 10 days. After removal from the atmosphere, ^{210}Pb is deposited in the snow and ice of glaciers, in lakes, and across the landscape. In fresh water lakes ^{210}Pb is rapidly adsorbed onto particles, and deposited as sediment on the lake floor. In addition to this "excess" ^{210}Pb, sediments contain a background level of supported ^{210}Pb in secular equilibrium with parent nuclides in the ^{238}U decay series. The excess ^{210}Pb is unsupported, so its decay can be employed as a geochronometer.

Determination of the activity of ^{210}Pb in the sediment requires addition of a radioactive spike of ^{208}Po, an artificial radionuclide with a half life of 2.93 years. On the alpha counter, ^{208}Po and ^{210}Po are measured, with the ^{208}Po acting as a yield and efficiency monitor. ^{210}Po ($t_{½}$ = 138.4 days) is a daughter product of ^{210}Pb and is assumed to be in secular equilibrium with ^{210}Pb, so their activities are equal. The measured activities of ^{208}Po and ^{210}Po are then used to calculate the amount of ^{210}Pb in the sample.

The process of the analysis began by weighing approximately 0.5 grams of dried sediment into separate Erlenmeyer flasks. One milliliter (6.35 dpm) of the spike, ^{208}Po, and 50 ml of 6N HCl were added to each sample. The samples

were heated at 100 °C for four hours and then cooled and filtered through a Whatman #10 filter. The sample volume was reduced down to approximately 5 ml by heating and evaporation. The pH was checked and adjusted to ~0.5 to 1.0 using either NaOH or HCl. Next between 0.1 and 0.2 g of ascorbic acid was added. The resulting solution was placed in a Nalgene bottle along with a copper disk, and was placed in an oven at 100 °C overnight. The ascorbic acid prevented any iron from precipitating onto the copper disks while they were being plated with Po. The disks were then removed and rinsed with DI water and ethanol before being counted in the alpha collector.

3.4 ^{210}Pb Calculations

Calculations for age and sediment accumulation rate followed approaches summarized by Oldfield and Appleby (1983). For Lake Superior sediments it was assumed that the ^{210}Pb flux was constant, so at steady-state the rate of decay of ^{210}Pb in the sediment column equals the rate of ^{210}Pb deposition:

$$w_o C_o = \lambda A_{(o)} \qquad (1)$$

If the rate of ^{210}Pb flux is constant, any changes in surface concentration are due to changes in sedimentation rate. As this is the case at the sediment-water interface, z = 0, it is also true for any depth, x:

$$w_x C_x = \lambda A_{(x)} \qquad (2)$$

where

w_o = mass sedimentation rate at sediment-water interface

($g/cm^2/yr$)

w_x = mass sedimentation rate at depth x ($g/cm^2/yr$)

λ = decay constant for ^{210}Pb, $\approx 0.0311\ yr^{-1}$

$A_{(o)}$ = Integrated sum of the activity of ^{210}Pb for entire sediment column (pCi/cm^2)

$A_{(x)}$ = Integrated sum of the activity of ^{210}Pb below depth x (pCi/cm^2)

C_o = Activity of ^{210}Pb at sediment-water interface (pCi/g)

C_x = Activity of ^{210}Pb at depth x (pCi/g)

Equation 2 can be rearranged to yield an equation expressing sedimentation rate at the time of deposition of a layer of sediment now at depth x:

$$w_x = \frac{\lambda A_{(x)}}{C_x} \qquad (3)$$

This approach allows the calculation of a changing sedimentation rate.

The model can be modified to account for sediment mixing, such as that caused by bioturbation. The modification assumes rapid mixing throughout a zone of fixed thickness, and only affects age calculations, not sedimentation rates. Given the mass of dry sediment in the zone of mixing, the depth/age relation can be calculated using the formula:

$$t = \frac{1}{\lambda} \ln \frac{A_{(o)}}{A_{(s)} + WC_x} \qquad (4)$$

where

t = Time (yr.)

λ = Exponential decay constant for ^{210}Pb, $\approx 0.0311\ yr^{-1}$

$A_{(o)}$ = Total integrated sum of ^{210}Pb activity of sediment column (pCi/cm^2)

$A_{(s)}$ = Integrated sum of ^{210}Pb activity for a depth below the zone of mixing (pCi/cm^2)

W = Dry mass of sediment in the zone of mixing (g/cm^2)

C_x = Activity of ^{210}Pb in the zone of mixing (pCi/g)

These approaches yield sedimentation rates in $g/cm^2/yr$. Resulting values were normalized using porosity to obtain sedimentation rates in cm/yr, corrected for compaction.

3.5 X-RAY DIFFRACTION

X-ray diffraction (XRD) was used to identify the general clay mineralogy at each site, and to determine whether a site had been affected by taconite mining. Taconite mining operations disposed of waste directly into the lake, beginning around 1956 (Cook, personal communication), along the North Shore, from Two Harbors to Silver Bay. Taconite tailings contain the iron oxide mineral grunerite which has a distinctive XRD signature and can be used to determine their presence (Cook, 1975). Evidence of mine waste should only be present in the depth range between 0.5 to 5 cm, given the low sedimentation rates of Lake

Superior. If bioturbation is also considered, the depth range would be increased to 0 to 6 cm.

Approximately 60 samples were analyzed on the XRD, representing cores LS96-1, 2, 3, 4, 5 and 6. The XRD shows that the sediments are primarily composed of clays, mostly chlorite, and montmorillonite (Table 7). Quartz was also identified in all the samples. Cores LS96-1, 2, and 5 were collected from the area most likely to be affected by taconite mining, and grunerite was identified in them. Of the remaining cores, one is from farther north along the shore off Grand Marais (site LS96-3), and the other two are from the middle of the western arm (sites LS96-4 and 6). In cores LS96-1 and 2 the top 5 to 5.5 cm were analyzed at 0.5 cm increments. In core LS96-1 the grunerite disappeared below the 4.0 to 4.5 cm sampling interval, in core LS96-2 the grunerite was no longer detectable below the 4.5 to 5.0 cm sampling interval (Table 7). Core LS96-5 was analyzed at 0.5 cm increments from 0 to 3 cm and at 1 cm increments form 3 to 11 cm. Grunerite was present down to 8-9 cm, being undetectable at 9-10 cm. In cores LS96-3, 4 and 6 the top 3 cm of each were analyzed for general lithology and to verify that there was no evidence of taconite mining. Additional samples from various depths in each core were analyzed for general lithology along the length of the core.

Table 7. Results of XRD analyses, Cores LS96-1 through 6.

Core	Mean depth, cm	Grunerite	Chlorite	Montmorillonite
LS96-1C	0.24	abundant	present	present
	0.73	abundant	present	present
	1.71	abundant	present	present
	2.19	abundant	absent	present
	2.68	abundant	absent	present
	3.17	abundant	present	present
	3.66	present	n/a	n/a
	4.14	present	n/a	n/a
	4.63	absent	n/a	n/a
	5.12	absent	n/a	n/a

Core	Mean depth, cm	Grunerite	Chlorite	Montmorillonite
LS96-2C	0.24	present	present	present
	0.73	present	present	present
	1.22	present	present	present
	1.71	present	present	present
	2.19	present	present	present
	2.68	present	present	present
	3.17	present	present	present
	3.66	present	n/a	n/a
	4.14	present	n/a	n/a
	4.63	present	n/a	n/a
	5.12	absent	n/a	n/a
	5.61	absent	n/a	n/a

Core	Mean depth, cm	Grunerite	Chlorite	Montmorillonite
LS96-3B	0.73	absent	present	present
	1.71	absent	present	present
	2.68	absent	present	present
	3.66	absent	present	present
	12.2	absent	present	present

Table 7 (continued). Results of XRD analyses, Cores LS96-1 through 6.

Core	Mean depth, cm	Grunerite	Chlorite	Montmorillonite
LS96-4C	0.24	absent	absent	present
	0.73	absent	present	present
	1.22	absent	present	absent
	1.71	absent	present	absent
	2.19	absent	present	absent
	2.68	absent	present	absent
	3.17	absent	present	absent

Core	Mean depth, cm	Grunerite	Chlorite	Montmorillonite
LS96-5B	0.73	present	present	absent
	1.22	present	absent	present
	1.71	abundant	absent	present
	2.19	abundant	present	present
	2.68	abundant	absent	present
	3.17	abundant	absent	present
	4.14	abundant	absent	present
	5.12	abundant	present	present
	6.09	abundant	absent	present
	7.07	abundant	present	present
	8.04	present	present	present
	9.02	present	present	present
	9.99	absent	present	present
	11.0	absent	present	present

Core	Mean depth, cm	Grunerite	Chlorite	Montmorillonite
LS96-6C	0.24	absent	present	present
	0.73	absent	present	present
	1.22	absent	present	present
	1.71	absent	present	present
	2.68	absent	present	present
	11.2	absent	present	present
	20.0	absent	present	present

3.6 Loss On Ignition

Loss on ignition (LOI) was used to determine the porosity (% H_2O by weight and volume), wet and dry bulk densities, percent organic content, and percent carbonate content of the sediments. This analysis was completed on the extruded sediment samples, one from each site, with the entire core being analyzed. The procedure involved weighing a measured volume of sediment, and then heating it at progressively higher temperatures, to burn off specific portions in the sediments. The samples are dried at 110 °C overnight and are then weighed. They are subsequently heated at 550 °C and 1000 °C for an hour each. After each step, the samples are allowed to cool and are then weighed.

The 110 °C heating is used to calculate the wet and dry bulk densities, and the percent water content in each sample, by volume and weight (equations 5-8) . The 550 °C heating step yields percent organic matter (equation 9), and the 1000 °C step can yield percent carbonates.

$$\text{Wet bulk density } (g/cm^3) = \frac{\text{Weight of fresh sample}}{\text{Volume of fresh sample}} \quad (5)$$

$$\text{Dry bulk density } (g/cm^3) = \frac{\text{Weight of dry sample}}{\text{Volume of fresh sample}} \quad (6)$$

$$\text{Porosity} = (\text{Wet bulk density} - \text{Dry bulk density}) \bullet 100\% \quad (7)$$

$$\text{Weight percent water} = \left(\frac{\text{Wet bulk density} - \text{Dry bulk density}}{\text{Wet bulk density}}\right) \bullet 100\% \quad (8)$$

$$\text{Percent Organic} = \frac{\text{Loss of mass from } 110° \text{ to } 550°}{\text{Weight of dry sample}} \bullet 100\% \qquad (9)$$

There were no detectable amounts of carbonates in Lake Superior sediments using this procedure. In low carbonate sediments the loss of mass after the 1000 °C step is dominated by the loss of water of hydrated clays (Kane et al., 1993). The results of the LOI calculations are listed in the appendix, including the porosity and organic content (Figures 11-17).

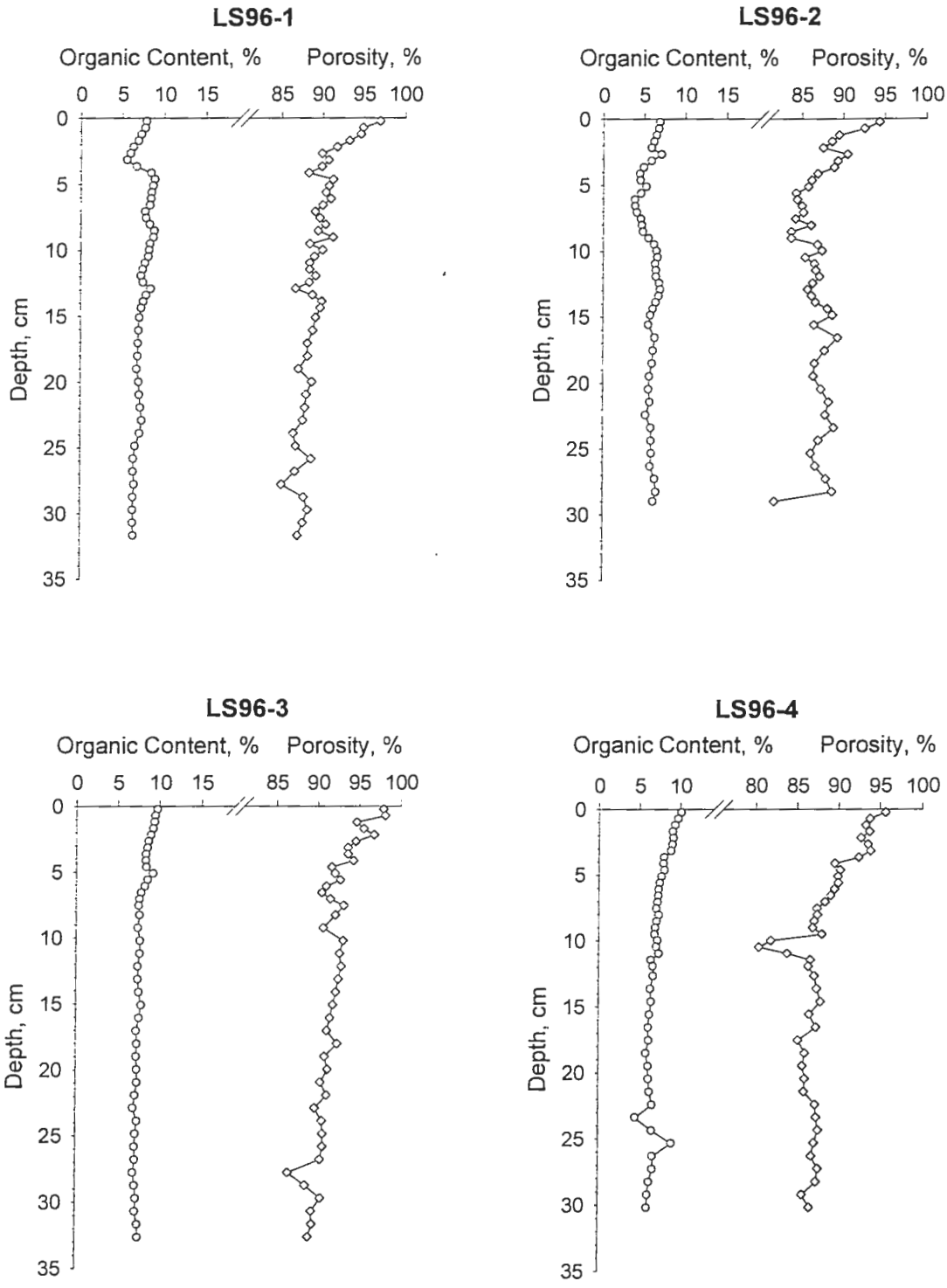

Figures 11-14. LOI results, porosity and organics, for cores LS96-1, 2, 3, and 4.

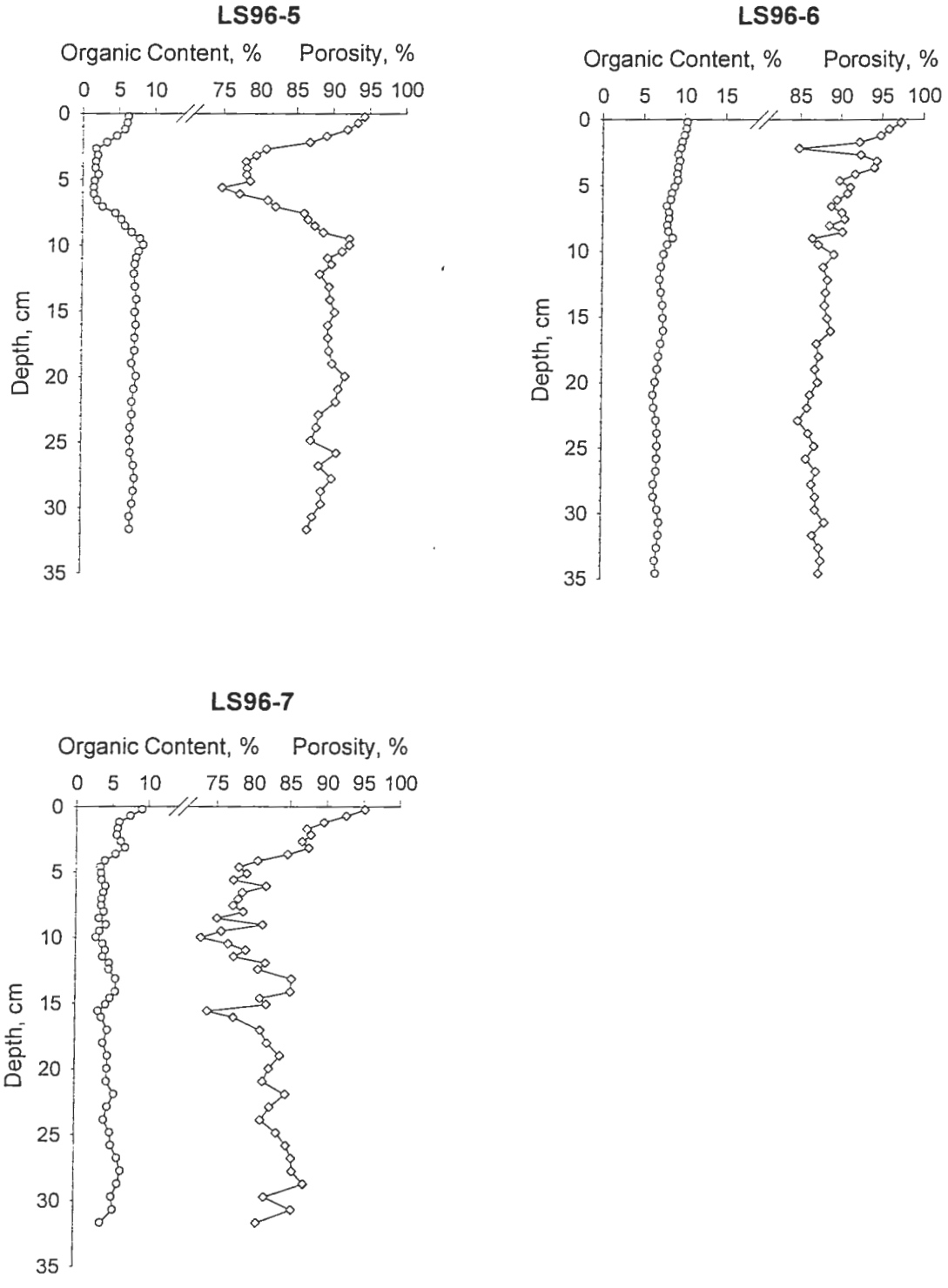

Figures 15-17. LOI results, porosity and organics, for cores LS96-5, 6, and 7.

4. RESULTS

For the purposes of this study, the sites were divided into 'in-depth study sites' and 'other study sites.' The criteria used to make this distinction depended on core quality and the quantities of pore waters available for analyses. 'In-depth' sites had high sampling densities for pore waters; consequently more sediment leach analyses as well as ^{210}Pb analyses for geochronology were completed. Core LS96-3, 4, 5, and 6 were 'in-depth study sites' while the remaining cores, LS96-1, 2, and 7, were placed in the 'other study sites' category.

In this presentation of results, points are connected by lines only as an aid in visualizing the data. In sediment cores the data points represent average values for the sampled depth interval. Numerical data are presented in the appendix.

4.1 In-Depth Study Sites

4.1a Coring Site LS96-3

Coring site LS96-3 is located east of Grand Marais, MN, at a water depth of 241 m (Figure 2).

The redox chemistry at site LS96-3 shows distinct peaks in the leachable solid phase at depths where pore water composition shows related changes

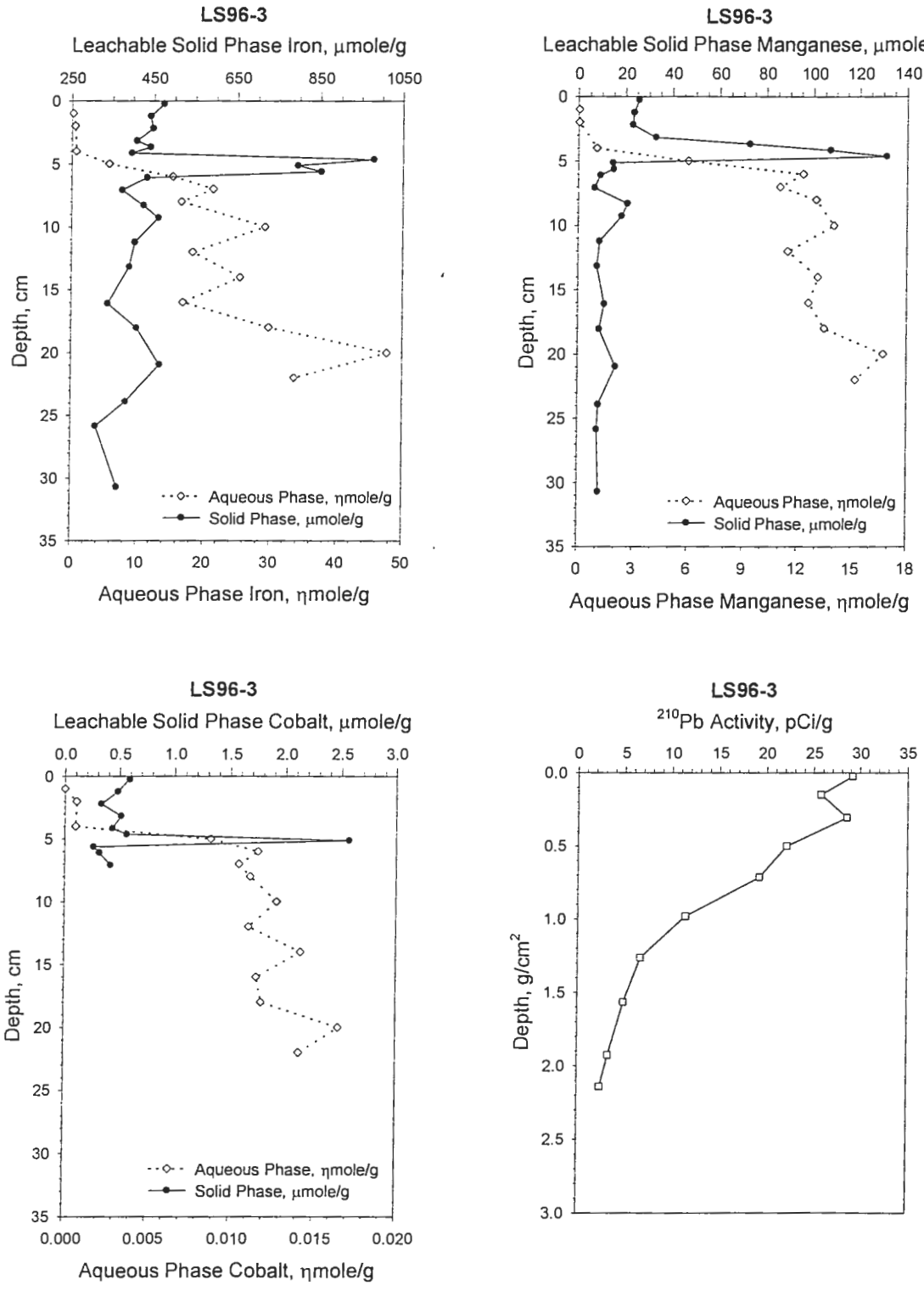

Figures 18-21. Core LS96-3, solid and aqueous phase data for Fe, Mn and Co, and ^{210}Pb.

(Figures 18-20). The solid phase Fe has a maximum concentration of 978 μmole/g at a depth of 4.75 cm. The Mn solid phase peak occurs with a concentration of 131 μmole/g at a depth of 4.75 cm. The solid phase peak for Co has a concentration of 2.57 μmole/g at 5.25 cm. The pore water profiles for Fe, Mn and Co have low concentrations near the sediment-water interface, with values increasing sharply at depth. The aqueous phase profile of Co affirms the presence of the redox boundary at 5 cm. The dissolved data for Fe and Mn also confirm the placement of their respective redox boundaries near the depth of 5 cm that the solid phase data suggests.

Lead-210 dating was completed for the top 10 cm of the core, at 1 cm increments (Figure 21). These data show a hundred-year average accumulation rate of 0.0178 $g/cm^2/yr$, or 0.059 cm/yr.

The XRD data for this core show a general clay lithology of chlorite and montmorillonite with quartz. Grunerite is not present, indicating that this site has not been affected by taconite mining. Given the distance of this site from the taconite mining along the North Shore, the presence of grunerite is not expected.

There is evidence at this site for the input of anthropogenic trace metals. Copper shows a dramatic increase at the sediment-water interface in the solid and aqueous phases (Figures 22-23). In the solid phase, Cu is enriched by approximately 4.5× over background concentrations deeper in the core. This site has an inventory of 1.8 $\mu mole/cm^2$ of anthropogenic Cu (i.e. above the background concentration) in the solid phase. In the aqueous phase,

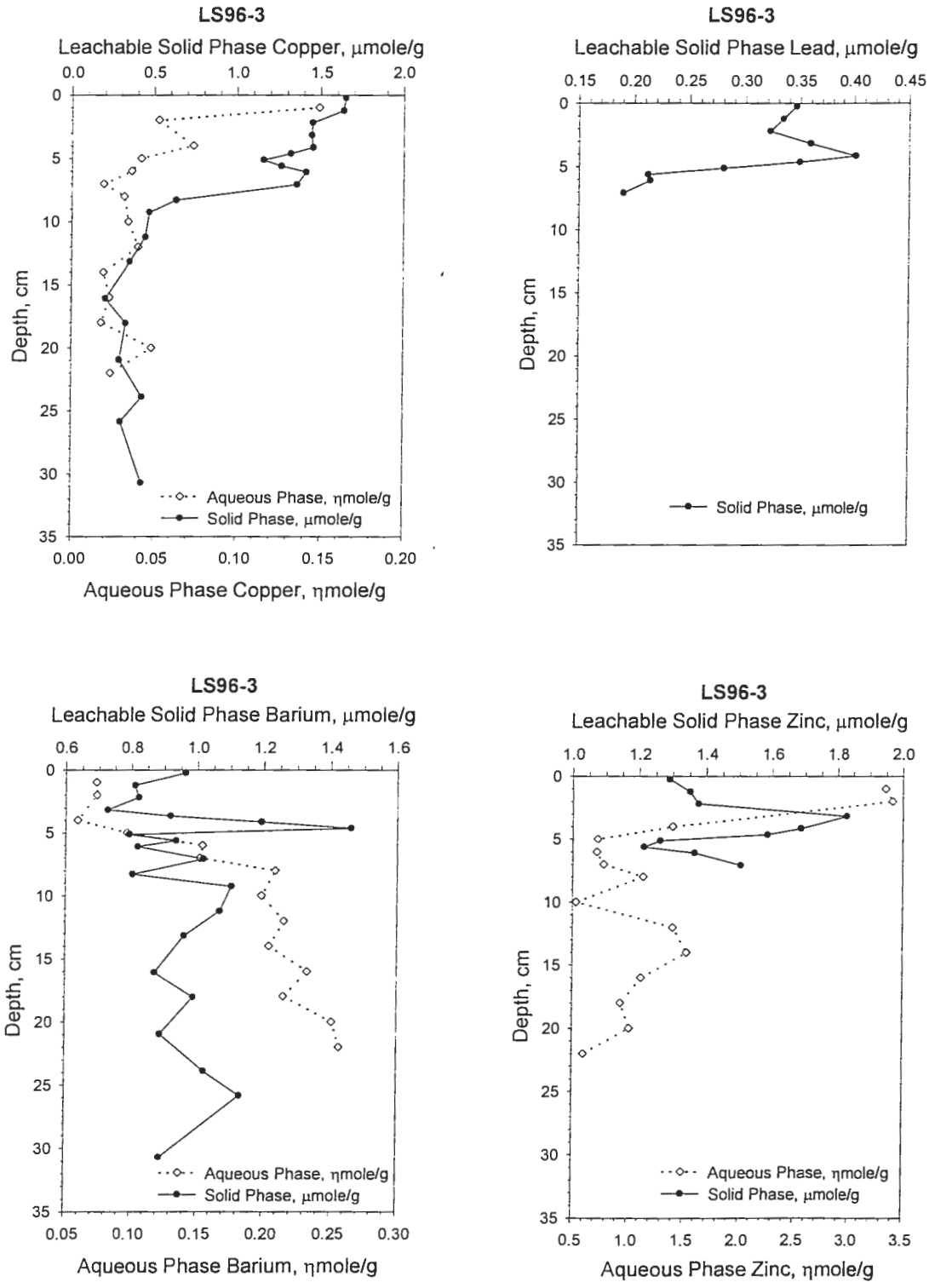

Figures 22-25. Core LS96-3, solid and aqueous phase data for Cu, Pb, Ba, and Zn.

near-surface Cu shows comparable enrichment over the deeper core. Lead profiles are difficult to interpret because the concentrations in the aqueous phase do not show a coherent trend. In the solid phase, Pb has a concentration increase of 2× at the sediment-water interface over that at 7 cm. Data for solid phase Pb is not available below 7 cm in this core, therefore it is possible that the enrichment is more than 2× above the deeper core, given the fact that the solid phase Cu did not decrease significantly until below 9.5 cm. This site has an inventory of 0.40 μmole/cm^2 of anthropogenic Pb in the solid phase.

As is the case in all of the cores, the Ba concentrations follow the Mn profiles in solid and aqueous phases (Figure 24). As Ba does not undergo changes in oxidation state under normal conditions (Oxtoby and Nachtrieb, 1987), its distributions are most likely due to adsorption onto reactive surfaces of Mn oxides.

The profiles of Zn show a solid phase depletion by 30 % at the sediment-water interface (Figure 25). The aqueous phase, however, are enriched by 4.5× over the concentration lower in the core.

4.1b Coring Site LS96-4

Coring site LS96-4 is located near the middle of the western basin of Lake Superior between Ontonagon, MI and Grand Marais, MN in a water depth of 171 m (Figure 2).

Core LS96-4 exhibits profiles of redox chemistry between the solid and aqueous phases that is consistent with steady-state early diagenesis. All three

metals, Fe, Mn and Co, have distinct oxidation and reduction zones, and individual redox boundaries (Figures 26-28). Iron, Mn, and Co show peaks of 1216 μmole/g at 11.25 cm, 546 μmole/g at 10.25, and 4.6 μmole/g at 6.25 cm, respectively. These values are factors of 4, 50 and 11 times the background concentration of Fe, Mn, and Co. The aqueous phase profile for the Fe confirms that the redox boundary lies below 11 cm. The aqueous phase profile for Mn verifies that the redox boundary in located below 10 cm. The aqueous phase profile for Co is difficult to interpret because the concentrations were at or below ICP-MS detection limits (Table 6).

The ^{210}Pb data for this site show an accumulation rate of 0.0113 g/cm^2/yr or 0.0477 cm/yr (Figure 29). The profile has a deviation from simple exponential behavior, between the depths of 4.75 to 5.25 cm. A similar feature is also present at around the same depth in the sediment column of core LS96-6, which is the closest core in proximity to core LS96-4 (Figure 2). Both cores are from the middle of the western arm of the lake and from comparable or mixing water depths, (174 and 211 m). It is possible that these two layers are the result of a single depositional event. The XRD data for this site shows no evidence of grunerite. This is expected due to the distance from taconite mining along the North Shore. The general clay lithology is montmorillonite, chlorite and some illite, and quartz is also present. This site shows effects of anthropogenic activities on both Cu and Pb inventories (Figures 30-31). Both metals are enriched in the solid phase at the surface-water interface. Copper

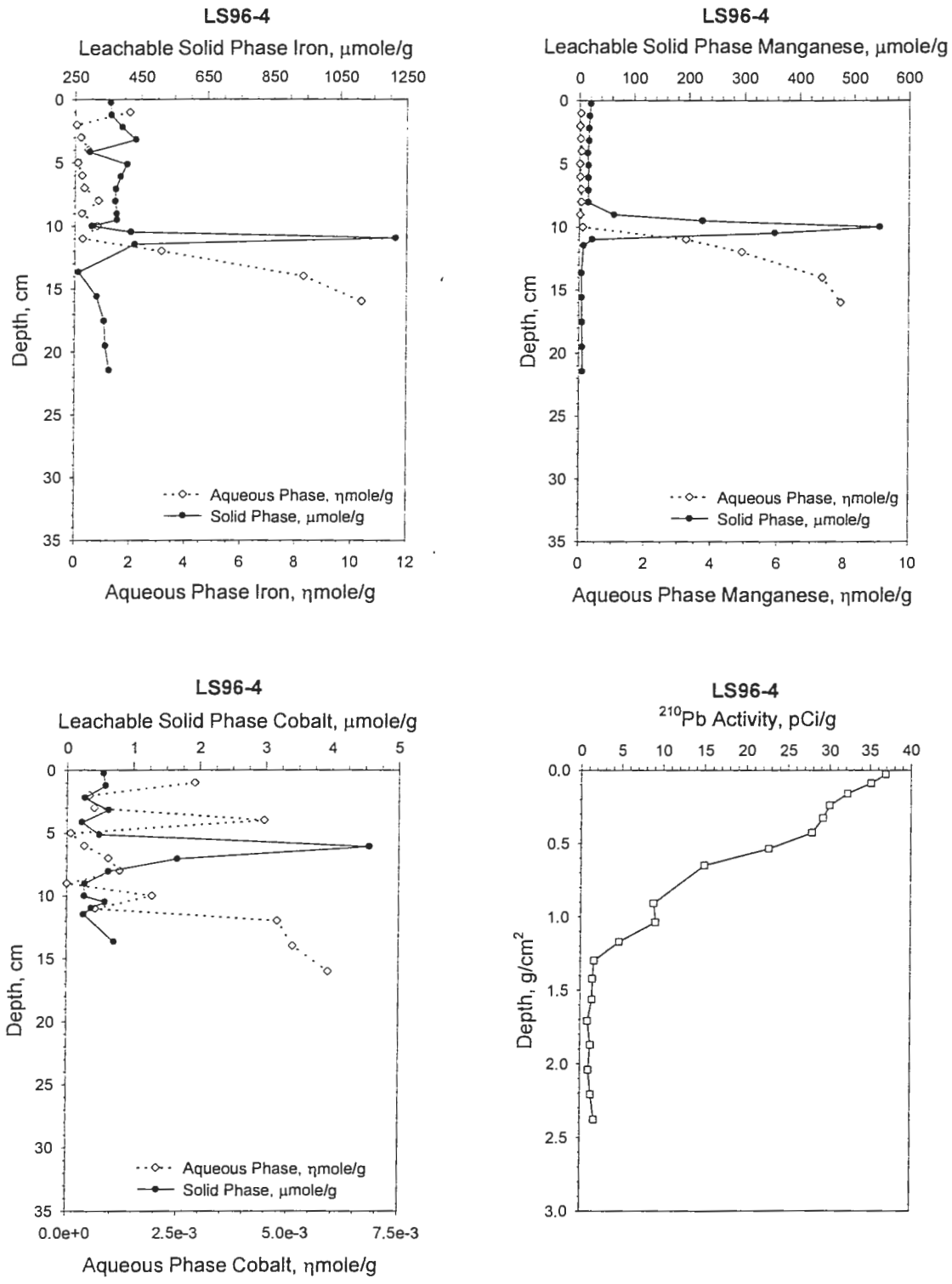

Figures 26-29. Core LS96-4, solid and aqueous phase data for Fe, Mn and Co, and ^{210}Pb.

concentrations are 1.868 μmole/g at 0.25 cm, which is 3.8× the concentration at 14 cm (0.491 μmole/g). This site has an inventory of 1.1 μmole/cm^2 of anthropogenic Cu in the solid phase. The dissolved Cu also show enrichment at the top of the core, being nearly 7× more concentrated than at 16 cm. The Pb concentration at the sediment-water interface is 0.40 μmole/g, which is 10× higher than it is at 14 cm. This site has an inventory of 0.33 μmole/cm^2 of anthropogenic Pb in the solid phase.

Barium profiles are similar to the profiles of Mn (Figure 32).

The Zn aqueous phase is depleted by 80% at the sediment-water interface compared to lower in the core (Figure 33). In the solid phase, Zn is depleted by 40% at the sediment-water interface.

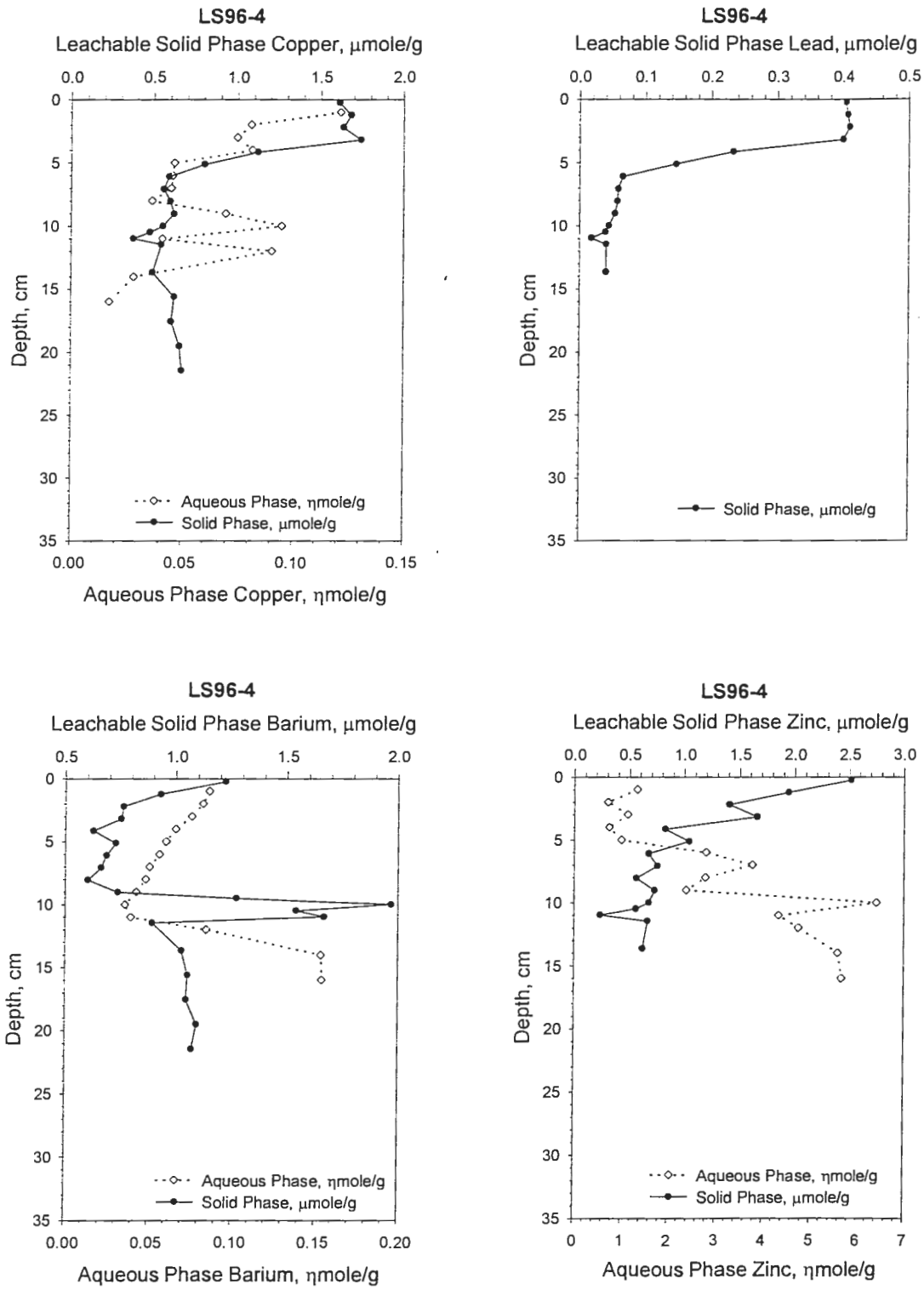

Figures 30-33. Core LS96-4, solid and aqueous phase data for Cu, Pb, Ba, and Zn.

4.1c Coring Site LS96-5

Coring site LS96-5 is located southeast of Two Harbors, MN in 251 m of water (Figure 2).

The redox chemistry at this site is complex (Figures 34-36). Manganese shows two distinct peaks, one of 218 μmole/g at 4.25 cm and one of 131 μmole/g at 10.25 cm. There is evidence of a smaller third peak of 46 μmole/g at 23.5 cm. The solid phase profile for Fe shows more 'noise' in the upper 10 cm of the core. Nevertheless, this core also shows two peaks, one of 629 μmole/g at 4.75 cm and one of 1150 μmole/g at 10.25 cm. Cobalt also has two peaks, one of 1.3 μmole/g at 3.5 cm and one of 1.5 μmole/g at 4.5 cm. The dissolved distributions of Fe and Mn confirm the presence of a redox boundary at the depth of the upper solid phase peaks, around 4 cm. The concentrations of dissolved Fe and Mn are highly variable in the equilibrium zone, which is below 12 cm, suggesting that the system is not in steady-state.

The ^{210}Pb distribution confirms the complex sedimentary history of this site (Figure 37). The ^{210}Pb data show that there has been mixing in the upper 2.25 cm and the layer below it has been mixed down to 9.25 cm. Below 9.25 cm the ^{210}Pb exponentially decays down to the supported background concentration. Due to the amount of mixing in this core it is not possible to calculate a representative accumulation rate.

The XRD data adds another line of evidence that helps clarify the complex sedimentation history of core LS96-5. The XRD shows a general clay lithology

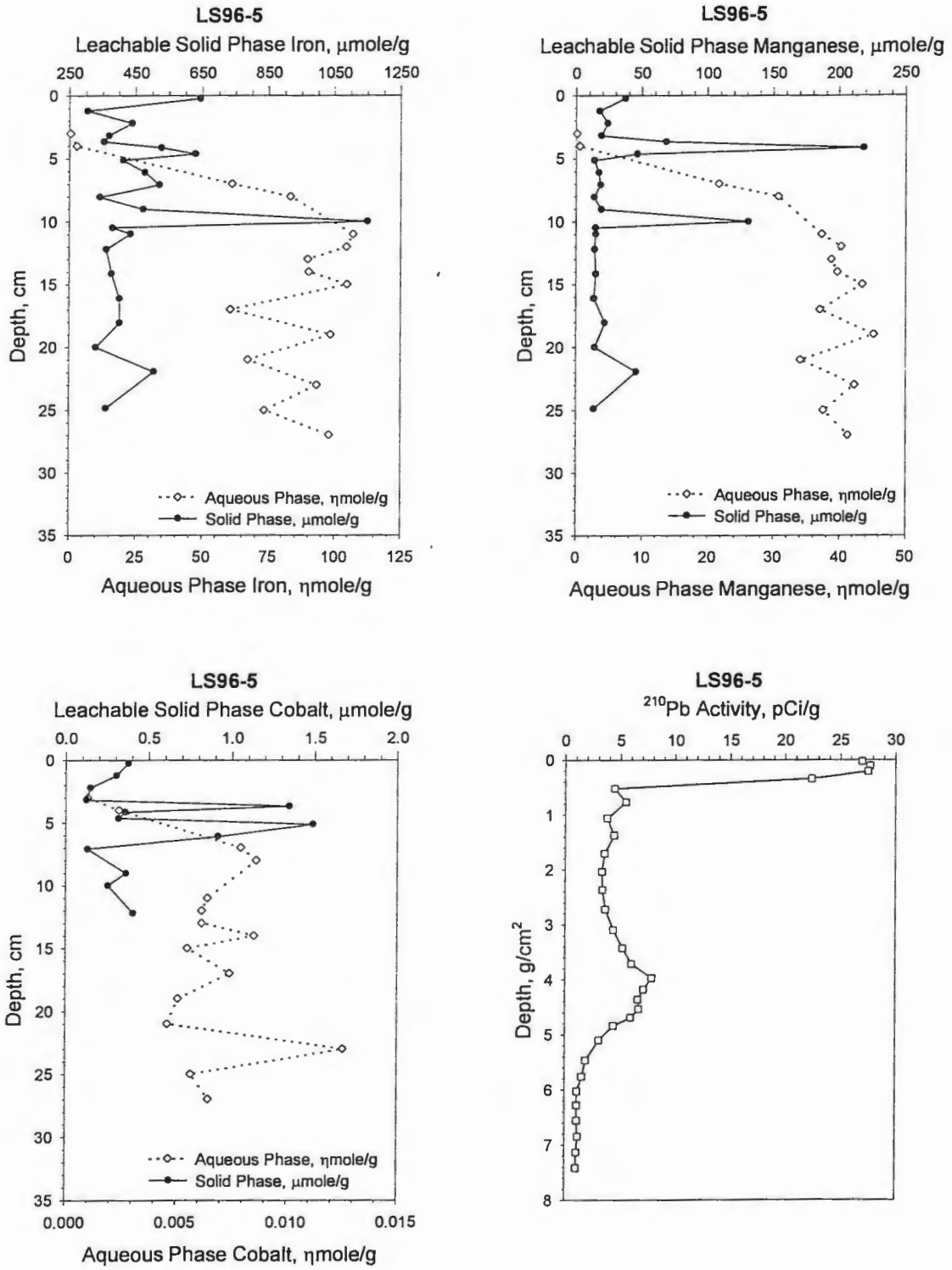

Figures 34-37. Core LS96-5, solid and aqueous phase data for Fe, Mn and Co, and ^{210}Pb.

of chlorite and montmorillonite with additional quartz. There is grunerite present at this site as well, down to a depth of 9 cm indicating that this site has been affected by taconite mining along the North Shore.

The solid phase profile for Cu shows enrichment at the sediment-water interface, with an additional peak at 10.25 cm (Figures 38). The concentration at the sediment-water interface is 6× the background value lower in the core. The peak at 10 cm is 3.5× the background concentration. This site has a solid phase inventory of anthropogenic Cu of 0.66 μmole/cm^2. The aqueous phase data show an increase near the top of the core, at 3 cm, which is the first pore water sample for this core. There does not appear to be any pattern in the rest of core. The solid phase profile for Pb again shows two peaks, one at the sediment-water interface and one at 9.25 cm (Figure 39). The solid phase has an inventory of anthropogenic Pb of 0.24 μmole/cm^2 at this site.

Barium follows the concentration profile of Mn, and becomes erratic below 10 cm (Figure 40). The solid phase peak at 4.75 cm is well defined and the pore water Ba distributions are consistent with a redox boundary at this depth.

The data for solid phase Zn do not show a definite trend. There appears to be a slight enrichment at the sediment-water interface (Figure 41). The aqueous phase data show an increase in the sample closest to the sediment-water interface, but low sample density makes more detailed evaluation difficult.

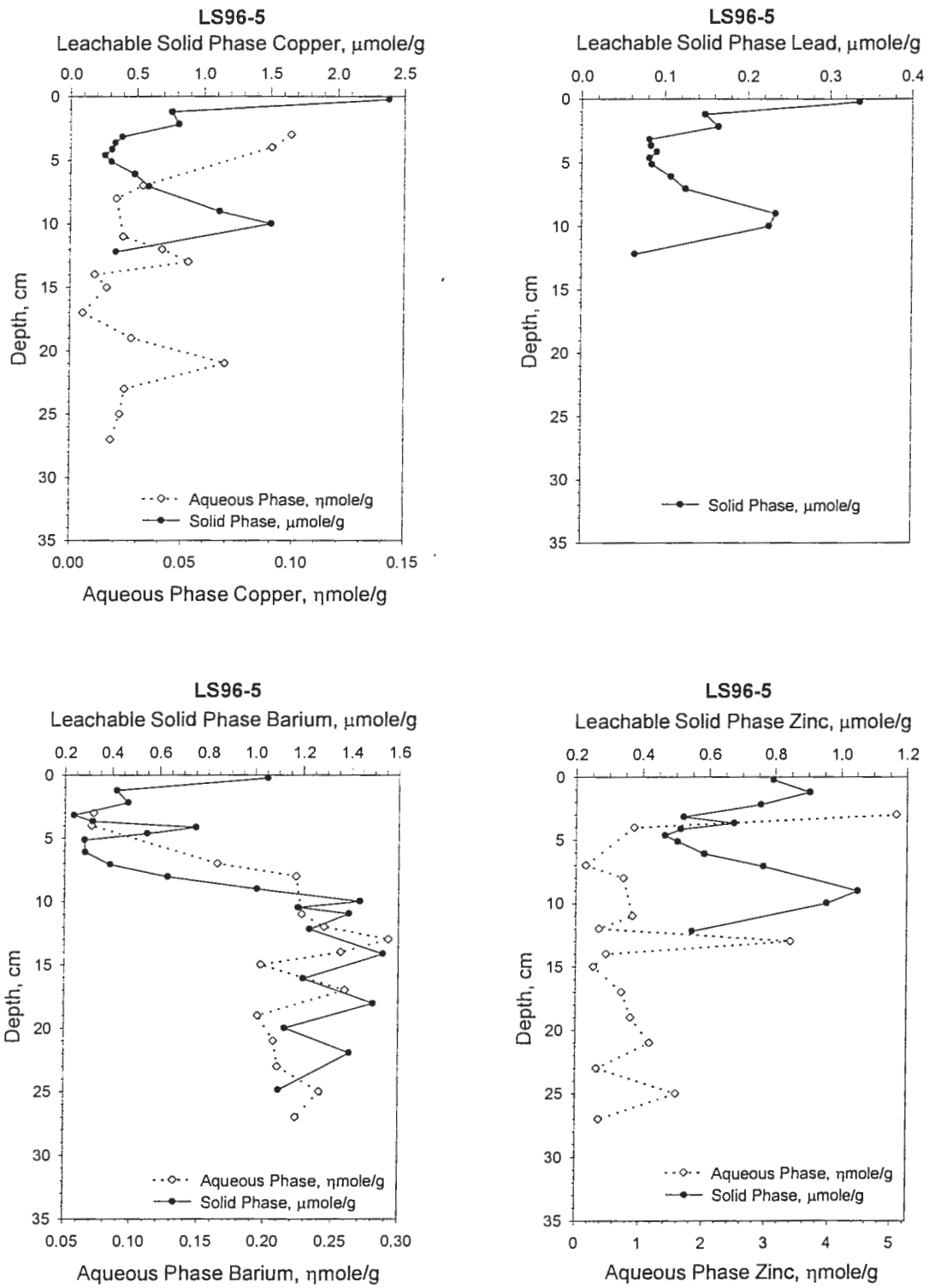

Figures 38-41. Core LS96-5, solid and aqueous phase data for Cu, Pb, Ba, and Zn.

4.1d Coring Site LS96-6

Coring site LS96-6 is located between Ontonagon, MI and Grand Marais, MN in 211 m water (Figure 2).

The redox chemistry at this site shows some deviation from the steady-state early diagenetic distribution of trace metals. As is expected in a steady-state system, the solid phase peaks of Fe, Mn and Co are present in a sequence corresponding to their redox potentials (Figures 42-44). The solid phase peak in Co occurs at 7.25 cm with a value of 3.1 μmole/g. The solid phase Mn peaks at 8.75 cm with a concentration of 211 μmole/g. The Fe peak in the solid phase is present at 9.25 cm with a concentration of 1515 μmole/g. In all 3 redox elements, the pore water data indicate redox boundaries lower in the core than suggested by the solid phase data. The aqueous phase data do not show a rapid increase but rather a gradual increase in concentration at the redox boundary. The mismatch between aqueous phase and solid phase profiles is an indication that this site may not be at steady-state.

The ^{210}Pb data for this core indicate a sedimentation rate of 0.012 $g/cm^2/yr$ or 0.051 cm/yr (Figure 45). This core also shows a deflection from simple exponential decay, similar to one observed in core LS96-4.

The XRD data shows the general clay lithology is chlorite and montmorillonite, with quartz. There is no grunerite present at this site, indicating that there has been no impact of taconite mining at this site.

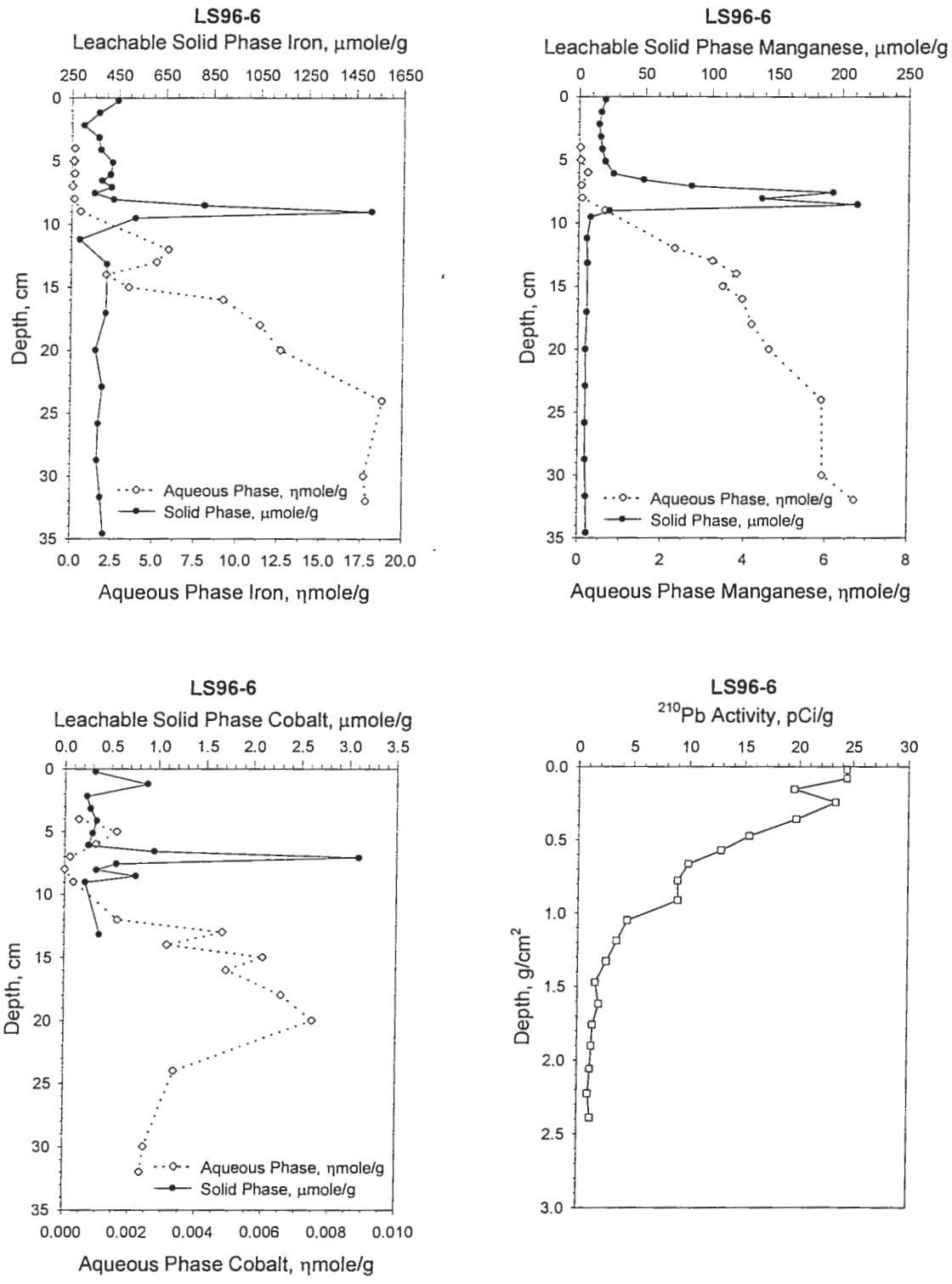

Figures 42-45. Core LS96-6, solid and aqueous phase data for Fe, Mn and Co, and ^{210}Pb.

Copper is enriched at the sediment-water interface by 5× in the solid phase (Figure 46). This site has an inventory of 1.4 μmole/cm^2 of anthropogenic Cu in the solid phase. Dissolved Cu is enriched near the sediment-water interface by 5× but also shows a peak at 14 cm. This second peak is not well understood. It is also present in analyses of Ni and Zn and is not confined to one, possibly contaminated sample; the peak in the Cu is comprised of two points. Lead is enriched at the sediment-water interface by 8× in the solid phase (Figure 47). The inventory of solid phase anthropogenic Pb at this site is 0.29 μmole/cm^2.

Barium concentration in the core follows the profiles of Mn in the solid phase, but deviates from the aqueous phase profiles (Figure 48). Barium shows a solid phase peak at 10 cm, which corresponds to the one for Mn. In the aqueous phase, Ba shows a peak at the same depth, 14 cm, that dissolved Cu shows a peak. The dissolved Mn at 14 cm shows a decrease in concentration. This feature, in addition to the others found in the aqueous phase of the different elements, show that this core is not in steady-state.

Solid phase Zn is depleted at the sediment-water interface by 60 % (Figure 49). The aqueous phase data shows two peaks, one at 6 cm and one at 14 cm, which correspond to the aqueous phase peaks in Cu and Ba.

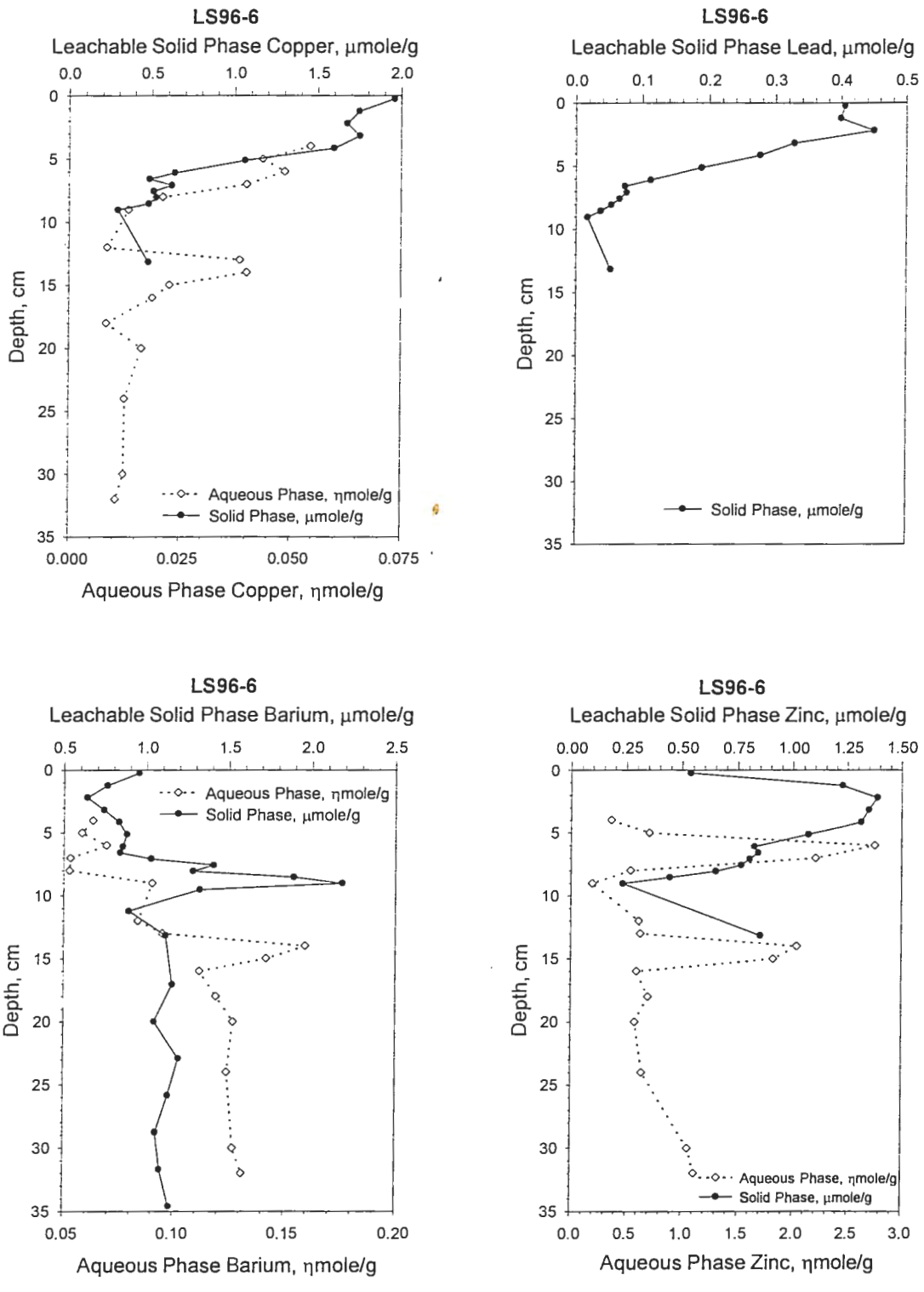

Figures 46-49. Core LS96-6, solid and aqueous phase data for Cu, Pb, Ba, and Zn.

4.2 Other Sites

The other coring sites in this study, cores LS96-1, 2 and 7, had fewer analyses run on them for a number of reasons. Core LS96-1 was discounted due to the fact that it was the first core collected in the study and there may have been problems in the collection. Core LS96-2 had no associated pore waters to analyze, therefore the information available to explain redox chemistry was limited. Core LS96-7 had a low collection of pore waters, and also showed significant variability among the four sub-cores, consequently this site fell out of line with the central topic of this thesis.

4.2a Coring Site LS96-1

Coring site LS96-1 is located between Silver Bay and Little Marais, MN in 191 m of water (Figure 2).

The redox boundaries in both Mn and Fe are well defined in this core (Figures 50-51). The Fe solid phase peak occurs at 14.25 cm with a concentration of 1300 μmole/g which is 4× the background value. The Mn solid phase peak occurs at 8.25 cm with a concentration of 270 μmole/g which is 10× the background concentration. The aqueous phase data for Mn confuse the matter, since it indicates that redox boundary might be higher in the sediment column. The increase in the aqueous phase occurs between 5 and 6 cm. The Fe aqueous phase data indicate that the redox boundary might be higher in the sediment column than the solid phase show. Another feature that suggests that

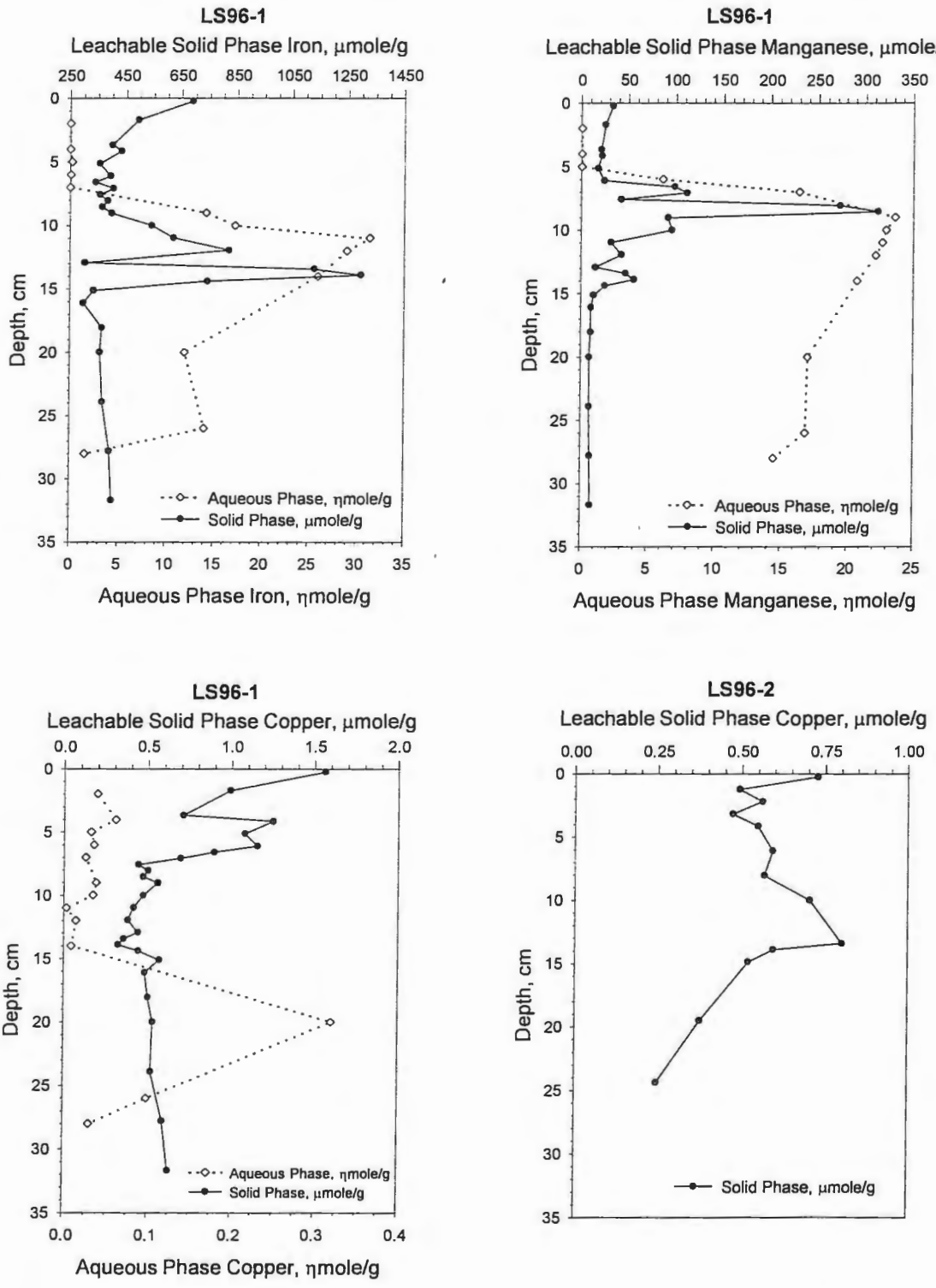

Figures 50-53. Cores LS96-1 and 2, solid and aqueous phase data for Fe, Mn and Cu.

this site is not in steady-state is the concentration of dissolved Fe increases from 9 to 11 cm, but then decreases deeper in the core.

XRD data for this core show a general clay lithology of chlorite and montmorillonite with quartz present. There is also grunerite found in this core down to a depth of 4.5 ± 0.25 cm. This indicates a possible sedimentation rate of 0.085 cm/yr, assuming 1.75 cm of bioturbation and 41 years since mining began.

The solid phase Cu shows an enrichment of 4× at the sediment-water interface (Figure 52). The concentrations remain high down to 7.25 cm in the core. The solid phase anthropogenic Cu inventory at this site is 0.96 μmole/cm^2. There is no Pb solid phase data. Copper aqueous phase data are difficult to interpret.

4.2b Coring Site LS96-2

Coring site LS96-2 is located between Duluth and Two Harbors, off the Knife River, in 143 m of water (Figure 2).

The XRD data for this site show a general lithology of chlorite, and montmorillonite with quartz present. There is also grunerite present at this site down to a depth of 6.00 ± 0.25 cm. This suggests a sedimentation rate of approximately 0.098 cm/yr, assuming 1.75 cm of bioturbation and 41 years since mining began.

Copper shows an enrichment of 3× at the sediment-water interface in the solid phase (Figure 53). The inventory of solid phase anthropogenic Cu at this

site is 1.1 μmole/cm^2. The profile of Cu suggests a high sedimentation rate, of the magnitude calculated by the grunerite data. Calculating a sedimentation rate from the Cu data, assuming mining started in force around 1895, with 2 cm of bioturbation gives a value of 0.098 cm/yr. This is in good agreement with the other estimate of sedimentation rate at this site.

4.2c Coring Site LS96-7

Coring site LS96-7 is located outside of Bayfield, WI in 94 m of water (Figure 2). This was the only site that showed variation between the sub-cores, demonstrating that it is unlikely to be at steady-state. The 3 cores acquired are different in make-up and appearance. The tops of all of the cores look the same, but at the bottom there is a bright orange, Fe rich mass that is 2 cm high in one core, 4 cm in another and absent in the third.

The redox chemistry for this site is sketchy because of the low sample density of pore water data (Figures 54-55). The Fe solid phase has a peak at 13.75 cm of 1500 μmole/g, which is approximately 7.5× the background value. But there is another peak around 36.5 cm that is 550 μmole/g in intensity, which is evidence of the orange material at the bottom of the core. The dissolved Fe data do not correspond with either of the two peaks. The increase in concentration around 28 cm into the core. This is also the furthest extent of the pore water data, so it is unknown what occurs in the aqueous phase at the lower solid phase peak. The solid phase Mn also exhibits two peaks, one peak at 12.25 cm of 230 μmole/g, which is ~20× that of the background value, and the

second, with an increase to 140 μmole/g at 36.5 cm. The Mn aqueous phase data indicate that the uppermost peak is the redox boundary.

Copper shows an enrichment of 5× at the sediment-water interface in the solid phase (Figure 56). The inventory of solid phase anthropogenic Cu at this site is 0.80 μmole/cm^2. The initial increase in Cu concentration can also be used to calculate a rough sedimentation rate. Doing so gives a sedimentation rate of 0.016 g/cm^2/yr, or 0.048 cm/yr.

There were no XRD or ^{210}Pb analyses done on these cores.

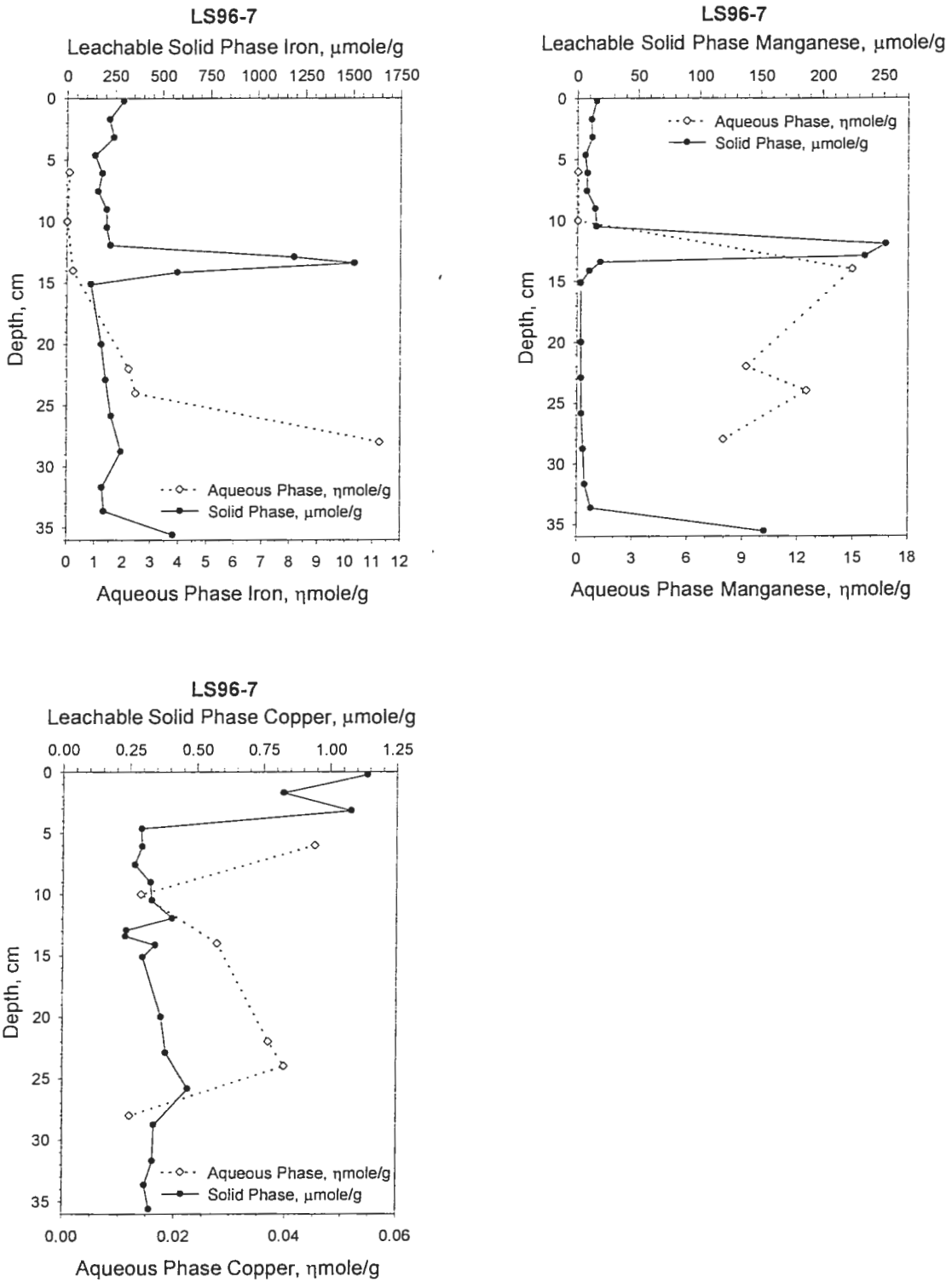

Figures 54-56. Core LS96-7, solid and aqueous phase data for Fe, Mn and Cu.

5. DISCUSSION

5.1 ANTHROPOGENIC SOURCES

Data from solid and aqueous phase analyses, in addition to ^{210}Pb geochronologies, were used to examine the history of deposition and distributions of Cu and Pb in Lake Superior.

5.1a Anthropogenic Copper

Copper mining began in the Keweenaw Peninsula in 1850. Between 1850 and 1968 at least a half billion tons of copper mine tailings, in the form of stamp sands, were dumped along shorelines and into connecting waterways. The mining peaked between 1890 and 1930 and ceased in 1968 (Kerfoot et al., 1994). There were two stamp mills that discharged material into Lake Superior, Freda/Redridge and Gay, which produced 45.5 and 22.6 million metric tons, respectively. The Freda/Redridge mill, which operated between 1895 and 1922, should have a more significant effect on the area of study in this thesis because it is on the western side of the Keweenaw Peninsula. The Gay mill discharged stamp sand into the eastern side of the Keweenaw Peninsula.

This study compares the historic production of stamp sands in the Keweenaw Peninsula, which should be correlated to levels of Cu introduced into the lake, to the Cu distribution found in ^{210}Pb-dated Lake Superior sediments of three cores (Figure 57). The results from core LS96-6 show a clear relationship

between the increase in Cu in the core, from 1860 to 1925, and the increase in stamp sand production. The sedimentary Cu concentrations remain high well after 1925. Core LS96-4 shows a trend of increasing concentration, from 1920 to 1960, that lags behind that of core LS96-6. This might be explained by the greater distance from the Keweenaw to core LS96-4 or some inconsistencies in the core chronologies at the two sites. Core LS96-3 shows an increase in Cu concentration from 1880 to 1900, followed by a slight decrease that could correspond to a decrease in production. In all of the cores, Cu concentrations remain high in sediments deposited well after Cu production ceased in the Keweenaw. However, since mine tailings are still present along the shores of Lake Superior, it is likely that Cu rich particles are being resuspended and transported into lake sediments.

The inventory of Cu was calculated at each site as an excess above natural background value, in $\mu mole/cm^2$. A map of Lake Superior displaying Cu inventories at each site (Figure 58) shows a general trend of decreasing concentrations with distance from the Keweenaw, considering the general counter-clockwise circulation pattern of this part of the lake.

5.1b Anthropogenic Lead

The dominant source of anthropogenic Pb to lake sediments is believed to be from the atmosphere. Lead has a short residence time in the water column of the Great Lakes and is quickly transported to lake sediments through particulate scavenging processes. Therefore, the sources of anthropogenic Pb added to

lake sediments should have a close relation in time and quantity to atmospheric emissions of Pb (Graney et al., 1995). The major sources of emissions are from gasoline, ore smelting, coal, and wood. Atmospheric emissions peaked between 1970 and 1975 with the majority accounted for by leaded gasoline and primary metal/steel production.

Comparison of anthropogenic Pb emissions for the entire U.S., to the Pb distributions in three ^{210}Pb-dated Lake Superior cores (Figure 59), shows a strong relationship between emission and deposition. The results for cores LS96-3 and 6 show a strong relation with the timing of the increase and subsequent decrease of Pb emissions. Core LS96-4 shows the increase to higher concentrations, but does not show the post-1970 decrease associated with lowered Pb emissions. It appears that the sampling density in core LS96-4 was too low to resolve the peak in Pb concentration. In all cases, the concentration of Pb in the sediments does not decrease as dramatically as the decrease in emissions, which can be explained by bioturbation recycling the Pb in the surficial sediments.

The inventory of Pb was calculated at each site as an excess above natural background value, in μmole/cm^2. A map of Lake Superior displaying Pb inventories at each site (Figure 60) shows that they are fairly uniform around the basin, averaging 0.35 μmole/cm^2.

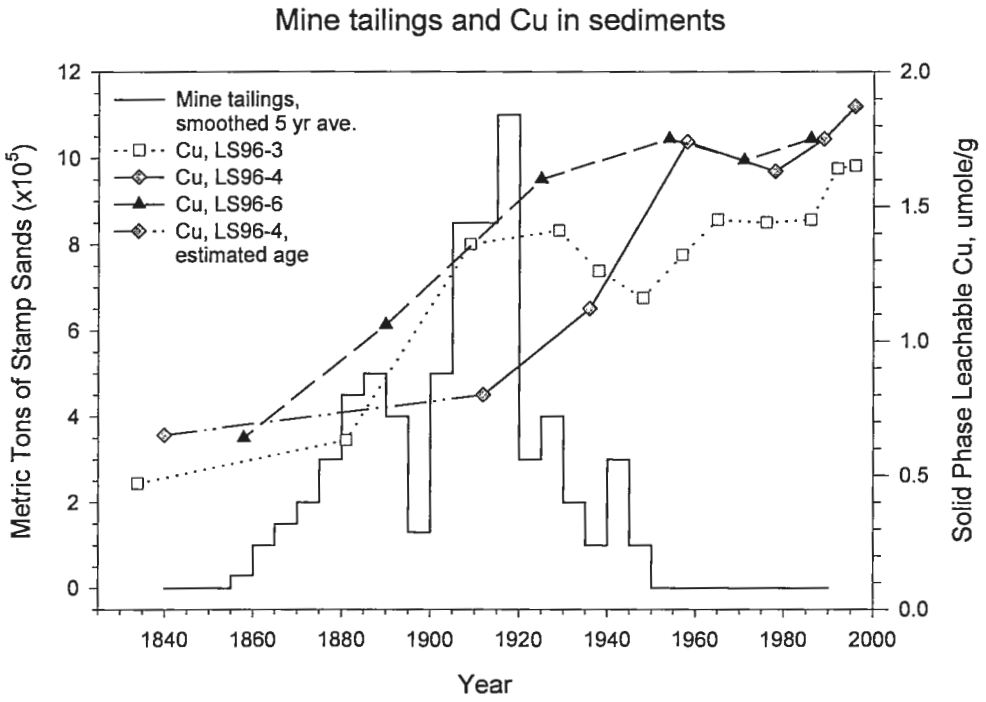

Figure 57. Mine tailings production with Cu inventory of sediments.

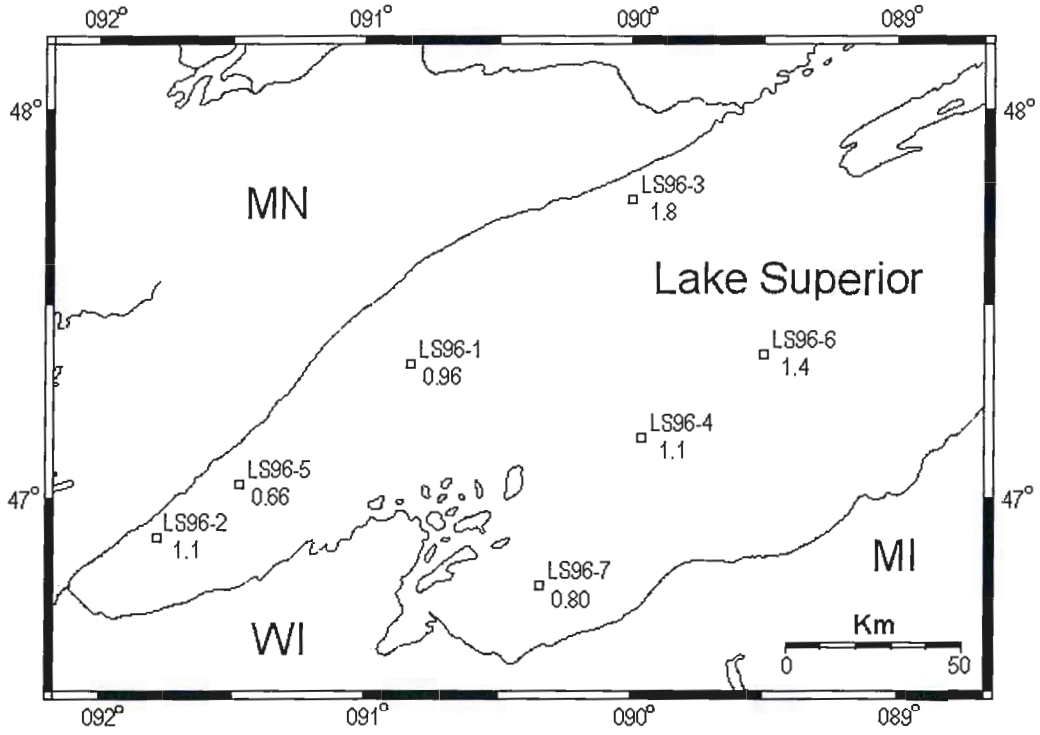

Figure 58. Map of Lake Superior showing relative Cu inventory by site (μmoles/cm^2).

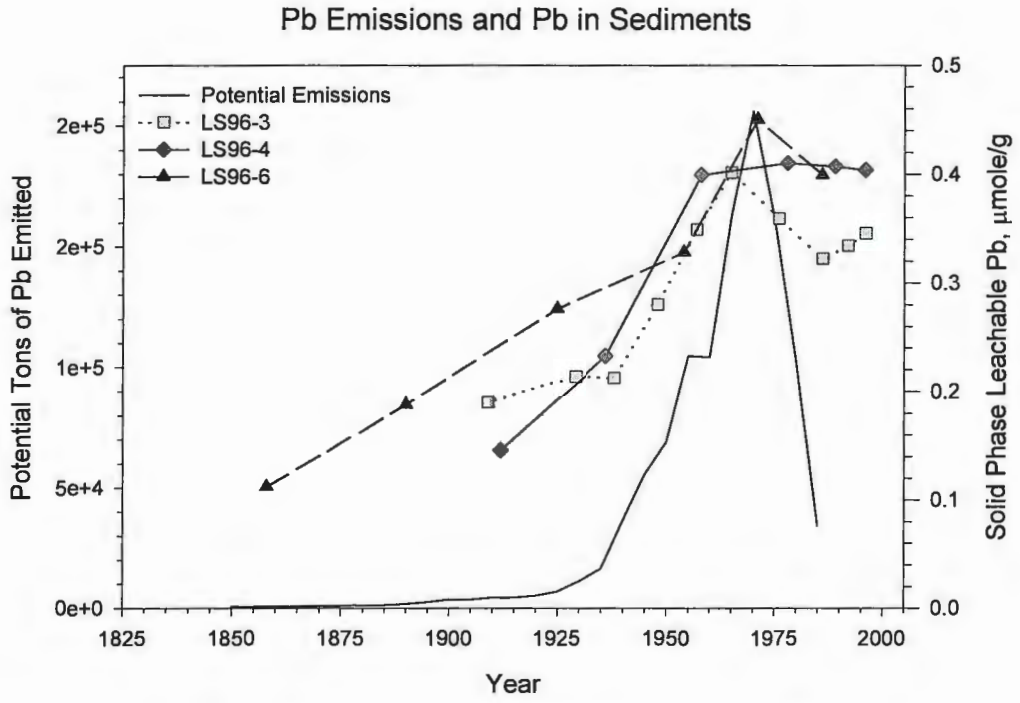

Figure 59. Atmospheric Pb emissions with Pb inventory in sediments.

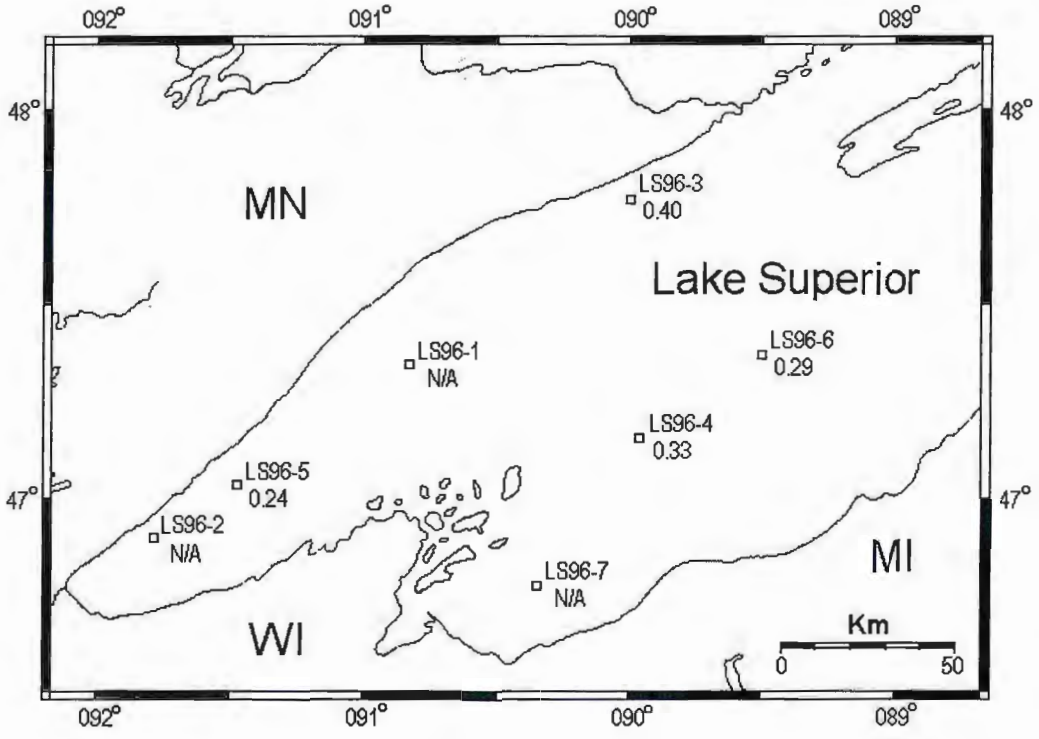

Figure 60. Map of Lake Superior showing relative Pb inventory by site (µmole/cm^2).

5.2 Sedimentation Rates

Sedimentation rates were calculated using three different methods: ^{210}Pb geochronology; the appearance of taconite tailings, which were disposed of in the lake from 1956 until 1978; and first appearance of Cu enrichment in the sediments, assumed to represent sediments deposited in 1897.

Sedimentation rates based on the first appearances of Cu and taconite tailings were calculated for cores LS96-1, 3, 4, 6, and 7 and for cores LS96-1 and 2, respectively (Table 9). The Cu-based sedimentation rates correspond well with those based on ^{210}Pb, in cores LS96-3, 4, and 6 (Tables 8 and 9). These sedimentation rates are comparable to previously published ^{210}Pb-based rates for Lake Superior (Figure 61).

The sedimentation rates provided by ^{210}Pb-based dating indicate that sedimentation rate has steadily increased over the past one hundred years (Figures 62-64). This may be associated with a change in land-use as human activities (lumbering and agriculture) introduced larger amounts of sediment into the lake.

Table 8. Results of ^{210}Pb analyses for cores LS96-3, 4 and 6.

Site	100 Year Ave. Sedimentation		Sedimentation range	
	($g/cm^2/yr$)	(cm/yr)	($g/cm^2/yr$)	(cm/yr)
LS96-3	0.0176	0.0594	0.011 *to* 0.025	0.041 *to* 0.088
LS96-4	0.0113	0.0477	0.005 *to* 0.018	0.018 *to* 0.091
LS96-6	0.0132	0.0462	0.005 *to* 0.021	0.026 *to* 0.084

Table 9. Results of sedimentation calculations of Cu and taconite.

Site	Sed rate using Cu		Sed rate using taconite	
	($g/cm^2/yr$)	(cm/yr)	($g/cm^2/yr$)	(cm/yr)
LS96-1	0.014	0.06	0.016	0.07
LS96-2	N/A	N/A	0.034	0.10
LS96-3	0.015	0.07	N/A	N/A
LS96-4	0.009	0.04	N/A	N/A
LS96-6	0.011	0.05	N/A	N/A
LS96-7	0.010	0.03	N/A	N/A

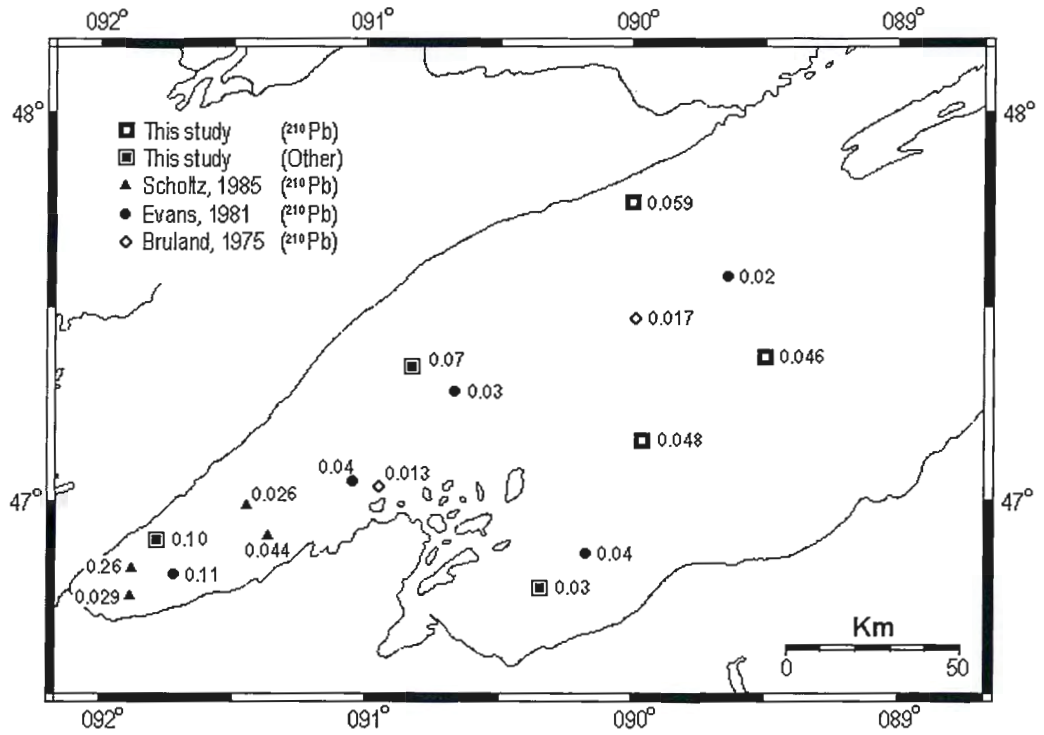

Figure 61. Map of Lake Superior sedimentation rates (cm/yr) of this study and others.

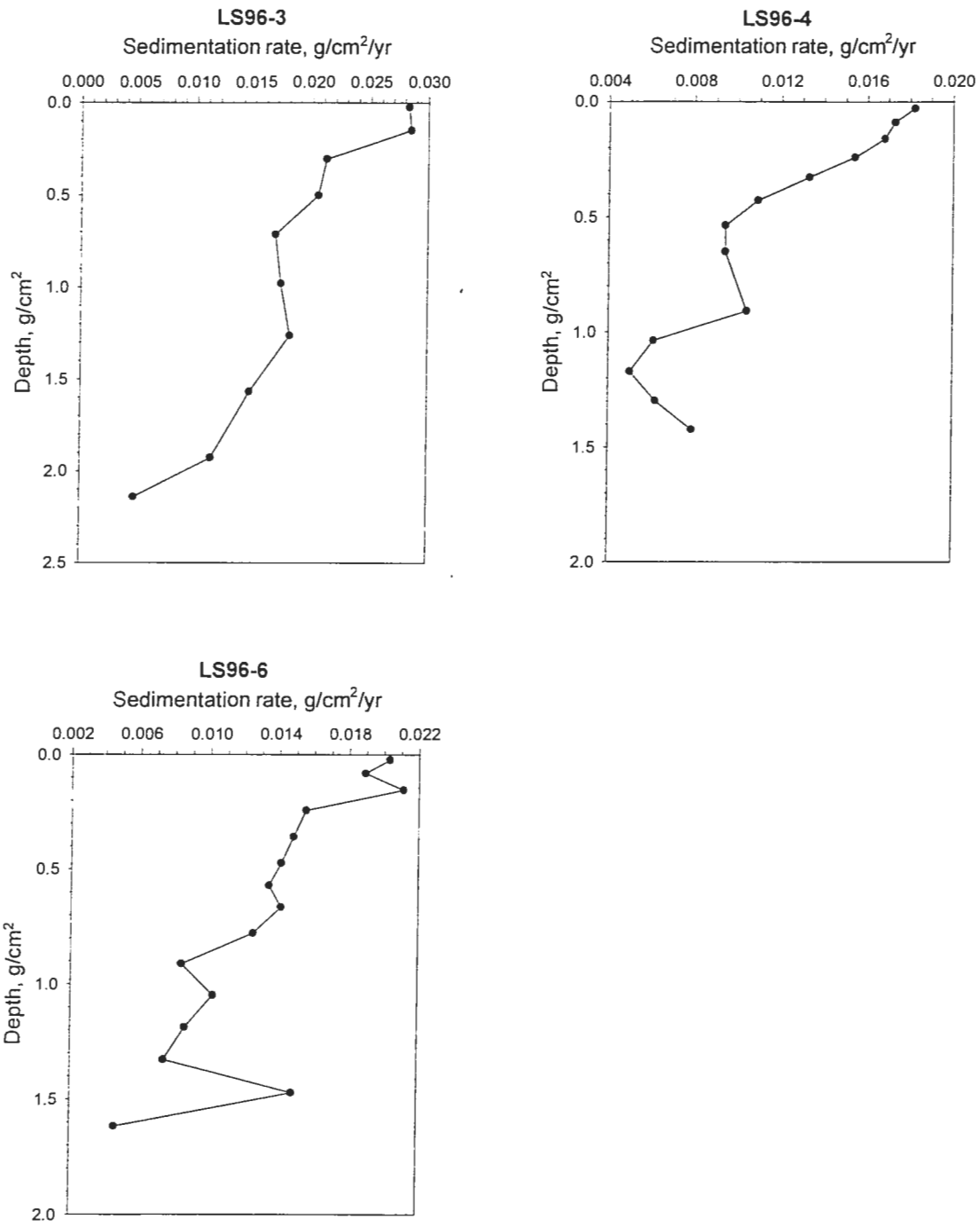

Figures 62-64. Sedimentation rate vs. depth, cores LS96-3, 4, and 6.

5.3 Diagenetic Modeling

5.3a Derivation of diagenetic equations

This study compares the data for solid and aqueous phase Fe, Mn and Co with the results of a mathematical model based on that of Burdige and Gieskes (1983). Burdige and Gieskes presented a model for steady-state Mn diagenesis that accounts for changes in both pore waters and solids due to advection, diffusion, and redox reactions. The reaction rates obtained from this modeling procedure, when combined with appropriate laboratory data on the mechanisms of these reactions and/or other measured quantities, should lead to a better understanding of the dynamics of Fe and Mn redox reactions (Burdige and Gieskes, 1983).

In order to use the model, the following parameters are required from each core: sedimentation rate in cm/yr.; average porosity of the oxidation and reduction zones; the depth of the upper boundary of the oxidizing zone; the depth of the redox boundary; and the concentration of the element in the solid phase in the oxidized zone. The sedimentation rate is calculated by ^{210}Pb geochronology, the porosity by LOI, the top of the oxidizing zone by the pore water data and the redox boundary and initial concentration by the sediment leach analyses.

The model only considers the oxidation and reduction zones (Figure 1). The concentrations of solid and aqueous phase species are held constant in the

oxidized and equilibrium zones. The model also assumes that: steady-state diagenesis is occurring; migration of dissolved species occurs only by molecular diffusion following Fick's Law; porosity and diffusion coefficients are constant over the depth range considered; and the sedimentation rate and the supply of reducible trace metal to the sediment are constant.

Equations 10 and 11 balance the input of dissolved Mn to the oxidation zone by advection and diffusion (Equation 10) with the removal (precipitation) by oxidation (Equation 11). Equations 12 and 13 are the counterparts to Equations 10 and 11 for the reduction zone.

The equations describing steady-state diagenesis in the oxidation and the reduction zones are:

For the oxidation zone ($L1 \leq z \leq L2$) pore waters,

$$D_b \frac{\partial^2 C_p^{ox}}{\partial z^2} - w \frac{\partial C_p^{ox}}{\partial z} - k_{ox} C_p^{ox} = 0 \qquad (10)$$

For the oxidation zone sediments,

$$-w \frac{\partial C_s^{ox}}{\partial z} + \frac{\phi}{1-\phi} k_{ox} C_p^{ox} = 0 \qquad (11)$$

For the reduction zone ($L2 \leq z \leq L3$) pore waters,

$$D_b \frac{\partial^2 C_p^{red}}{\partial z^2} - w \frac{\partial C_p^{red}}{\partial z} + \frac{1-\phi}{\phi} k_{red} C_s^{red} = 0 \qquad (12)$$

For the reduction zone sediments,

$$-w \frac{\partial C_s^{red}}{\partial z} - k_{red} C_s^{red} = 0 \qquad (13)$$

where

D_b = bulk sediment diffusion coefficient (cm^2/yr)

C_p = Concentration of element in pore water (μmole/g)

C_s = Concentration of element in solid phase (μmole/g)

$C_s°$ = Concentration of element at z = 0 (μmole/g)

w = sedimentation rate (cm/yr)

k_{ox} = 1st order rate constant for oxidation (yr^{-1})

k_{red} = 1st order rate constant for reduction (yr^{-1})

ϕ = porosity

z = depth (cm)

The superscripts *ox* and *red* refer to concentrations in the oxidation and the reduction zones, respectively. The bulk sediment diffusion coefficient, D_b, is calculated from Lerman (1975) using the equation:

$$D_b = D° * \phi^2 \qquad (14)$$

where D° is calculated from Li and Gregory (1974) by assuming the temperature of the sediment is 4 °C and that D versus T is linear between 0 °C and 18 °C, the value for D° can be interpolated for 4 °C. The values used for D° are:

1. Mn^{+2}, D° = 3.5×10^{-6} cm^2/sec = 115.2 cm^2/yr
2. Fe^{+2}, D° = 3.95×10^{-6} cm^2/sec = 124.5 cm^2/yr
3. Co^{+2}, D ° = 3.92×10^{-6} cm^2/sec = 123.8 cm^2/yr

The boundary conditions used to solve the equations describing steady-state diagenesis for this model, as described in Burdige and Gieskes, are:

1. $C_p^{ox}(L1) = 0$
2. $C_s^{ox}(L1) = C_s°$
3. Continuity of concentrations at the redox boundary. This implies that

   $C_p^{ox}(L2) = C_p^{red}(L2)$

   $C_s^{ox}(L2) = C_s^{red}(L2)$

4. Continuity of fluxes across the redox boundary. For the solids, this is equivalent to the previous equation. For pore waters, assuming ϕ, w and D_b are constant with depth, the boundary condition is

$$\left(\frac{\partial C_p^{ox}}{\partial z}\right)_{L2} = \left(\frac{\partial C_p^{red}}{\partial z}\right)_{L2}$$

5. As $z \rightarrow \infty$, C_p remains finite.

With these boundary conditions, the solutions to equations 10 to 13 are:

$$C_p^{ox} = A\sinh(\alpha(z-L1)) \quad (15)$$

$$C_p^{red} = G - \frac{1-\phi}{\phi}\frac{Ew^2}{k_{red}D_b}e^{-\beta(z-L2)} \quad (16)$$

$$C_s^{ox} = C_s^{\circ}\cosh(\alpha(z-L1)) \quad (17)$$

$$C_s^{red} = Ee^{-\beta(z-L2)} \quad (18)$$

where

$$\alpha = \sqrt{k_{ox}/D_b} \quad (19)$$

$$\beta = k_{red}/w \quad (20)$$

$$L_{ox} = L2 - L1 \quad (21)$$

$$A = \frac{C_s^{\circ}(1-\phi)w}{\phi\alpha D_b} \quad (22)$$

$$E = C_s^{\circ}\cosh\alpha L_{ox} \quad (23)$$

$$G = A(\sinh\alpha L_{ox} + \alpha/\beta\cosh\alpha L_{ox}) \quad (24)$$

5.3b Application of the model

This model was applied to cores LS96-3, and 4, which were studied most extensively and have all of the necessary information available. Data from cores from two other sites, LS96-5 and 6, indicate that the sediments are not undergoing steady-state diagenesis and therefore are beyond the scope of the

model. In addition to the current redox boundary, core LS96-5 shows a second and possibly third peak of Mn and Fe, a feature which is less distinct for Co. It is hypothesized that this is the result of a depositional event which buried the redox boundary. The lower Fe and Mn peaks are relict features which are slowly being reduced and redeposited at the current redox boundary. This site is, therefore, not in steady-state. Core LS96-6 has an unusual set of anomalies that occur in the aqueous phase. In addition to the pore water enrichment of Cu, Ni and Zn near the sediment-water interface there is another peak for all of those elements that occurs around 15 cm. Therefore, core LS96-6 does not appear to be in steady-state.

Some data normalizations are required when applying the model. The first normalization removes the background concentration of the elements. The model requires that the solid phase concentration goes to zero below the redox boundary; this is not always the case with this data set. It appears that the sediment leaching procedure also dissolves some matrix-bound trace metals that would not be available to diagenetic reactions. This raises the solid phase concentration below the redox boundary, causing the model to predict spuriously high pore water concentrations. In order to fit the diagenetic model to this data it is necessary to subtract out the background concentration. This was accomplished by subtracting the average concentration below the redox boundary.

Another variation from the approach of BG is the method by which C_s° is

calculated. In the BG model $C_s°$ is the concentration of the element at the sediment-water interface. In this study the average concentration of the element in the oxidized zone was used. There are some cases in these cores where the concentration at the sediment-water interface is elevated, and therefore not representative of the oxidized zone. This normalization has the effect of lowering the concentration of pore water below the redox boundary predicted by the model.

The model was fit by least squares of the predicted and real data to the solid phase profiles by changing the k_{ox} and k_{red} variables. Fitting to the solid phase data provided better results than fitting to the aqueous phase data. When fitted to the aqueous phase data, the peak in the solid phase decreases dramatically and often disappears. The results and variables used in the calculations are listed in Table10.

Table 10. Variables and results of diagenetic model.

Parameter	LS96-3, Mn	LS96-4, Mn	LS96-3, Fe	LS96-4, Fe	LS96-3, Co
D_b (cm^2/yr)	95.5	79.4	105.6	89.5	106.4
w (cm/yr)	0.0594	0.0477	0.0594	0.0477	0.0594
ϕ	0.93	0.848	0.921	0.848	0.927
$C_s°$ (μmole/g)	12.02	7.58	51	37.1	0.15
L_{ox} (cm)	1.63	0.99	0.63	0.25	1.12
Ave. subtracted (μmole/g)	11.44	8.21	391	342.1	0.33
k_{ox} (yr^{-1})	345	2019	2254	21270	968
k_{red}(yr^{-1})	0.45	0.081	0.069	0.22	0.69

5.3c Coring Site LS96-3

This site provided the most successful application of the BG model (Figures 65-67). The model accurately predicted solid and aqueous phase distributions of Fe, Mn and Co that were close to the real data. The parameters and resulting constants are listed in Table 10. This showed that the redox sensitive elements at this site, Fe, Mn and Co, are undergoing early diagenetic redistribution and are close to steady-state equilibrium.

The model worked well, predicting reasonable redox kinetics. The rate constants that are reported in other studies, both those that were calculated from laboratory experiments and those fit to real data, cover a wide range (Burdige and Gieskes, 1983). The rate constants for Fe and Mn in core LS96-3 are reasonable when compared to other reported values.

5.3d Coring Site LS96-4

Applying the model to this site was less successful than for core LS96-3 (Figures 68-69). Core LS96-4 appears to be an example of solid phase Fe and Mn have been accumulating undisturbed for a long time. As a result, the solid phase peaks are many times higher in core LS96-4 than LS96-3, and the pore water concentrations are lower. The oxidation and reduction constants, therefore, have to be an order of magnitude higher in core LS96-4 over core LS96-3. Iron and Mn were predicted with moderate success. The Mn model was fit to the solid phase peak, which yielded much higher aqueous phase concentrations than are present in the data, by as much as an order of

magnitude. The resulting shape of the predicted curve matches that of the real data, but cannot be fit any closer. The model was applied in the same way to the Fe data. The solid phase data was fit, leaving the pore water data to compare the fit of the model. The aqueous phase data fit better than the Mn, being no more than 7× off of the real data.

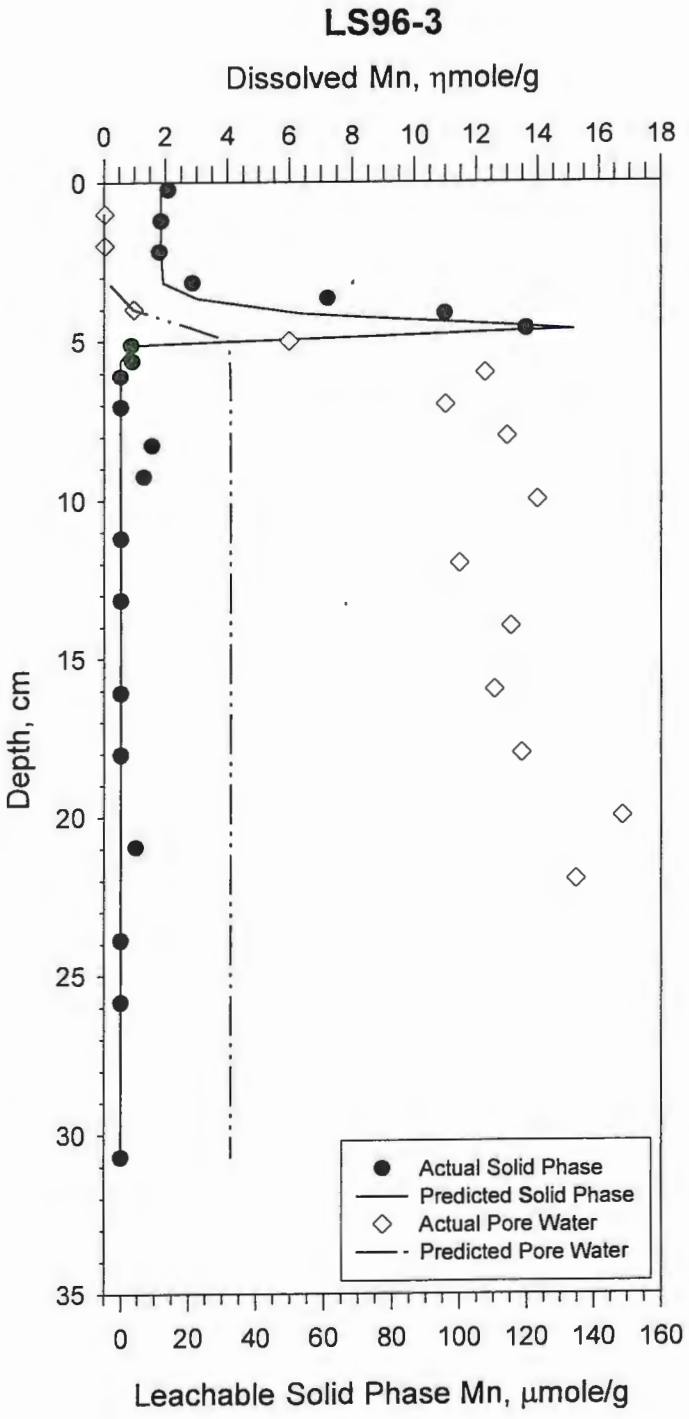

Figure 65. Core LS96-3 Mn diagenetic model results.

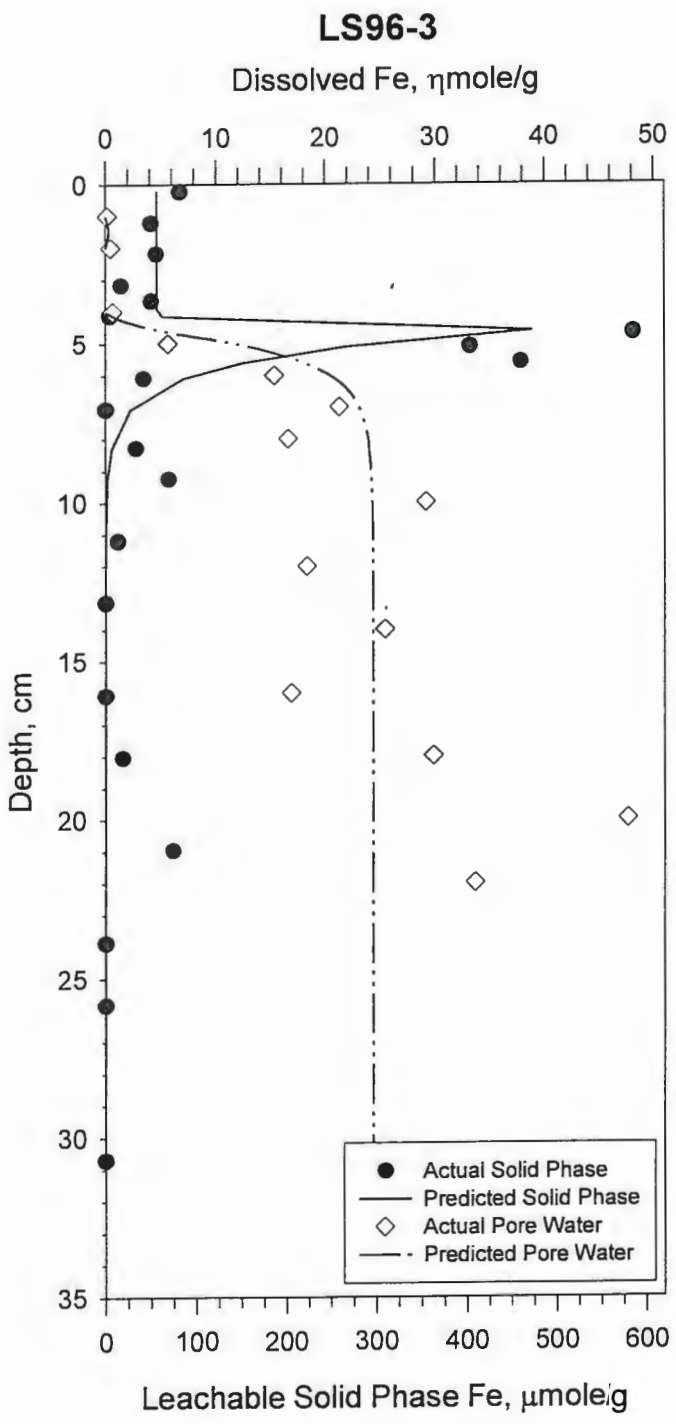

Figure 66. Core LS96-3 Fe diagenetic model results.

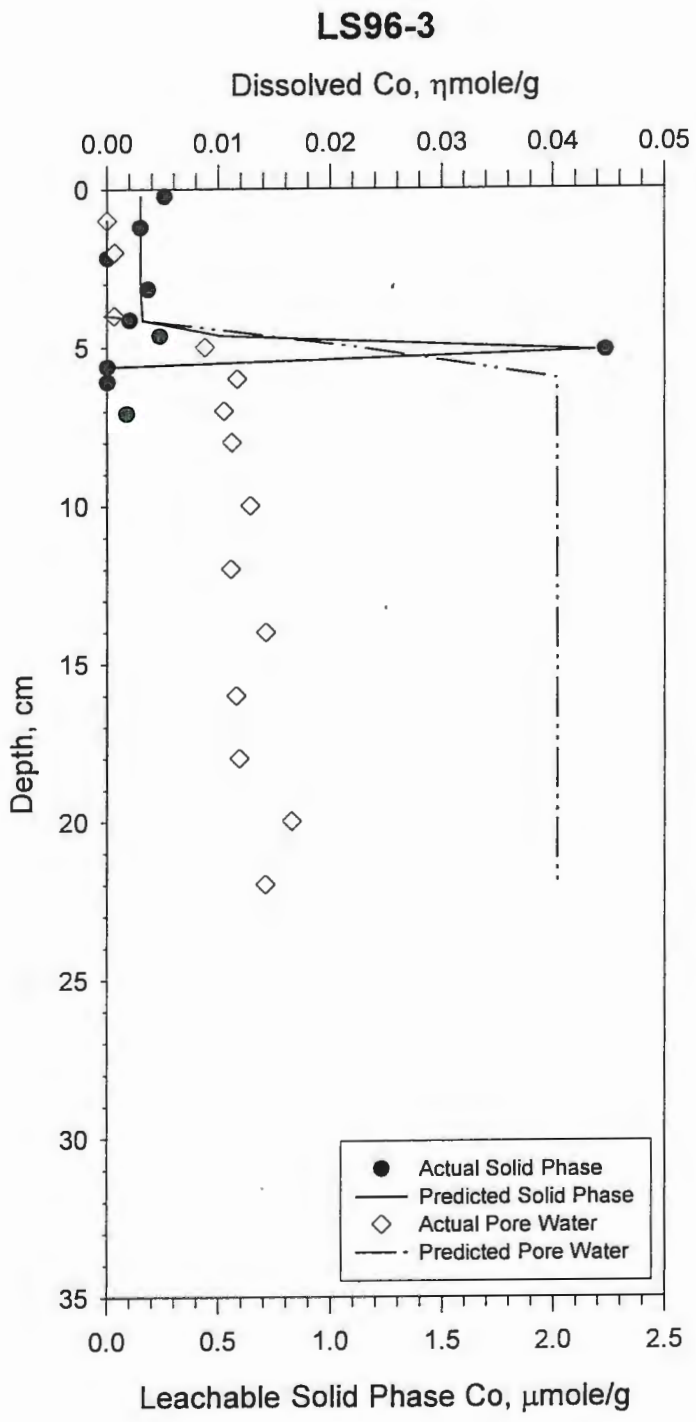

Figure 67. Core LS96-3 Co diagenetic model results.

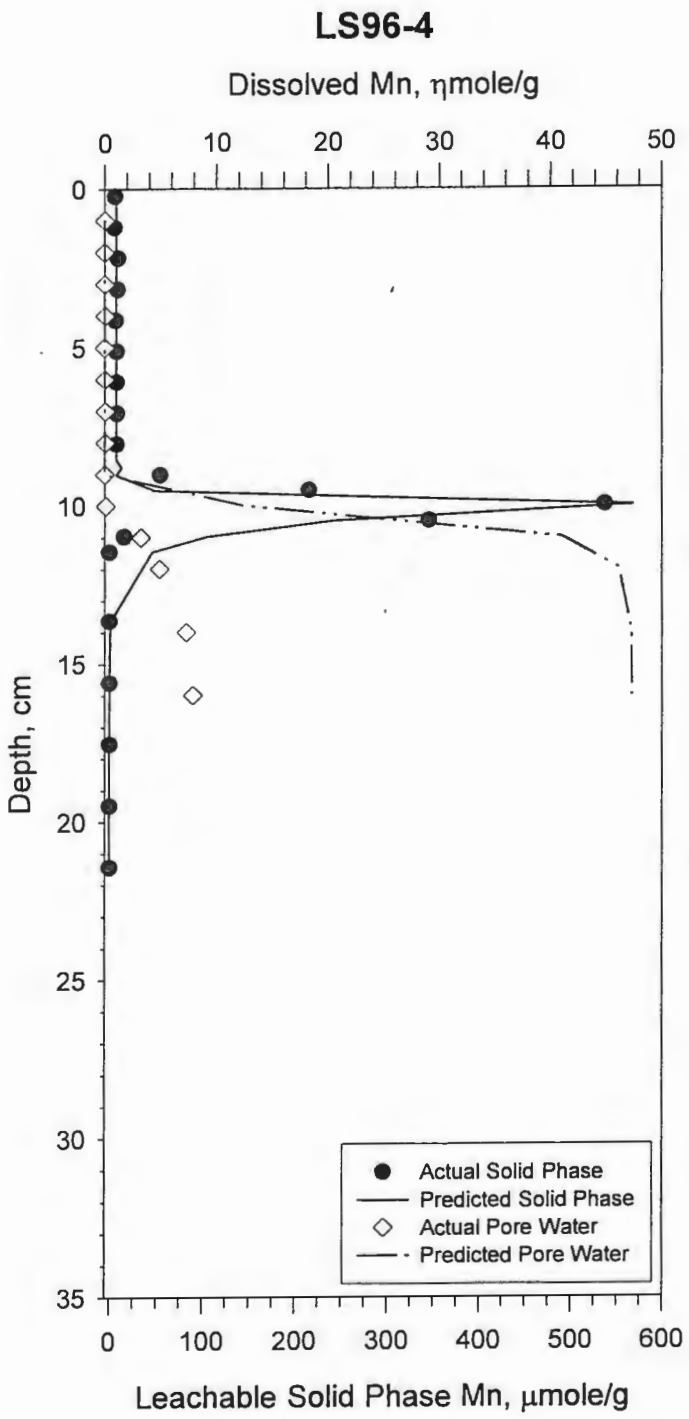

Figure 68. Core LS96-4 Mn diagenetic model results.

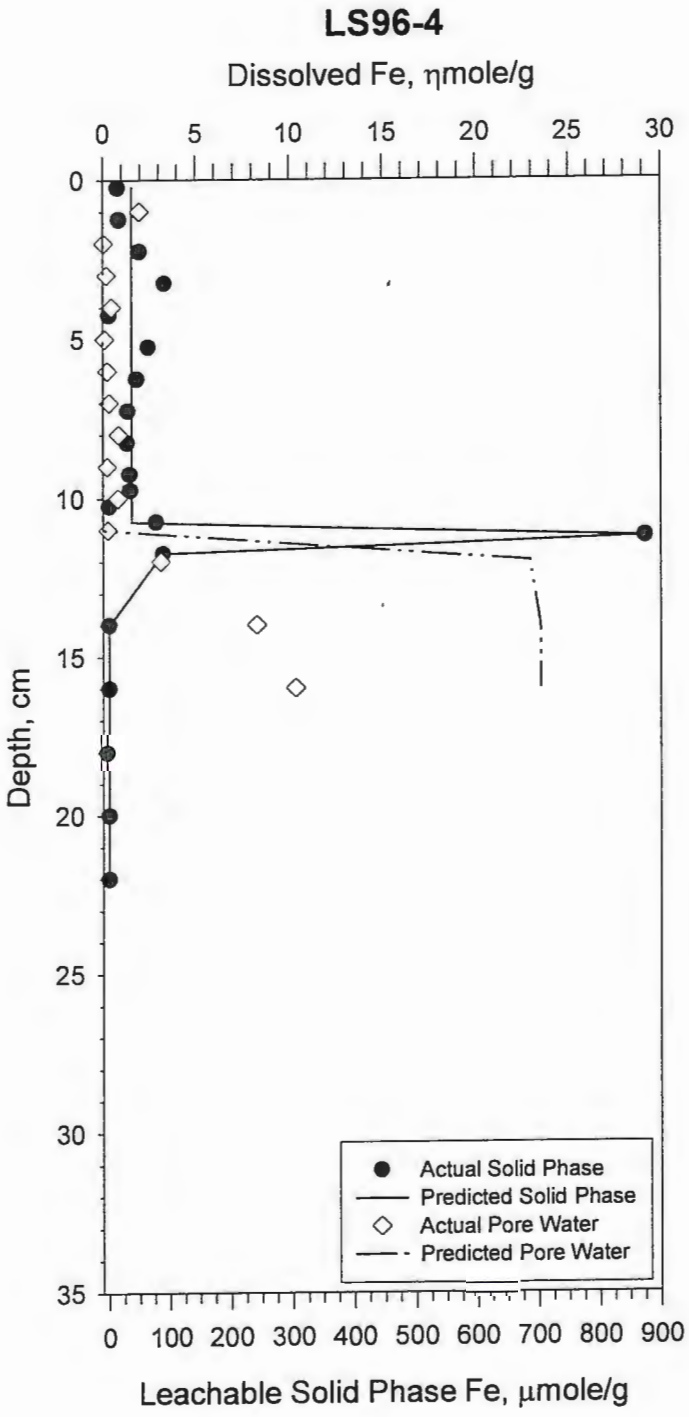

Figure 69. Core LS96-4 Fe diagenetic model results.

5.4 Trace Metal Fluxes, Results and Discussion

In order to study trace metal fluxes, the amount diffusing out of the sediment column is compared to the amount being buried in the sediment. The equation describing diffusive flux out of the sediments is (Berner, 1980):

$$J_s = -\phi D_s \frac{\partial C}{\partial x} \qquad (25)$$

where

J_s = diffusion flux out of sediments ($g / cm^2 / yr$)
D_s = whole sediment diffusion coefficient (cm^2 / yr)
$\frac{\partial C}{\partial x}$ = concentration gradient ($nmole / g / cm$), and
ϕ = porosity (%)

This equation assumes no advection of pore waters. Using this equation the fluxes have been calculated for Cu and Zn. Gradients across the sediment-water interface were calculated using this pore water data and bottom water concentrations from Nriagu et al. (1996). Concentrations of Cu in the bottom water are 10× smaller than those in the pore waters, and those of Zn are as much as 1000× smaller. These values are assumed to exist right to the sediment-water interface. Porosity was averaged over the upper part of the core, from the depth of the first pore water sample to the sediment-water interface. The concentration gradient was calculated from the uppermost pore water sample to the bottom water, and was assumed to be linear across that range. The diffusion coefficient was calculated from Li and Gregory (1974) for

each element, assuming a temperature of 4 °C.

In order to find the net flux, the rate at which the trace metals are being buried into the sediment is calculated. The equation used is:

$$J = C_o \bullet w \qquad (26)$$

where

J = burial rate into sediments (μmole/cm^2/yr)

C_o = solid phase concentration at sediment-water interface (μmole/g)

w = sedimentation rate (g/cm^2/yr)

The solid phase concentration at the sediment-water interface was obtained from the sediment leach data for each element. The sedimentation rate used was the 100 year average. The variables used in all calculations are listed in Table 11.

Table 11. Variables used in flux calculations.

Core	Element	BW Conc. (ηmole/g)	PW Conc. (ηmole/g)	at depth (cm)	ϕ	w (g/cm^2/yr)	C_o (μmole/g)
LS96-3	Cu	0.012	0.15	1	0.97	0.018	1.7
LS96-4	Cu	0.012	0.12	1	0.94	0.011	1.9
LS96-3	Zn	0.0050	3.3	1	0.97	0.018	1.3
LS96-4	Zn	0.0050	1.3	1	0.94	0.011	0.99

Trace metal flux of Cu and Zn were calculated for cores LS96-3 and 4 that show significant enrichments in pore waters relative to bottom waters. In both

cases the reported fluxes are minima due to the nature of the calculation. The apparent slope of the concentration gradient across the sediment-water interface depends on the position of the uppermost pore water samples; sites where near-surface pore water samples are unavailable would yield inaccurate flux estimates, and are not presented here. As a result of the uppermost samples being too deep in the core, the flux calculations for cores LS96-5 and 6 are less accurate. For cores LS96-3 and 4 high sample density in the upper portion of the core allows an accurate calculation.

The fluxes into and out of the sediments, as well as the net flux, are reported for Cu and Zn for cores LS96-3 and 4 (Table 12). At both sites the Cu flux into the sediment is higher than that exiting the sediments into the overlying water; approximately 50% of the leachable Cu appears to be remobilized by diagenetic reactions in the upper few cm. This may contribute to the observed increase in dissolved Cu in the near-surface relative to deeper sediments. The increased concentration of Cu in the pore waters near the sediment-water interface (Figures 22 and 30) is the result of remobilization by diagenetic reactions. The profiles also show that Cu is dissolving at depth and diffusing upward to the sediment-water interface, which would be shown be high concentrations at depth that decrease upward in the sediment column. The aqueous phase concentrations in cores LS96-3 and 4 are low in the deep in the core, increase in the near-surface sediments and then decrease at the sediment-water interface.

Table 12. Copper and Zinc flux for Cores LS96-3 and 4.

Site	Element	Flux in (ηmole/cm^2/yr)	Flux out (ηmole/cm^2/yr)	Total
LS96-3	Cu	-29	17	-12
LS96-4	Cu	-21	13	-8
LS96-3	Zn	-23	400	377
LS96-4	Zn	-11	155	144

The calculated Zn fluxes for cores LS96-3 and 4 show a greater amount leaving the sediment column than entering it. The fluxes of Zn out of the sediment are as much as 20× greater than the inward flux. The small influx indicates another source of solid phase Zn that has not been taken into account in these calculations; it is not possible for a steady-state system to have more material leaving the sediment than coming in. It appears that diagenesis remobilizes Zn from phases (probably organic matter) not subject to attack by the hydroxylamine-acetic acid leaching technique. The outward flux is consistent with the suggestion of Nriagu et al. (1996), of regeneration of Zn from Lake Superior sediments.

The water column profiles in Lake Superior assembled by Nriagu et al. (1996) show an increase in Zn concentration relative to the upper water column, of approximately 100 ng/L, in the bottom 50 m at nearby sites. It is likely that this enrichment developed over a three month period from spring turnover (June) to the time of sampling (August). This corresponds to an annual flux of 40 nmole/cm^2/yr, of the same order of magnitude as the flux 150 nmole/cm^2/yr at

site LS96-3.

Nriagu et al. (1996) also report an estimate of the amount of dust input into Lake Superior of 66 nmole/cm^2/yr, which is an estimate of input and not of the amount that dissolves, that is part of the source of solid phase Zn into the system. This flux is of the same magnitude as the other annual fluxes calculated in this study.

The time required to accumulate the observed Fe and Mn peaks was estimated by comparing depositional fluxes of Fe and Mn to the inventory of solid phase Fe and Mn found in the peak. The fluxes of redox-mobile Fe and Mn were calculated using the average initial solid phase concentrations of Fe and Mn above the redox boundary (μmole/g) and the average sedimentation rate, in g/cm^2/yr. The peak inventory was calculated as the sum of concentrations (in excess of the average incoming concentration) times the depth increments they represent.

The results indicate that the present peaks could have accumulated over relatively short time periods (Table 13) considering that early diagenesis has been occurring since the last glaciers receded from the Lake Superior Basin, approximately 10,000 years ago. This apparent inconsistency may be due to past episodes of enhanced burial of Fe and Mn or to a recent increase in fluxes of redox-mobile Fe and Mn.

Table 13. Peak accumulation.

	LS96-3 Mn	LS96-4 Mn	LS96-3 Fe	LS96-4 Fe
Sedimentation rate, g/cm^2/yr	0.018	0.011	0.018	0.011
Initial concentration, μmole/g	16.9	7.6	51.0	37.1
Flux, μmole/cm^2/yr	0.305	0.083	0.918	0.408
Estimated inventory,μmole/cm^2	30	210	181	181
Estimated time of build up (years)	**98.**	**2519**	**197**	**444**

5.5 Physical Disturbances To Cores

5.5a Coring Site LS96-5

Data from core LS96-5, beginning with field observations of an iron-oxide layer at ~3 cm overlying a manganese-oxide layer at ~10 cm, indicate a complex sedimentary history. The notion of perturbation to the sediments is borne out by the distribution of ^{210}Pb in the core, which shows a major deflection from natural exponential decay (Figure 37). High ^{210}Pb activity is limited to a few samples at the sediment-water interface. Below 2.25 cm, the ^{210}Pb concentrations drop to a constant value that is significantly above background levels until 9.25 cm where there is an increase in activity and a return to simple exponential behavior. This suggests that the zone above 9.25 cm has been disturbed, and that sediments below 9.25 cm are unaffected and undisturbed by fluctuation in the sedimentation rate.

This was further investigated using x-ray diffraction (XRD) to examine distributions of taconite ore tailings in the sediment column. One would expect to

find evidence of taconite tailings at this site due to the close proximity to Silver Bay. Disposal of tailings in Lake Superior initiated in 1956, assuming a sedimentation rate of 0.015 g/cm^2/yr and 2 cm of bioturbation, taconite tailings would be expected to be present to a depth of approximately 5 cm. However, XRD data show grunerite present to a depth of 9 cm. This corresponds well with the ^{210}Pb data as that is the depth that there is a return to a normal exponential decay with no deflections.

The hypothesis for sedimentation at this site involves slumping of material from higher up on the slope of the trench. The slumped material moved down slope and became homogenized as it was deposited, mixing up the unsupported ^{210} Pb in the sediments, and the grunerite from the taconite tailings. It is unknown what would have caused this depositional event, but the evidence is there to support the claim. Approximately 9 cm of sediment was rapidly deposited at this location. Since that time approximately 1 cm of new sediment has been deposited.

This hypothesis is consistent with the observed solid and aqueous phase metal distributions of Fe and Mn (Figures 34-35). There are two sets of solid phase Fe and Mn peaks, suggesting that the redox boundary may have shifted and indicating that the sediments and pore waters are not presently at steady-state. The initial field description of this core can be reevaluated keeping this hypothesis in mind. "Top 4 cm is tan in color. Then there is the orange layer which is ~ 2 mm thick. The color changes to light gray for 4 cm. The next 3 cm

is black or very dark gray. The remaining core is dark brownish gray." It appears that the redox boundary had been at what is presently 10 cm depth, and migrated up in the sediment column to its present location at 4 cm after the rapid sedimentation event. The orange layer at 4 cm is the current redox boundary for Fe. The black layer between 8 and 11 cm would be the relict redox boundary. Because this relict redox boundary is now in the reduction zone, the Fe and Mn found there is being reduced, remobilized, and redeposited at the current redox boundary. This process is occurring more rapidly for Mn than for Fe. In the solid phase, the upper Mn peak is already well-defined and higher in concentration than the lower peak; this is not the case with the Fe profile which still has the dominant peak at 10.25 cm. This is understandable because Mn-oxides are less stable than Fe-oxides at the current oxidation potential at 10.25 cm, therefore the Mn will remobilize more readily than the Fe.

The Cu data is also consistent with the theory of a relict sediment-water interface (Figure 38). The peak in the solid phase at 10.25 cm is a relict enrichment that was once near the sediment-water interface, but it was buried by the rapid sedimentation event. The aqueous phase data support this, showing an increase in concentration between 12 and 13 cm in addition to one at the sediment-water interface.

The LOI profile at this site shows a decrease in porosity over the depth range of 2.5 to 10.0 cm (Figure 15). There is also a decrease in the organic content of the sediment in that depth range. Both of these observations show

that the sediment between 2.5 and 10.0 cm has different characteristics than other sediment at that site.

Core LS96-5 was collected at a site where the sediment column had been physically disturbed, making it difficult to interpret trace metal profiles. However, several lines of evidence, including ^{210}Pb geochronology, X-ray diffractometry, and sediment leach and pore water trace metal concentrations, permit deconvolution of the complex history of sedimentation at this location.

6. SUMMARY

Sediment cores were collected from Lake Superior and were analyzed for a suite of trace metals in solid and aqueous phases. Pore water concentration profiles were used to evaluate remobilization and enrichment of trace metals in the sediments. There have been very few previous studies examining the redox chemistry of trace metals and the effects of early diagenesis on metal distributions in Lake Superior sediments.

In this study, redox chemistry of Fe, Mn and Co were examined, in addition to the concentration profiles of Cu, Pb, Zn and Ba. The redox-sensitive elements showed distributions consistent with steady-state early diagenesis, featuring distinct solid phase peaks corresponding to the depth below which rapid increases in aqueous phase concentrations occur. A mathematical model was used to predict early diagenetic distributions of the redox elements (Fe, Mn and Co) in solid and aqueous phase assuming simple one-dimensional diffusion. The results of the model were generally consistent with the actual vertical profiles of these metals.

Concentration profiles of Cu and Pb were used to identify amount of anthropogenic loading in the lake, making it possible to discern historical events in the sediment record. Both the beginning of Cu mining in Michigan and the rise and fall of alkyl lead consumption in the U.S. were seen in the sedimentary record. In the western basin, sedimentary inventories of anthropogenic Cu

appeared to show a general decrease with distance from Cu sources, particularly when the general counterclockwise pattern of circulation was considered.

Trace metal flux of Cu and Zn into and out of the sediments were calculated. There was significant regeneration and release of Zn into the water column; the calculated flux was consistent with the magnitude of deepwater enrichment observed in water column profiles. Regeneration of Cu was less significant.

Sedimentation rates and core chronologies based on ^{210}Pb analyses were calculated and compared to sedimentation rates based on appearance of evidence of taconite tailings and anthropogenic Cu. Lead-210 analyses yielded 100-year average sedimentation rates between 0.011 to 0.018 g/cm^2/yr (0.046 to 0.059 cm/yr). Taconite tailing disposal in the lake began in 1956; the first appearance of taconite tailings was used to estimate sedimentation rates of 0.016 and 0.034 g/cm^2/yr (0.07 and 0.10 cm/yr) at two sites adjacent to the North Shore. These rates are consistent with previously reported ^{210}Pb-based rates. Sedimentation rates calculated from first appearance of Cu, assumed to have occurred in 1895, range from 0.009 to 0.015 (0.03 to 0.07 cm/yr) and are in good agreement with those calculated by the ^{210}Pb method.

7. REFERENCES

Anderson, K.A., 1997, A seismic stratigraphic study of Western Lake Superior. Masters Thesis, University of Minnesota-Duluth.

Berner, R.A., 1980, Early diagenesis - A theoretical approach. Princeton University Press.

Bruland, K.W., Koide, M., Bowser, C., Maher, L.J., and Goldberg, E.D., 1975, ^{210}Pb and pollen geochronologies on Lake Superior sediments. Quaternary Research, p.89-98.

Burdige, D.J., and Gieskes, J.M., 1983, A pore water/solid phase diagenetic model for manganese in marine sediments. American Journal of Science, v.283, p.29-47.

Callender, E., and Bowser, C.J., 1980, Manganese and copper geochemistry of interstitial fluids from manganese nodule-rich pelagic sediments of the northeastern equatorial pacific ocean. American Journal of Science, v.280, p.1063-1096.

Cook, P.M., 1975, Semi-quantitative determination of asbestiform amphibole mineral concentrations in western Lake Superior water samples. In: Advances in X-ray Analysis, v.18. Pickles, W.L., Barrett, C.S., Newkirk, J.B., and Ruud, C.O. (Eds.), p557-567.

Evans, J.E., Johnson, T.C., Alexander, Jr., E.C., Lively, R.S., and Eisenreich, S.J., 1981, Sedimentation rates and depositional processes in Lake Superior from ^{210}Pb geochronology. Journal of Great Lakes Research, v.7(3), p.299-310.

Faure, G., 1986, Principles of isotope geology, second edition. John Wiley and Sons, Inc.

Graney, J.R., Halliday, A.N., Keeler, G.J., Nriagu, J.O., Robbins, J.A., and Norton, S.A., 1995, Isotopic record of lead pollution in lake sediments from the northeastern United States. Geochimica et Cosmochimica Acta, v.59, p.1715-1728.

Heggie, D.T., and Lewis, T., 1984, Cobalt in pore waters of marine sediments. Nature, v.311 (4), p.453-455.

Kane, J.S., and Skeen, C.J., 1993, A study to determine source of inter-laboratory variability in measured Loss On Ignition (LOI) for Devonian Ohio shale SDO-1. U.S. Geological Survey Bulletin 2046, p. F1-F9.

Kemp, A.L.W., Williams, J.D.H., Thomas, R.L., and Gregory, M.L., 1978, Impact of man's activities on the chemical composition of the sediments of Lakes Superior and Huron. Water, Air and Soil Pollution???

Kerfoot, W.C., Lauster, G., and Robbins, J.A., 1994, Paleolimnological study of copper mining around Lake Superior: Artificial varves from Portage Lake provide a high resolution record. Limnology and Oceanography, v.39, p.649-669.

Klinkhammer, G.P., Heggie, D.T., and Graham, D.W., 1982, Metal diagenesis in oxic marine sediments. Earth and Planetary Science Letters, v.61, p.211-219.

Klinkhammer, G.P., 1980, Early diagenesis in sediments from the eastern equatorial Pacific, II. Pore water metal results. Earth and Plantary Science Letters, v.49, p.81-101.

Krishnaswamy, S., Martin, J.M., and Meybeck, M., 1971, Geochronology of lake sediments. Earth and Planetary Science Letters, v.11, p.407-414.

Li, Y.-H., and Gregory, S., 1974, Diffusion of ions in sea water and in deep-sea sediments. Geochimica et Cosmochimica Acta, v.38, p.703-714.

Manheim, F.T., 1966, A hydraulic squeezer for obtaining interstitial water from consolidated and unconsolidated sediments. U.S. Geological Survey Professional Papers, 550C, p.256-261.

McKee, J.D., Wilson, T.P., Long, D.T., and Owen, R.M., 1989a, Geochemical partitioning of Pb, Zn, Cu, Fe, and Mn across the sediment-water interface in large lakes. Journal of Great Lakes Research, v.15(1), p.46-58.

McKee, J.D., Wilson, T.P., Long, D.T., and Owen, R.M., 1989b, Pore water profiles and early diagenesis of Mn, Cu, and Pb in sediments from large lakes. Journal of Great Lakes Research, v.15(1), p.68-83.

Nriagu, J.O., Lawson, G., Wong, H.K.T., and Cheam, V., 1996, Dissolved trace metals in Lakes Superior, Erie, and Ontario. Environmental Science and Technology, v.30, p.178-187.

Oldfield, F., and Appleby, P.G., 1983, Empirical testing of ^{210}Pb-dating models for lake sediments. In: Lake sediments in Environmental History, Haworth, E.W., Lund, J.W.G., eds., Minneapolis, University of Minnesota Press, p.93-124.

Oxtoby, D.W., and Nachtrieb, N.H., 1987, Principles of modern chemistry. Saunders College Publishing, p.563.

Robbins, J.A., and Callender, E., 1975, Diagenesis of manganese in Lake Michigan sediments. American Journal of Science, v.275, p.512-533.

Scholtz, C.A., 1985, Sediment distribution and sedimentation rates in the western arm of Lake Superior using 3.5 kHz seismic reflection profiles and ^{210}Pb geochronology. Masters Thesis, University of Minnesota.

Schultz, H.D., Dahmke, A., Schinzel, U., Wallmann, K., and Zabel, M., 1994, Early diagenetic processes, fluxes, and reaction rates in sediments of the South Atlantic. Geochimica et Cosmochimica Acta, v.58, p.2041-2060.

Shaw, T.J., Gieskes, J.M., and Jahnke, R.A., 1990, Early diagenesis in differing depositional environments: The response of transition metals in pore water. Geochimica et Cosmochimica Acta, v.54, p.1233-1246.

Tessier, A., Campbell, P.G.C., and Bisson, M., 1979, Sequential extraction procedure for the speciation of particulate trace metals. Analytical Chemistry, v.51, p.844-851.

8. APPENDIX

LS96-1 Mean depth, cm		Wet (g/cc)	Dry (g/cc)	LOSS ON IGNITION % Organic	H2O Vol %	H2O Wt %
0.24		1.087	0.118	7.9	97.0	89.2
0.73		1.109	0.160	7.7	94.9	85.5
1.22		1.116	0.170	7.3	94.6	84.8
1.71		1.129	0.197	6.9	93.2	82.6
2.19		1.162	0.245	6.3	91.7	78.9
2.68		1.157	0.258	6.0	89.9	77.7
3.17		1.179	0.272	5.5	90.7	76.9
3.66		1.186	0.288	6.7	89.9	75.7
4.14		1.157	0.274	8.5	88.3	76.3
4.63		1.160	0.247	8.9	91.3	78.7
5.12		1.072	0.235	8.7	90.8	78.1
5.61		1.164	0.260	8.5	90.4	77.7
6.09		1.205	0.295	8.5	91.0	75.5
6.58		0.958	0.206	8.3	90.0	78.5
7.07		1.190	0.299	7.8	89.1	74.9
7.56		1.099	0.266	7.9	89.7	75.8
8.04		1.192	0.288	8.3	90.3	75.8
8.53		1.188	0.294	8.8	89.5	75.3
9.02		1.186	0.274	8.7	91.2	76.9
9.51		1.175	0.291	8.3	88.5	75.3
9.99		1.203	0.303	8.2	90.0	74.8
10.48		1.211	0.321	8.1	89.0	73.5
10.97		1.190	0.305	7.7	88.4	74.4
11.46		1.229	0.345	7.5	88.4	72.0
11.94		1.218	0.326	7.3	89.2	73.2
12.43		1.230	0.346	7.5	88.4	71.9
12.92		1.241	0.374	8.4	86.8	69.9
13.41		1.241	0.354	7.9	88.8	71.5
13.89		1.239	0.340	7.5	89.9	72.6
14.38		1.219	0.321	7.3	89.7	73.6
15.11	*	1.210	0.319	7.1	89.2	73.7
16.09	*	1.213	0.325	7.0	88.8	73.2
17.06	*	1.215	0.333	6.9	88.2	72.6
18.04	*	1.222	0.339	6.9	88.2	72.2
19.01	*	1.207	0.336	6.8	87.1	72.2
19.99	*	1.199	0.312	7.0	88.7	74.0
20.96	*	1.227	0.346	7.1	88.1	71.8
21.94	*	1.205	0.326	7.3	87.9	73.0
22.91	*	1.178	0.302	7.4	87.7	74.4
23.89	*	1.232	0.367	7.2	86.5	70.2
24.86	*	1.210	0.342	6.6	86.8	71.7
25.84	*	1.230	0.343	6.4	88.7	72.1
26.81	*	1.245	0.378	6.4	86.7	69.6
27.79	*	1.220	0.369	6.5	85.1	69.8
28.76	*	1.224	0.347	6.4	87.8	71.7
29.74	*	1.241	0.358	6.4	88.3	71.2
30.71	*	1.226	0.349	6.4	87.7	71.5
31.69	*	1.244	0.373	6.4	87.1	70.0

Asterisk denotes 1 cm depth increment, all others 0.5 cm depth increment.

LS96-2			LOSS ON IGNITION			
Mean depth, cm		Wet (g/cc)	Dry (g/cc)	% Organic	H2O Vol %	H2O Wt %
0.24		1.124	0.180	6.9	94.4	84.0
0.73		1.133	0.207	6.8	92.6	81.7
1.22		1.167	0.272	6.5	89.5	76.7
1.71		1.188	0.302	6.2	88.6	74.6
2.19		1.223	0.348	5.9	87.6	71.6
2.68		1.210	0.306	7.1	90.5	74.8
3.17		1.204	0.311	5.9	89.3	74.2
3.66		1.265	0.376	4.9	88.9	70.3
4.14		1.258	0.389	4.5	86.9	69.1
4.63		1.271	0.409	4.5	86.2	67.8
5.12		1.207	0.350	5.2	85.8	71.1
5.61		1.289	0.446	4.6	84.3	65.4
6.09		1.292	0.448	3.9	84.4	65.3
6.58		1.266	0.416	3.9	85.0	67.1
7.07		1.283	0.431	4.1	85.2	66.4
7.56		1.294	0.452	4.6	84.2	65.1
8.04		1.268	0.407	4.7	86.1	67.9
8.53		1.298	0.461	4.8	83.7	64.5
9.02		1.253	0.416	5.6	83.7	66.8
9.51		1.247	0.378	6.2	86.9	69.7
9.99		1.241	0.366	6.5	87.6	70.5
10.48		1.263	0.409	6.6	85.4	67.6
10.97		1.238	0.373	6.4	86.5	69.9
11.46		1.256	0.389	6.5	86.7	69.1
11.94		1.313	0.441	6.5	87.2	66.4
12.43		1.260	0.397	6.9	86.3	68.5
12.92		1.254	0.397	7.0	85.7	68.4
13.41		1.249	0.388	6.8	86.2	69.0
13.89		1.251	0.385	6.4	86.7	69.3
14.38		1.245	0.364	6.1	88.1	70.8
14.87		1.244	0.357	5.8	88.7	71.3
15.6	*	1.244	0.378	5.5	86.5	69.6
16.58	*	1.204	0.311	6.3	89.3	74.2
17.55	*	1.207	0.329	6.1	87.8	72.7
18.53	*	1.246	0.381	6.0	86.6	69.5
19.5	*	1.253	0.389	5.7	86.4	69.0
20.48	*	1.232	0.358	5.6	87.4	70.9
21.45	*	1.201	0.318	5.8	88.3	73.5
22.43	*	1.248	0.369	5.2	87.9	70.4
23.4	*	1.244	0.355	5.9	88.9	71.5
24.38	*	1.275	0.404	5.9	87.1	68.3
25.35	*	1.268	0.406	6.0	86.2	68.0
26.33	*	1.247	0.380	5.8	86.7	69.5
27.3	*	1.230	0.351	6.4	88.0	71.5
28.28	*	1.215	0.328	6.5	88.8	73.0
29.01	*	1.157	0.339	6.2	81.8	70.7

Asterisk denotes 1 cm depth increment, all others 0.5 cm depth increment.

LS96-3			LOSS ON IGNITION			
Mean depth, cm		Wet (g/cc)	Dry (g/cc)	% Organic	H2O Vol %	H2O Wt %
0.24		1.076	0.097	9.7	97.9	91.0
0.73		1.106	0.125	9.5	98.1	88.7
1.22		1.101	0.155	9.4	94.7	86.0
1.71		1.106	0.151	9.3	95.5	86.4
2.19		1.134	0.167	9.0	96.8	85.3
2.68		1.154	0.208	8.7	94.6	81.9
3.17		1.135	0.199	8.6	93.6	82.5
3.66		1.142	0.206	8.4	93.6	82.0
4.14		1.184	0.241	8.4	94.3	79.6
4.63		1.188	0.271	8.4	91.7	77.2
5.12		1.207	0.287	9.2	92.1	76.3
5.61		1.205	0.278	8.6	92.7	76.9
6.09		1.197	0.287	8.2	91.0	76.0
6.58		1.207	0.303	7.9	90.5	74.9
7.07		1.241	0.326	7.7	91.5	73.8
7.56		1.210	0.279	7.6	93.1	77.0
8.29	*	1.199	0.278	7.7	92.1	76.8
9.26	*	1.207	0.301	7.5	90.6	75.1
10.24	*	1.199	0.268	7.7	93.1	77.7
11.21	*	1.154	0.227	7.7	92.6	80.3
12.19	*	1.175	0.246	7.4	92.8	79.0
13.16	*	1.202	0.278	7.4	92.5	76.9
14.14	*	1.184	0.262	7.6	92.2	77.9
15.11	*	1.206	0.288	7.9	91.8	76.2
16.09	*	1.203	0.289	7.6	91.5	76.0
17.06	*	1.205	0.294	7.3	91.1	75.6
18.04	*	1.204	0.280	7.4	92.4	76.8
19.01	*	1.211	0.303	7.3	90.8	75.0
19.99	*	1.199	0.287	7.4	91.2	76.1
20.96	*	1.209	0.306	7.4	90.4	74.7
21.94	*	1.195	0.283	7.2	91.1	76.3
22.91	*	1.217	0.320	6.9	89.7	73.7
23.89	*	1.207	0.302	7.4	90.6	75.0
24.86	*	1.210	0.304	7.2	90.6	74.9
25.84	*	1.215	0.309	7.1	90.7	74.6
26.81	*	1.204	0.301	7.2	90.4	75.0
27.79	*	1.174	0.309	7.0	86.5	73.7
28.76	*	1.209	0.324	7.2	88.6	73.2
29.74	*	1.241	0.336	7.3	90.4	72.9
30.71	*	1.221	0.327	7.2	89.3	73.2
31.69	*	1.234	0.340	7.5	89.4	72.5
32.66	*	1.242	0.353	7.6	89.0	71.6

Asterisk denotes 1 cm depth increment, all others 0.5 cm depth increment.

LS96-4		LOSS ON IGNITION				
Mean depth, cm		Wet (g/cc)	Dry (g/cc)	% Organic	H2O Vol %	H2O Wt %
0.24		1.071	0.115	10.1	95.6	89.3
0.73		1.065	0.127	9.7	93.8	88.0
1.22		1.089	0.156	9.3	93.3	85.6
1.71		1.101	0.164	9.1	93.7	85.1
2.19		1.109	0.182	9.1	92.7	83.6
2.68		1.153	0.217	9.0	93.6	81.1
3.17		1.157	0.218	8.9	93.9	81.1
3.66		1.161	0.237	8.0	92.4	79.6
4.14		1.162	0.266	7.9	89.5	77.1
4.63		1.166	0.264	8.1	90.2	77.3
5.12		1.152	0.253	7.7	89.9	78.0
5.61		1.184	0.285	7.5	90.0	76.0
6.09		0.888	0.222	7.4	89.5	75.0
6.58		1.167	0.276	7.3	89.0	76.3
7.07		1.165	0.281	7.2	88.4	75.8
7.56		1.180	0.306	7.1	87.4	74.1
8.04		1.218	0.344	7.4	87.4	71.8
8.53		1.204	0.334	7.1	87.0	72.3
9.02		1.201	0.332	7.0	86.9	72.3
9.51		1.231	0.351	6.9	88.0	71.5
9.99		1.190	0.371	7.2	81.8	68.8
10.48		1.164	0.360	7.1	80.4	69.1
10.97		1.263	0.425	7.4	83.8	66.4
11.46		1.239	0.373	6.4	86.6	69.9
11.94		1.247	0.383	6.7	86.4	69.3
12.68	*	1.255	0.384	6.7	87.1	69.4
13.65	*	1.261	0.387	6.4	87.4	69.3
14.63	*	1.235	0.356	6.5	87.8	71.1
15.6	*	1.258	0.393	6.3	86.5	68.7
16.58	*	1.230	0.357	6.1	87.3	71.0
17.55	*	1.225	0.373	6.2	85.2	69.5
18.53	*	1.253	0.393	5.9	86.0	68.6
19.5	*	1.243	0.386	6.1	85.7	68.9
20.48	*	1.255	0.395	6.2	86.0	68.5
21.45	*	1.242	0.383	6.3	85.9	69.1
22.43	*	1.242	0.370	6.7	87.3	70.2
23.4	*	1.232	0.359	4.5	87.4	70.9
24.38	*	1.225	0.349	6.6	87.6	71.5
25.35	*	1.202	0.331	9.0	87.1	72.4
26.33	*	1.224	0.356	6.7	86.8	70.9
27.3	*	1.220	0.344	6.7	87.6	71.8
28.28	*	1.256	0.382	6.3	87.4	69.6
29.25	*	1.165	0.308	6.1	85.7	73.6
30.23	*	1.251	0.386	6.0	86.6	69.2

Asterisk denotes 1 cm depth increment, all others 0.5 cm depth increment.

LS96-5		LOSS ON IGNITION				
Mean depth, cm		Wet (g/cc)	Dry (g/cc)	% Organic	H2O Vol %	H2O Wt %
0.24		1.073	0.131	6.3	94.2	87.8
0.73		1.116	0.183	6.1	93.3	83.6
1.22		1.138	0.219	5.8	91.9	80.7
1.71		1.202	0.312	4.7	89.1	74.1
2.19		1.258	0.390	3.3	86.8	69.0
2.68		1.410	0.602	1.8	80.8	57.3
3.17		1.367	0.572	2.1	79.5	58.1
3.66		1.455	0.674	1.8	78.1	53.7
4.14		1.439	0.657	1.8	78.2	54.3
4.63		1.447	0.666	2.2	78.2	54.0
5.12		1.448	0.661	1.7	78.7	54.3
5.61		1.507	0.759	1.5	74.8	49.6
6.09		1.515	0.743	1.5	77.2	51.0
6.58		1.390	0.579	2.0	81.1	58.3
7.07		1.387	0.566	2.8	82.2	59.2
7.56		1.322	0.462	4.5	86.1	65.1
8.04		1.239	0.373	5.4	86.6	69.9
8.53		1.233	0.358	5.9	87.5	70.9
9.02		1.211	0.324	6.8	88.7	73.2
9.51		1.225	0.303	8.0	92.2	75.3
9.99		1.212	0.290	8.5	92.2	76.1
10.48		1.158	0.245	7.8	91.3	78.8
10.97		1.162	0.269	7.5	89.3	76.9
11.46		1.173	0.275	7.3	89.8	76.6
12.19	*	1.197	0.315	7.2	88.2	73.7
13.16	*	1.176	0.280	7.3	89.5	76.1
14.14	*	1.145	0.248	7.6	89.6	78.3
15.11	*	1.161	0.258	7.3	90.3	77.8
16.09	*	1.188	0.294	7.5	89.4	75.2
17.06	*	1.183	0.289	7.3	89.4	75.6
18.04	*	1.179	0.284	7.4	89.5	75.9
19.01	*	1.188	0.287	6.9	90.0	75.8
19.99	*	1.167	0.249	7.6	91.8	78.7
20.96	*	1.162	0.253	7.3	90.8	78.2
21.94	*	1.172	0.266	7.0	90.5	77.3
22.91	*	1.200	0.318	7.0	88.2	73.5
23.89	*	1.185	0.306	6.8	87.9	74.2
24.86	*	1.230	0.359	6.7	87.2	70.9
25.84	*	1.168	0.262	6.8	90.7	77.6
26.81	*	1.185	0.302	7.2	88.3	74.5
27.79	*	1.180	0.279	7.4	90.0	76.3
28.76	*	1.187	0.301	7.3	88.6	74.6
29.74	*	1.213	0.327	7.1	88.6	73.0
30.71	*	1.215	0.341	6.8	87.4	71.9
31.69	*	1.229	0.361	6.8	86.7	70.6

Asterisk denotes 1 cm depth increment, all others 0.5 cm depth increment.

LS96-6		LOSS ON IGNITION				
Mean depth, cm		Wet (g/cc)	Dry (g/cc)	% Organic	H2O Vol %	H2O Wt %
0.24		1.063	0.090	10.3	97.3	91.5
0.73		1.103	0.145	10.2	95.9	86.9
1.22		1.096	0.148	10.0	94.8	86.5
1.71		1.128	0.205	9.7	92.3	81.8
2.19		1.106	0.257	9.6	84.8	76.7
2.68		1.126	0.202	9.2	92.4	82.1
3.17		1.131	0.187	9.4	94.4	83.4
3.66		1.130	0.189	9.2	94.1	83.3
4.14		1.182	0.264	9.1	91.7	77.6
4.63		1.170	0.271	9.2	89.8	76.8
5.12		1.186	0.275	8.8	91.2	76.8
5.61		1.190	0.282	8.5	90.8	76.3
6.09		1.175	0.280	8.3	89.5	76.2
6.58		1.179	0.291	7.9	88.8	75.3
7.07		1.195	0.294	8.1	90.1	75.4
7.56		1.175	0.271	8.1	90.4	77.0
8.04		1.190	0.304	7.9	88.6	74.5
8.53		1.227	0.325	8.1	90.2	73.5
9.02		1.207	0.342	8.6	86.5	71.7
9.51		1.190	0.318	7.9	87.2	73.3
10.24	*	1.191	0.299	7.5	89.2	74.9
11.21	*	1.183	0.304	7.2	87.9	74.3
12.19	*	1.190	0.306	7.0	88.4	74.3
13.16	*	1.202	0.320	7.2	88.2	73.3
14.14	*	1.199	0.318	7.4	88.0	73.4
15.11	*	1.206	0.323	7.4	88.4	73.2
16.09	*	1.192	0.304	7.5	88.8	74.5
17.06	*	1.216	0.345	7.2	87.1	71.6
18.04	*	1.231	0.357	6.9	87.4	71.0
19.01	*	1.231	0.362	6.8	86.9	70.6
19.99	*	1.221	0.348	6.5	87.3	71.5
20.96	*	1.228	0.365	6.3	86.3	70.3
21.94	*	1.235	0.375	6.4	86.0	69.6
22.91	*	1.220	0.371	6.7	84.9	69.6
23.89	*	1.231	0.370	6.8	86.2	70.0
24.86	*	1.242	0.374	6.8	86.9	69.9
25.84	*	1.226	0.367	6.8	85.9	70.0
26.81	*	1.229	0.358	6.7	87.1	70.9
27.79	*	1.220	0.354	6.4	86.5	70.9
28.76	*	1.228	0.358	6.4	87.0	70.9
29.74	*	1.208	0.338	6.9	87.0	72.1
30.71	*	1.201	0.319	7.1	88.2	73.4
31.69	*	1.213	0.346	7.0	86.7	71.5
32.66	*	1.221	0.345	6.8	87.5	71.7
33.64	*	1.226	0.349	6.6	87.7	71.6
34.61	*	1.218	0.343	6.7	87.5	71.9

Asterisk denotes 1 cm depth increment, all others 0.5 cm depth increment.

LS96-7		LOSS ON IGNITION				
Mean depth, cm		Wet (g/cc)	Dry (g/cc)	% Organic	H2O Vol %	H2O Wt %
0.24		1.081	0.130	9.1	95.1	88.0
0.73		1.117	0.192	7.5	92.6	82.9
1.22		1.173	0.277	5.9	89.6	76.4
1.71		1.208	0.336	5.7	87.2	72.2
2.19		1.193	0.315	5.6	87.8	73.6
2.68		1.216	0.350	6.1	86.6	71.2
3.17		1.248	0.372	6.7	87.5	70.2
3.66		1.262	0.416	5.4	84.7	67.1
4.14		1.368	0.562	4.0	80.6	58.9
4.63		1.394	0.613	3.4	78.0	56.0
5.12		1.403	0.612	3.5	79.1	56.4
5.61		1.423	0.649	3.5	77.3	54.4
6.09		1.344	0.526	4.1	81.8	60.8
6.58		1.384	0.599	3.8	78.5	56.7
7.07		1.381	0.601	3.6	77.9	56.5
7.56		1.387	0.615	3.5	77.3	55.7
8.04		1.382	0.595	3.9	78.7	56.9
8.53		1.352	0.601	3.2	75.1	55.6
9.02		1.331	0.518	4.2	81.3	61.1
9.51		1.449	0.692	3.3	75.7	52.2
9.99		1.476	0.746	2.8	72.9	49.4
10.48		1.423	0.657	3.7	76.6	53.8
10.97		1.352	0.561	4.1	79.0	58.5
11.46		1.398	0.624	3.8	77.4	55.4
11.94		1.338	0.520	4.7	81.7	61.1
12.43		1.341	0.534	4.7	80.8	60.2
13.16		1.375	0.522	5.6	85.3	62.1
14.14		1.258	0.406	5.6	85.2	67.7
14.63		1.276	0.465	4.8	81.0	63.5
15.11		1.373	0.554	4.2	81.9	59.7
15.6		1.456	0.717	3.2	73.9	50.7
16.09	*	1.398	0.624	3.7	77.4	55.4
17.06	*	1.327	0.516	4.5	81.1	61.1
18.04	*	1.366	0.546	3.9	82.0	60.0
19.01	*	1.274	0.436	4.5	83.8	65.8
19.99	*	1.300	0.477	4.5	82.3	63.3
20.96	*	1.318	0.504	4.4	81.5	61.8
21.94	*	1.269	0.424	5.5	84.6	66.6
22.91	*	1.324	0.500	4.5	82.4	62.3
23.89	*	1.341	0.529	4.1	81.2	60.5
24.86	*	1.282	0.448	4.9	83.4	65.0
25.84	*	1.280	0.433	5.0	84.7	66.2
26.81	*	1.263	0.409	6.0	85.4	67.6
27.79	*	1.251	0.395	6.4	85.6	68.4
28.76	*	1.223	0.352	6.0	87.1	71.2
29.74	*	1.223	0.406	5.2	81.7	66.8
30.71	*	1.256	0.401	5.4	85.5	68.1
31.69	*	1.341	0.533	3.7	80.7	60.2

Asterisk denotes 1 cm depth increment, all others 0.5 cm depth increment.

^{210}Pb, raw data

LS96-3 Mean depth cm	Mean depth g/cm^2	Activity pCi/g	LS96-4 Mean depth cm	Mean depth g/cm^2	Activity pCi/g
0.24	0.024	29.2	0.24	0.029	36.9
1.22	0.15	25.7	0.73	0.089	35.1
2.19	0.31	28.6	1.22	0.16	32.2
3.17	0.50	22.1	1.71	0.24	30.0
4.14	0.71	19.2	2.19	0.33	29.2
5.12	0.98	11.4	2.68	0.43	27.9
6.09	1.26	6.67	3.17	0.54	22.7
7.07	1.57	4.88	3.66	0.65	15.0
8.04	1.93	3.27	4.63	0.91	8.89
9.02 (*)	2.22	2.42	5.12	1.04	9.12
			5.61	1.17	4.72
			6.09	1.30	1.69
			6.58	1.42	1.48
			7.07	1.56	1.46
			7.56	1.71	0.92
			8.04	1.87	1.28
			8.53	2.04	1.04
			9.02	2.21	1.33
			9.51	2.38	1.73

Asterisk denotes 1 cm depth increment, all others 0.5 cm depth increment.

^{210}Pb, raw data

LS96-5 Mean depth cm	Mean depth g/cm^2	Activity pCi/g	LS96-6 Mean depth cm	Mean depth g/cm^2	Activity pCi/g
0.24	0.033	27.0	0.24	0.023	24.4
0.73	0.11	27.7	0.73	0.081	24.4
1.22	0.21	27.5	1.22	0.15	19.5
1.71	0.34	22.4	1.71	0.24	23.3
2.19	0.52	4.44	2.19	0.36	19.7
2.68	0.77	5.47	2.68	0.47	15.4
3.17	1.06	3.77	3.17	0.57	12.9
3.66	1.37	4.40	3.66	0.66	9.90
4.14	1.71	3.54	4.14	0.78	8.96
4.63	2.04	3.31	4.63	0.91	8.99
5.12	2.37	3.35	5.12	1.05	4.46
5.61	2.72	3.61	5.61	1.19	3.49
6.09	3.10	4.33	6.09	1.33	2.58
6.58	3.43	5.21	6.58	1.47	1.61
7.07	3.72	6.01	7.07	1.62	1.93
7.56	3.97	7.86	7.56	1.76	1.37
8.04	4.18	7.10	8.04	1.90	1.28
8.53	4.36	6.62	8.53	2.06	1.16
9.02	4.53	6.68	9.02	2.23	0.98
9.51	4.69	5.94	9.51	2.39	1.20
9.99	4.84	4.38			
10.97	5.10	3.05			
12.19 (*)	5.46	1.87			
13.16 (*)	5.76	1.54			
14.14 (*)	6.03	1.10			
15.11 (*)	6.28	1.09			
16.09 (*)	6.55	1.09			
17.06 (*)	6.85	1.18			
18.04 (*)	7.13	1.05			
19.01 (*)	7.42	1.01			

Asterisk denotes 1 cm depth increment, all others 0.5 cm depth increment.

Solid and aqueous phase data

LS96-1		Leachable Solid Phase, all concentrations in μmole / g					
Mean depth, cm		Cu	Std. dev.	Fe	Std. dev.	Mn	Std. dev.
0.24		1.6E+00	1.1E-01	686	10.5	33.0	7.8E-01
1.71		9.9E-01	3.6E-02	493	7.5	25.2	6.2E-01
3.66		7.1E-01	2.9E-02	399	6.5	20.9	5.8E-01
4.14		1.3E+00	3.8E-02	431	6.6	21.5	5.4E-01
5.12		1.1E+00	3.2E-02	353	4.3	17.6	3.4E-01
6.09		1.2E+00	4.6E-02	392	6.9	24.3	8.2E-01
6.58		9.0E-01	4.9E-02	339	10.1	98.6	3.8E+00
7.07		6.9E-01	4.9E-02	402	7.1	111.6	3.8E+00
7.56		4.4E-01	3.4E-02	355	10.6	42.2	1.6E+00
8.04		5.0E-01	4.2E-02	383	6.8	271.9	9.2E+00
8.53		4.7E-01	4.0E-02	363	10.8	312.6	1.2E+01
9.02		5.6E-01	3.6E-02	396	7.0	91.6	3.1E+00
9.99		4.7E-01	3.3E-02	542	9.5	95.7	3.2E+00
10.97		4.1E-01	3.5E-02	619	9.8	31.6	7.5E-01
11.94		3.8E-01	4.3E-02	819	24.4	42.5	1.6E+00
12.92		4.4E-01	3.9E-02	302	9.0	15.1	5.9E-01
13.41		3.5E-01	3.2E-02	1127	17.8	47.0	1.1E+00
13.89		3.2E-01	4.0E-02	1295	29.0	55.8	1.9E+00
14.38		4.4E-01	3.5E-02	742	11.8	25.1	6.0E-01
15.11	*	5.7E-01	5.9E-02	333	7.5	13.4	5.5E-01
16.09	*	4.8E-01	3.0E-02	296	4.5	10.6	2.4E-01
18.04	*	5.0E-01	3.2E-02	364	5.5	10.4	2.4E-01
19.99	*	5.3E-01	3.6E-02	356	5.4	8.9	2.1E-01
23.89	*	5.2E-01	3.5E-02	366	5.6	8.9	2.1E-01
27.79	*	5.9E-01	3.7E-02	392	6.5	9.7	3.3E-01
31.69	*	6.3E-01	4.3E-02	400	6.6	10.3	3.5E-01

LS96-1		Aqueous Phase, all concentrations in ηmole / g					
Mean depth, cm		Cu	Std. dev.	Fe	Std. dev.	Mn	Std. dev.
2	*	3.9E-02	2.1E-03	0.00	0.0E+00	0.036	1.7E-03
4	*	6.1E-02	7.3E-03	0.00	0.0E+00	0.037	3.4E-03
5	*	3.2E-02	1.7E-03	0.181	2.2E-01	0.041	3.8E-03
6	*	3.5E-02	4.5E-03	0.066	2.9E-01	6.16	8.8E-02
7	*	2.5E-02	1.4E-03	0.00	0.0E+00	16.4	2.6E-01
9	*	3.8E-02	2.7E-03	14.2	4.0E-01	23.6	4.0E-01
10	*	3.4E-02	2.8E-03	17.3	2.8E-01	22.9	2.1E-01
11	*	3.1E-03	3.9E-03	31.4	4.5E-01	22.7	2.4E-01
12	*	1.4E-02	1.8E-03	29.0	5.9E-01	22.2	2.9E-01
14	*	8.8E-03	1.7E-03	26.0	6.6E-01	20.8	3.9E-01
20	*	3.2E-01	2.8E-03	12.0	4.3E-01	17.0	1.8E-01
26	*	9.9E-02	3.3E-03	14.1	3.4E-01	16.9	4.9E-02
28	*	3.1E-02	4.0E-03	1.61	3.0E-01	14.5	9.1E-02

Asterisk denotes 1 cm depth increment, all others 0.5 cm depth increment.

LS96-2		Leachable Solid Phase, all concentrations in μmole / g	
Mean depth, cm		Cu	Std. dev.
0.24		7.3E-01	7.6E-02
1.22		4.9E-01	3.9E-02
2.19		5.6E-01	3.1E-02
3.17		4.7E-01	3.5E-02
4.14		5.5E-01	5.5E-02
6.09		5.9E-01	3.4E-02
8.04		5.7E-01	3.1E-02
9.99		7.0E-01	3.8E-02
13.41		8.0E-01	3.4E-02
13.89		5.9E-01	3.1E-02
14.87		5.2E-01	3.9E-02
19.50	*	3.8E-01	3.3E-02
24.38	*	2.5E-01	3.7E-02

Asterisk denotes 1 cm depth increment, all others 0.5 cm depth increment.

LS96-3 Leachable Solid Phase, all concentrations in μmole / g									
Mean depth, cm		Ba	Std. dev.	Co	Std. dev.	Cu	Std. dev.	Fe	Std. dev.
0.24		9.6E-01	3.7E-02	5.9E-01	1.7E-02	1.6E+00	4.8E-02	473	7.2
1.22		8.1E-01	3.4E-02	4.8E-01	2.0E-02	1.6E+00	3.0E-02	441	6.8
2.19		8.2E-01	3.1E-02	3.3E-01	2.0E-02	1.5E+00	5.2E-02	447	6.8
3.17		7.3E-01	2.3E-02	5.1E-01	1.3E-02	1.4E+00	3.2E-02	408	7.4
3.66		9.2E-01	2.8E-02					441	9.3
4.14		1.2E+00	3.3E-02	4.3E-01	1.5E-02	1.5E+00	5.7E-02	396	7.2
4.63		1.5E+00	3.4E-02	5.6E-01	1.3E-02	1.3E+00	3.1E-02	978	17.6
5.12		7.9E-01	2.5E-02	2.6E+00	2.9E-02	1.2E+00	2.7E-02	794	14.3
5.61		9.4E-01	2.5E-02	2.6E-01	1.4E-02	1.3E+00	1.6E-02	852	15.4
6.09		8.2E-01	2.6E-02	3.1E-01	1.1E-02	1.4E+00	4.5E-02	433	6.6
7.07		1.0E+00	2.8E-02	4.2E-01	5.0E-03	1.4E+00	2.0E-02	372	5.7
8.29	*	8.0E-01	3.4E-02			6.3E-01	6.2E-02	425	9.2
9.26	*	1.1E+00	3.0E-02			4.7E-01	4.5E-02	461	7.0
11.21	*	1.1E+00	3.1E-02			4.5E-01	5.1E-02	405	6.2
13.16	*	9.6E-01	2.9E-02			3.5E-01	5.0E-02	391	7.1
16.09	*	8.7E-01	2.7E-02			2.1E-01	4.5E-02	339	6.2
18.04	*	9.9E-01	3.2E-02			3.3E-01	5.8E-02	410	7.5
20.96	*	8.9E-01	2.6E-02			2.9E-01	4.2E-02	465	8.4
23.89	*	1.0E+00	2.9E-02			4.3E-01	4.5E-02	384	7.0
25.84	*	1.1E+00	3.0E-02			3.0E-01	5.2E-02	311	4.8
30.71	*	8.9E-01	2.5E-02			4.3E-01	4.2E-02	364	4.6

LS96-3 Aqueous Phase, all concentrations in ηmole / g									
Mean depth, cm		Ba	Std. dev.	Co	Std. dev.	Cu	Std. dev.	Fe	Std. dev.
1	*	7.3E-02	2.1E-03	0.0E+00	0.0E+00	1.5E-01	7.5E-03	0.16	3.1E-01
2	*	7.3E-02	1.4E-03	7.0E-04	1.2E-03	5.3E-02	4.4E-03	0.47	2.8E-01
4	*	5.9E-02	2.4E-03	6.5E-04	9.0E-04	7.3E-02	7.5E-03	0.66	3.4E-01
5	*	9.7E-02	1.1E-03	8.8E-03	1.3E-03	4.2E-02	4.5E-03	5.67	3.1E-01
6	*	1.5E-01	3.0E-03	1.2E-02	1.0E-03	3.6E-02	5.4E-03	15.3	3.5E-01
7	*	1.5E-01	3.4E-03	1.1E-02	1.5E-03	1.9E-02	3.3E-03	21.3	4.5E-01
8	*	2.1E-01	2.9E-03	1.1E-02	1.9E-03	3.2E-02	3.9E-03	16.6	2.9E-01
10	*	2.0E-01	2.6E-03	1.3E-02	1.1E-03	3.4E-02	4.8E-03	29.2	6.2E-01
12	*	2.2E-01	3.1E-03	1.1E-02	2.5E-03	4.1E-02	6.6E-03	18.3	5.7E-01
14	*	2.0E-01	3.0E-03	1.4E-02	1.5E-03	1.9E-02	2.7E-03	25.5	6.0E-01
16	*	2.3E-01	3.8E-03	1.2E-02	1.7E-03	2.3E-02	2.8E-03	16.9	3.8E-01
18	*	2.2E-01	5.0E-03	1.2E-02	2.5E-03	1.8E-02	2.6E-03	29.8	4.4E-01
20	*	2.5E-01	4.4E-03	1.7E-02	1.8E-03	4.9E-02	3.8E-03	47.7	6.2E-01
22	*	2.6E-01	2.9E-03	1.4E-02	1.2E-03	2.4E-02	4.5E-03	33.7	5.1E-01

Asterisk denotes 1 cm depth increment, all others 0.5 cm depth increment.

LS96-3		Leachable Solid Phase, all concentrations in μmole / g							
Mean depth, cm		Mn	Std. dev.	Ni	Std. dev.	Pb	Std. dev.	Zn	Std. dev.
0.24		25.5	0.77	2.32	9.9E-02	3.5E-01	2.1E-02	1.3E+00	1.5E-01
1.22		23.5	0.71	0.83	4.4E-02	3.3E-01	1.5E-02	1.4E+00	1.2E-01
2.19		22.9	0.69	1.12	2.8E-02	3.2E-01	1.0E-02	1.4E+00	1.3E-01
3.17		32.7	1.14	2.43	8.3E-02	3.6E-01	1.0E-02	1.8E+00	9.0E-02
3.66		72.6	1.60						
4.14		107	3.72	1.74	8.2E-02	4.0E-01	4.0E-03	1.7E+00	1.2E-01
4.63		131	4.56	1.71	4.2E-02	3.5E-01	1.1E-02	1.6E+00	8.4E-02
5.12		14.5	0.51	0.95	3.6E-02	2.8E-01	9.0E-03	1.3E+00	1.1E-01
5.61		14.8	0.52	0.47	2.1E-02	2.1E-01	1.0E-02	1.2E+00	1.2E-01
6.09		9.2	0.20	0.56	3.9E-02	2.1E-01	8.0E-03	1.4E+00	8.4E-02
7.07		6.8	0.15	0.59	5.7E-02	1.9E-01	1.2E-02	1.5E+00	3.6E-02
8.29	*	20.8	0.57						
9.26	*	18.4	0.39						
11.21	*	9.0	0.20						
13.16	*	7.9	0.19						
16.09	*	11.2	0.26						
18.04	*	9.0	0.22						
20.96	*	16.0	0.37						
23.89	*	8.8	0.21						
25.84	*	8.2	0.12						
30.71	*	8.9	0.12						

LS96-3		Aqueous Phase, all concentrations in ηmole / g							
Mean depth, cm		Mn	Std. dev.	Ni	Std. dev.	Pb	Std. dev.	Zn	Std. dev.
1	*	0.036	4.0E-03	2.7E-02	7.6E-03	1.6E-04	2.5E-04	3.3E+00	3.5E-02
2	*	0.041	4.0E-03	5.6E-03	4.2E-03	2.1E-03	6.8E-04	3.4E+00	3.5E-02
4	*	0.99	1.6E-02	4.7E-03	4.4E-03	3.0E-03	7.0E-04	1.4E+00	2.8E-02
5	*	6.0	8.3E-02	1.1E-02	6.4E-03	8.0E-04	7.5E-04	7.3E-01	2.1E-02
6	*	12.3	1.6E-01	1.7E-02	7.2E-03	9.9E-04	4.8E-04	7.2E-01	1.6E-02
7	*	11.0	1.2E-01	8.3E-03	7.4E-03	1.7E-03	3.1E-04	7.8E-01	1.2E-02
8	*	13.0	9.0E-02	1.2E-02	6.5E-03	1.1E-03	4.2E-04	1.1E+00	2.5E-02
10	*	14.0	2.0E-01	1.8E-02	6.9E-03	1.1E-03	4.7E-04	5.3E-01	3.3E-02
12	*	11.5	7.5E-02	2.5E-02	3.0E-03	1.4E-03	4.8E-04	1.4E+00	2.8E-02
14	*	13.1	9.0E-02	1.7E-02	4.9E-03	2.2E-04	4.9E-04	1.5E+00	4.5E-02
16	*	12.6	7.2E-02	3.2E-02	5.7E-03	1.6E-03	5.3E-04	1.1E+00	2.9E-02
18	*	13.5	5.5E-02	3.8E-02	5.4E-03	4.1E-04	3.5E-04	9.4E-01	1.0E-02
20	*	16.8	1.3E-01	3.5E-02	8.1E-03	1.5E-03	6.8E-04	1.0E+00	2.0E-02
22	*	15.2	1.3E-01	3.6E-02	5.4E-03	9.9E-04	4.8E-04	6.0E-01	1.9E-02

Asterisk denotes 1 cm depth increment, all others 0.5 cm depth increment.

LS96-4		Leachable Solid Phase, all concentrations in μmole / g							
Mean depth, cm		Ba	Std. dev.	Co	Std. dev.	Cu	Std. dev.	Fe	Std. dev.
0.24		1.2E+00	4.5E-02	5.4E-01	2.0E-02	1.6E+00	6.0E-02	356	5.5
1.22		9.3E-01	4.0E-02	5.7E-01	2.3E-02	1.7E+00	4.0E-02	358	5.6
2.19		7.6E-01	3.8E-02	2.6E-01	8.0E-03	1.6E+00	6.5E-02	391	6.3
3.17		7.5E-01	3.7E-02	6.2E-01	4.1E-02	1.7E+00	6.0E-02	433	6.9
4.14		6.2E-01	3.4E-02	2.2E-01	9.0E-03	1.1E+00	4.4E-02	293	4.7
5.12		7.3E-01	3.2E-02	4.8E-01	1.7E-02	8.0E-01	3.3E-02	406	6.4
6.09		6.8E-01	2.8E-02	4.6E+00	9.1E-02	5.9E-01	2.8E-02	387	6.1
7.07		6.6E-01	2.4E-02	1.7E+00	4.7E-02	5.6E-01	1.9E-02	372	5.7
8.04		6.0E-01	4.0E-02	6.2E-01	2.0E-02	6.0E-01	3.3E-02	371	8.4
9.02		7.4E-01	2.8E-02	2.6E-01	1.4E-02	6.2E-01	2.4E-02	375	5.8
9.51		1.3E+00	2.8E-02					376	7.9
9.99		2.0E+00	4.5E-02	2.6E-01	7.0E-03	5.5E-01	1.4E-02	301	4.7
10.48		1.5E+00	3.8E-02	5.7E-01	1.2E-02	4.8E-01	1.8E-02	419	6.4
10.97		1.7E+00	4.1E-02	3.6E-01	5.0E-03	3.7E-01	1.3E-02	1216	23.9
11.46		8.9E-01	2.6E-02	2.5E-01	1.1E-02	5.4E-01	2.4E-02	430	8.5
13.65	*	1.0E+00	2.9E-02	7.1E-01	1.8E-02	4.9E-01	2.7E-02	261	5.2
15.6	*	1.1E+00	3.2E-02			6.2E-01	5.6E-02	316	6.3
17.55	*	1.0E+00	3.2E-02			6.1E-01	5.9E-02	338	6.7
19.5	*	1.1E+00	3.2E-02			6.6E-01	5.0E-02	342	5.6
21.45	*	1.1E+00	4.7E-02			6.7E-01	8.2E-02	354	8.1

LS96-4		Aqueous Phase, all concentrations in ηmole / g							
Mean depth, cm		Ba	Std. dev.	Co	Std. dev.	Cu	Std. dev.	Fe	Std. dev.
1	*	8.6E-02	1.5E-03	2.9E-03	3.7E-04	1.2E-01	5.5E-03	1.97	1.6E-01
2	*	8.3E-02	3.3E-03	5.0E-04	7.1E-04	8.1E-02	4.2E-03	0.05	1.9E-01
3	*	7.6E-02	1.6E-03	6.1E-04	6.6E-04	7.5E-02	4.2E-03	0.21	1.5E-01
4	*	6.6E-02	6.0E-04	4.5E-03	9.1E-04	8.2E-02	3.9E-03	0.47	1.9E-01
5	*	6.1E-02	1.4E-03	8.0E-05	6.0E-04	4.7E-02	5.0E-03	0.10	1.8E-01
6	*	5.7E-02	1.6E-03	3.9E-04	8.5E-04	4.6E-02	3.8E-03	0.25	2.3E-01
7	*	5.1E-02	1.7E-03	9.3E-04	8.4E-04	4.5E-02	3.5E-03	0.34	3.3E-01
8	*	4.8E-02	1.3E-03	1.2E-03	6.9E-04	3.7E-02	3.1E-03	0.85	3.6E-01
9	*	4.3E-02	9.0E-04	0.0E+00	0.0E+00	7.0E-02	3.4E-03	0.24	3.2E-01
10	*	3.6E-02	1.7E-03	1.9E-03	5.9E-04	9.5E-02	4.6E-03	0.81	3.5E-01
11	*	4.0E-02	6.0E-04	6.4E-04	1.0E-03	4.1E-02	5.0E-03	0.28	3.3E-01
12	*	8.5E-02	1.3E-03	4.8E-03	1.3E-03	9.1E-02	6.4E-03	3.14	3.6E-01
14	*	1.5E-01	3.0E-03	5.1E-03	1.5E-03	2.8E-02	3.9E-03	8.29	4.8E-01
16	*	1.5E-01	2.7E-03	5.9E-03	6.8E-04	1.7E-02	1.5E-03	10.38	3.1E-01

Asterisk denotes 1 cm depth increment, all others 0.5 cm depth increment.

LS96-4		Leachable Solid Phase, all concentrations in μmole / g							
Mean depth, cm		Mn	Std. dev.	Ni	Std. dev.	Pb	Std. dev.	Zn	Std. dev.
0.24		20.4	2.5E-01	7.0E-01	5.3E-02	4.0E-01	2.0E-02	2.5E+00	8.2E-02
1.22		18.2	2.4E-01	7.5E-01	5.2E-02	4.1E-01	2.0E-02	1.9E+00	9.7E-02
2.19		17.3	3.0E-01	6.1E-01	5.8E-02	4.1E-01	2.0E-02	1.4E+00	7.8E-02
3.17		17.2	2.9E-01	7.8E-01	2.7E-02	4.0E-01	1.0E-02	1.7E+00	1.4E-01
4.14		15.0	2.6E-01	5.2E-01	4.6E-02	2.3E-01	1.0E-02	8.2E-01	1.1E-01
5.12		16.1	2.7E-01	6.6E-01	2.9E-02	1.5E-01	6.0E-03	1.0E+00	1.0E-01
6.09		16.2	2.7E-01	1.2E+00	4.3E-02	6.5E-02	3.0E-03	6.7E-01	7.0E-02
7.07		16.4	2.6E-01	9.1E-01	3.9E-02	5.8E-02	4.0E-03	7.5E-01	6.6E-02
8.04		16.0	3.8E-01	6.2E-01	3.9E-02	5.7E-02	5.0E-03	5.6E-01	8.6E-02
9.02		63.0	9.7E-01	7.9E-01	2.7E-02	5.3E-02	6.0E-03	7.3E-01	9.4E-02
9.51		224	4.9E+00						
9.99		546	8.3E+00	6.1E-01	2.5E-02	4.4E-02	3.0E-03	6.8E-01	2.4E-02
10.48		354	5.4E+00	5.7E-01	1.9E-02	3.9E-02	4.0E-03	5.6E-01	6.2E-02
10.97		23.9	4.5E-01	3.6E-01	1.9E-02	1.8E-02	3.0E-03	2.4E-01	4.9E-02
11.46		7.9	1.6E-01	5.0E-01	2.1E-02	4.0E-02	3.0E-03	6.7E-01	3.6E-02
13.65	*	4.3	9.0E-02	5.3E-01	2.1E-02	4.0E-02	2.0E-03	6.2E-01	3.2E-02
15.6	*	4.9	1.1E-01						
17.55	*	5.4	1.2E-01						
19.5	*	6.1	1.1E-01						
21.45	*	6.6	1.7E-01						

LS96-4		Aqueous Phase, all concentrations in ηmole / g							
Mean depth, cm		Mn	Std. dev.	Ni	Std. dev.	Pb	Std. dev.	Zn	Std. dev.
1	*	3.6E-02	2.0E-03	3.3E-02	2.2E-03	2.4E-03	2.2E-04	1.3E+00	2.7E-02
2	*	1.3E-02	2.7E-03	1.6E-02	3.5E-03	1.1E-03	2.8E-04	7.1E-01	2.1E-02
3	*	3.5E-02	2.1E-03	2.1E-02	4.3E-03	1.4E-03	4.0E-04	1.1E+00	2.7E-02
4	*	6.4E-02	3.7E-03	2.0E-02	5.8E-03	5.1E-03	6.4E-04	7.3E-01	2.1E-02
5	*	1.4E-02	1.7E-03	7.9E-03	2.5E-03	9.9E-04	5.0E-04	9.9E-01	1.6E-02
6	*	2.5E-02	1.3E-03	1.5E-02	3.2E-03	1.6E-03	4.8E-04	2.8E+00	2.4E-02
7	*	5.8E-02	5.2E-03	1.3E-02	1.9E-03	1.1E-03	4.8E-04	3.8E+00	5.2E-02
8	*	6.1E-02	3.1E-03	1.2E-02	3.5E-03	1.7E-03	5.7E-04	2.8E+00	4.1E-02
9	*	2.5E-02	3.1E-03	7.4E-03	2.2E-03	1.4E-03	5.8E-04	2.4E+00	3.0E-02
10	*	1.0E-01	5.4E-03	1.9E-02	4.5E-03	1.8E-04	5.3E-04	6.4E+00	8.5E-02
11	*	3.2E+00	3.3E-02	9.2E-03	4.9E-03	1.5E-04	7.4E-04	4.3E+00	5.4E-02
12	*	4.9E+00	4.3E-02	7.4E-02	7.9E-03	6.5E-03	5.7E-04	4.7E+00	8.1E-02
14	*	7.3E+00	1.3E-01	1.4E-02	1.9E-03	1.7E-03	6.7E-04	5.6E+00	6.2E-02
16	*	7.9E+00	7.9E-02	1.9E-02	3.4E-03	3.7E-03	1.0E-03	5.7E+00	9.7E-02

Asterisk denotes 1 cm depth increment, all others 0.5 cm depth increment.

LS96-5		Leachable Solid Phase, all concentrations in μmole / g							
Mean depth, cm		Ba	Std. dev.	Co	Std. dev.	Cu	Std. dev.	Fe	Std. dev.
0.24		1.0E+00	1.1E-01	3.7E-01	3.5E-02	2.4E+00	1.1E-01	643	10.8
1.22		4.2E-01	1.7E-02	3.0E-01	1.5E-02	7.6E-01	3.3E-02	304	4.7
2.19		4.7E-01	1.8E-02	1.5E-01	5.0E-03	8.1E-01	2.3E-02	438	6.8
3.17		2.4E-01	9.0E-03	1.2E-01	5.0E-03	3.9E-01	1.2E-02	369	5.7
3.66		3.2E-01	9.0E-03	1.3E+00	2.0E-02	3.4E-01	6.0E-03	354	5.4
4.14		7.5E-01	2.2E-02	3.6E-01	1.2E-02	3.1E-01	1.1E-02	526	8.1
4.63		5.5E-01	1.3E-02	3.2E-01	7.0E-03	2.6E-01	9.0E-03	629	12.3
5.12		2.8E-01	1.2E-02	1.5E+00	2.8E-02	3.1E-01	1.2E-02	411	11.4
6.09		2.9E-01	1.1E-02	9.1E-01	1.2E-02	4.8E-01	1.4E-02	477	9.4
7.07		3.9E-01	1.3E-02	1.3E-01	1.1E-02	5.9E-01	1.9E-02	521	9.5
8.04		6.3E-01	2.9E-02					341	6.3
9.02		1.0E+00	3.0E-02	3.6E-01	2.9E-02	1.1E+00	2.3E-02	473	8.6
9.99		1.4E+00	4.3E-02	2.5E-01	1.5E-02	1.5E+00	4.9E-02	1150	20.9
10.48		1.2E+00	2.8E-02					380	8.0
10.97		1.4E+00	3.3E-02					434	6.6
12.19	*	1.2E+00	3.3E-02	4.1E-01	2.1E-02	3.5E-01	2.7E-02	361	6.6
14.14	*	1.5E+00	4.1E-02					377	6.2
16.09	*	1.2E+00	3.5E-02					401	6.6
18.04	*	1.5E+00	3.7E-02					402	6.6
19.99	*	1.1E+00	3.1E-02					330	5.4
21.94	*	1.4E+00	3.6E-02					505	8.3
24.86	*	1.1E+00	2.9E-02					360	5.9

LS96-5		Aqueous Phase, all concentrations in ηmole / g							
Mean depth, cm		Ba	Std. dev.	Co	Std. dev.	Cu	Std. dev.	Fe	Std. dev.
3	*	7.2E-02	1.6E-03	9.8E-04	5.6E-04	9.9E-02	7.1E-03	0.37	2.3E-01
4	*	7.0E-02	6.0E-04	2.4E-03	6.6E-04	9.0E-02	8.4E-03	2.73	2.8E-01
7	*	1.6E-01	4.2E-03	7.9E-03	7.2E-04	3.3E-02	2.8E-03	61.1	1.5E+00
8	*	2.2E-01	3.9E-03	8.6E-03	2.1E-03	2.1E-02	1.7E-03	83.1	6.5E-01
11	*	2.3E-01	3.5E-03	6.4E-03	1.1E-03	2.4E-02	4.8E-03	107.1	6.9E-01
12	*	2.4E-01	1.5E-03	6.1E-03	1.0E-03	4.1E-02	2.9E-03	104.6	6.9E-01
13	*	2.9E-01	4.0E-03	6.1E-03	1.6E-03	5.3E-02	4.2E-03	89.8	7.9E-01
14	*	2.6E-01	3.6E-03	8.5E-03	6.7E-04	1.1E-02	1.9E-03	90.2	1.3E+00
15	*	2.0E-01	3.0E-03	5.5E-03	9.6E-04	1.7E-02	2.8E-03	104.8	6.4E-01
17	*	2.6E-01	3.1E-03	7.4E-03	8.6E-04	5.8E-03	4.1E-03	60.6	4.6E-01
19	*	2.0E-01	1.5E-03	5.1E-03	8.8E-04	2.8E-02	2.1E-03	98.5	8.7E-01
21	*	2.1E-01	2.0E-03	4.6E-03	1.4E-03	7.0E-02	4.1E-03	67.3	7.7E-01
23	*	2.1E-01	2.2E-03	1.3E-02	1.5E-03	2.5E-02	2.5E-03	93.2	1.5E+00
25	*	2.4E-01	2.1E-03	5.7E-03	9.4E-04	2.3E-02	2.7E-03	73.5	4.9E-01
27	*	2.2E-01	2.7E-03	6.4E-03	1.8E-03	1.9E-02	2.2E-03	98.0	6.0E-01

Asterisk denotes 1 cm depth increment, all others 0.5 cm depth increment.

LS96-5		Leachable Solid Phase, all concentrations in μmole / g							
Mean depth, cm		Mn	Std. dev.	Ni	Std. dev.	Pb	Std. dev.	Zn	Std. dev.
0.24		37.0	6.7E-01	7.4E-01	8.9E-02	3.4E-01	2.8E-02	7.9E-01	2.3E-01
1.22		17.6	3.0E-01	3.4E-01	3.0E-02	1.5E-01	6.0E-03	9.0E-01	7.8E-02
2.19		23.7	4.0E-01	1.8E-01	1.7E-02	1.6E-01	8.0E-03	7.6E-01	9.1E-02
3.17		18.9	3.1E-01	1.1E-01	1.2E-02	8.1E-02	2.0E-03	5.2E-01	3.4E-02
3.66		68.3	1.1E+00	4.4E-01	1.0E-02	8.3E-02	4.0E-03	6.7E-01	3.1E-02
4.14		218.4	3.5E+00	1.1E-01	1.0E-02	9.0E-02	2.0E-03	5.1E-01	2.9E-02
4.63		46.3	9.9E-01	8.8E-02	8.0E-03	8.1E-02	3.0E-03	4.7E-01	2.7E-02
5.12		13.9	4.2E-01	4.0E-01	9.0E-03	8.4E-02	1.0E-03	5.0E-01	2.6E-02
6.09		17.1	3.7E-01	2.5E-01	1.4E-02	1.1E-01	5.0E-03	5.8E-01	3.2E-02
7.07		18.2	3.6E-01	1.4E-01	1.3E-02	1.3E-01	3.0E-03	7.6E-01	3.8E-02
8.04		13.6	2.9E-01						
9.02		19.0	3.8E-01	5.5E-01	4.5E-02	2.3E-01	8.0E-03	1.1E+00	4.5E-02
9.99		130.7	2.5E+00	5.5E-01	3.5E-02	2.3E-01	1.2E-02	9.6E-01	1.6E-01
10.48		14.7	3.3E-01						
10.97		14.8	2.4E-01						
12.19	*	13.9	2.9E-01	7.5E-01	2.4E-02	6.4E-02	3.0E-03	5.5E-01	7.9E-02
14.14	*	14.9	2.8E-01						
16.09	*	13.5	2.5E-01						
18.04	*	21.7	3.9E-01						
19.99	*	14.1	2.6E-01						
21.94	*	45.5	8.0E-01						
24.86	*	13.5	2.5E-01						

LS96-5		Aqueous Phase, all concentrations in ηmole / g							
Mean depth, cm		Mn	Std. dev.	Ni	Std. dev.	Pb	Std. dev.	Zn	Std. dev.
3	*	0.13	5.2E-03	1.2E-02	4.5E-03	1.0E-03	4.0E-04	5.1E+00	1.1E-01
4	*	0.56	2.5E-02	1.3E-02	3.5E-03	1.7E-03	5.6E-04	9.1E-01	2.9E-02
7	*	21.7	4.9E-01	1.3E-02	3.6E-03	1.9E-03	5.3E-04	1.5E-01	1.1E-02
8	*	30.7	1.4E-01	1.5E-02	2.3E-03	5.3E-04	3.7E-04	7.5E-01	2.1E-02
11	*	37.2	1.2E-01	1.5E-02	4.0E-03	3.0E-03	7.0E-04	8.9E-01	1.9E-02
12	*	40.3	3.5E-01	1.6E-02	3.7E-03	5.0E-03	5.6E-04	3.7E-01	1.7E-02
13	*	38.7	2.9E-01	3.8E-02	6.3E-03	8.1E-04	5.3E-04	3.4E+00	6.0E-02
14	*	39.7	4.6E-01	2.5E-02	2.9E-03	0.0E+00	0.0E+00	4.8E-01	1.7E-02
15	*	43.5	3.8E-01	1.9E-02	3.6E-03	2.6E-04	3.8E-04	2.8E-01	9.0E-03
17	*	37.0	1.8E-01	1.7E-02	5.0E-03	0.0E+00	0.0E+00	7.3E-01	2.6E-02
19	*	45.3	2.3E-01	2.1E-02	4.9E-03	2.2E-04	4.4E-04	8.7E-01	2.8E-02
21	*	34.1	1.7E-01	2.7E-02	4.7E-03	9.8E-04	4.9E-04	1.2E+00	2.1E-02
23	*	42.3	5.4E-01	3.1E-02	4.1E-03	4.0E-04	6.2E-04	3.4E-01	1.9E-02
25	*	37.5	1.3E-01	2.3E-02	5.3E-03	6.0E-05	4.9E-04	1.6E+00	4.8E-02
27	*	41.3	1.9E-01	2.4E-02	4.1E-03	1.7E-04	4.5E-04	3.7E-01	1.6E-02

Asterisk denotes 1 cm depth increment, all others 0.5 cm depth increment.

LS96-6		Leachable Solid Phase, all concentrations in μmole / g							
Mean depth, cm		Ba	Std. dev.	Co	Std. dev.	Cu	Std. dev.	Fe	Std. dev.
0.24		9.5E-01	5.2E-02	3.2E-01	3.1E-02	2.0E+00	1.4E-01	446	7.6
1.22		7.6E-01	3.1E-02	8.8E-01	2.5E-02	1.7E+00	8.7E-02	366	6.1
2.19		6.4E-01	2.5E-02	2.3E-01	6.8E-03	1.7E+00	2.9E-02	300	5.0
3.17		7.4E-01	2.7E-02	2.7E-01	1.9E-02	1.8E+00	4.7E-02	365	6.1
4.14		8.3E-01	3.6E-02	3.4E-01	1.8E-02	1.6E+00	1.7E-02	373	9.8
5.12		8.8E-01	2.9E-02	3.0E-01	1.7E-02	1.1E+00	5.4E-02	424	9.8
6.09		8.5E-01	2.8E-02	2.5E-01	1.2E-02	6.4E-01	2.1E-02	415	9.6
6.58		8.4E-01	2.3E-02	9.5E-01	2.4E-02	4.8E-01	1.5E-02	380	8.7
7.07		1.0E+00	2.9E-02	3.1E+00	2.5E-02	6.2E-01	1.8E-02	420	9.7
7.56		1.4E+00	3.4E-02	5.5E-01	2.1E-02	5.1E-01	2.2E-02	348	8.0
8.04		1.3E+00	3.4E-02	3.4E-01	1.1E-02	5.3E-01	2.3E-02	429	6.7
8.53		1.9E+00	4.1E-02	7.6E-01	1.4E-02	4.8E-01	2.6E-02	812	12.6
9.02		2.2E+00	4.6E-02	2.2E-01	1.1E-02	2.9E-01	1.5E-02	1515	23.4
9.51		1.3E+00	3.0E-02					523	7.9
11.21	*	8.9E-01	2.1E-02					285	4.4
13.16	*	1.1E+00	2.7E-02	3.7E-01	1.4E-02	4.8E-01	1.8E-02	403	6.3
17.06	*	1.2E+00	2.9E-02					399	6.2
19.99	*	1.0E+00	2.6E-02					356	5.5
22.91	*	1.2E+00	3.0E-02					385	5.9
25.84	*	1.1E+00	2.8E-02					369	5.7
28.76	*	1.1E+00	2.6E-02					364	5.6
31.69	*	1.1E+00	2.8E-02					380	5.9
34.61	*	1.1E+00	3.0E-02					393	7.9

LS96-6		Aqueous Phase, all concentrations in ηmole / g							
Mean depth, cm		Ba	Std. dev.	Co	Std. dev.	Cu	Std. dev.	Fe	Std. dev.
4	*	6.3E-02	8.3E-04	4.1E-04	4.6E-04	5.5E-02	2.7E-03	0.17	2.3E-01
5	*	5.8E-02	1.7E-03	1.6E-03	1.3E-03	4.4E-02	4.3E-03	0.12	3.3E-01
6	*	6.9E-02	1.5E-03	9.5E-04	9.4E-04	4.9E-02	2.9E-03	0.17	3.8E-01
7	*	5.3E-02	1.2E-03	1.6E-04	1.3E-03	4.0E-02	3.9E-03	0.04	3.7E-01
8	*	5.2E-02	2.0E-03	0.0E+00	0.0E+00	2.1E-02	2.2E-03	0.17	2.4E-01
9	*	9.0E-02	1.5E-03	2.7E-04	6.2E-04	1.3E-02	4.5E-03	0.54	1.9E-01
12	*	8.4E-02	1.1E-03	1.6E-03	1.1E-03	8.6E-03	2.0E-03	5.9	2.4E-01
13	*	9.5E-02	2.2E-03	4.8E-03	1.5E-03	3.9E-02	4.0E-03	5.2	3.4E-01
14	*	1.6E-01	2.6E-03	3.1E-03	1.5E-03	4.0E-02	4.3E-03	2.1	3.9E-01
15	*	1.4E-01	3.5E-03	6.0E-03	1.0E-03	2.3E-02	4.5E-03	3.5	3.7E-01
16	*	1.1E-01	2.1E-03	4.9E-03	9.8E-04	1.9E-02	4.0E-03	9.2	3.6E-01
18	*	1.2E-01	4.0E-04	6.6E-03	1.5E-03	8.3E-03	2.8E-03	11.4	3.9E-01
20	*	1.3E-01	3.2E-03	7.5E-03	4.0E-04	1.6E-02	4.2E-03	12.7	4.0E-01
24	*	1.2E-01	3.1E-03	3.3E-03	7.5E-04	1.3E-02	2.8E-03	18.8	5.0E-01
30	*	1.3E-01	1.6E-03	2.5E-03	6.3E-04	1.2E-02	1.5E-03	17.7	2.0E-01
32	*	1.3E-01	1.9E-03	2.4E-03	8.3E-04	1.1E-02	3.7E-03	17.8	2.9E-01

Asterisk denotes 1 cm depth increment, all others 0.5 cm depth increment.

LS96-6		Leachable Solid Phase, all concentrations in μmole / g							
Mean depth, cm		Mn	Std. dev.	Ni	Std. dev.	Pb	Std. dev.	Zn	Std. dev.
0.24		19.4	3.9E-01	7.0E-01	5.3E-02	4.1E-01	1.8E-02	5.4E-01	1.9E-01
1.22		16.5	3.2E-01	7.6E-01	5.4E-02	4.0E-01	9.1E-03	1.2E+00	1.2E-01
2.19		14.8	2.8E-01	4.8E-01	2.3E-02	4.5E-01	1.6E-02	1.4E+00	1.2E-01
3.17		16.0	3.0E-01	5.5E-01	2.7E-02	3.3E-01	1.5E-02	1.3E+00	8.0E-02
4.14		17.1	4.7E-01	5.6E-01	2.0E-02	2.8E-01	5.0E-03	1.3E+00	7.4E-02
5.12		19.6	4.9E-01	6.5E-01	2.4E-02	1.9E-01	6.3E-03	1.1E+00	6.6E-02
6.09		25.9	6.5E-01	6.2E-01	4.5E-02	1.1E-01	4.0E-03	8.2E-01	7.3E-02
6.58		48.7	1.2E+00	8.4E-01	2.3E-02	7.3E-02	5.1E-03	8.4E-01	3.4E-02
7.07		84.7	2.1E+00	1.6E+00	4.6E-02	7.6E-02	5.8E-03	8.0E-01	2.7E-02
7.56		192	4.7E+00	8.1E-01	2.9E-02	6.5E-02	4.3E-03	7.6E-01	4.4E-02
8.04		138	2.2E+00	7.5E-01	3.9E-02	5.3E-02	7.0E-03	6.5E-01	6.1E-02
8.53		211	3.3E+00	6.4E-01	3.8E-02	3.7E-02	2.7E-03	4.4E-01	4.8E-02
9.02		22.9	3.7E-01	4.5E-01	3.5E-02	1.7E-02	3.3E-03	2.3E-01	3.5E-02
9.51		8.9	1.5E-01						
11.21	*	6.1	1.0E-01						
13.16	*	6.7	1.2E-01	6.7E-01	2.4E-02	5.2E-02	4.9E-03	8.5E-01	3.0E-02
17.06	*	6.5	1.2E-01						
19.99	*	5.5	9.8E-02						
22.91	*	5.8	1.0E-01						
25.84	*	5.6	1.0E-01						
28.76	*	5.7	1.0E-01						
31.69	*	6.5	1.1E-01						
34.61	*	7.0	1.5E-01						

LS96-6		Aqueous Phase, all concentrations in ηmole / g							
Mean depth, cm		Mn	Std. dev.	Ni	Std. dev.	Pb	Std. dev.	Zn	Std. dev.
4	*	2.3E-02	4.8E-03	9.1E-03	2.4E-03	8.9E-03	6.3E-04	3.6E-01	1.0E-02
5	*	4.0E-02	3.6E-03	4.7E-03	4.4E-03	1.6E-04	3.9E-04	7.1E-01	4.2E-02
6	*	2.1E-01	9.8E-03	1.8E-02	5.1E-03	7.7E-04	3.9E-04	2.8E+00	2.3E-02
7	*	5.8E-02	3.1E-03	1.1E-02	2.2E-03	4.6E-04	4.6E-04	2.2E+00	5.6E-02
8	*	7.9E-02	2.8E-03	5.0E-03	5.3E-03	5.8E-05	3.9E-04	5.4E-01	6.7E-03
9	*	6.3E-01	1.1E-02	6.2E-03	3.2E-03	3.7E-04	3.6E-04	1.9E-01	5.6E-03
12	*	2.3E+00	2.7E-02	1.4E-02	2.9E-03	3.4E-04	4.4E-04	6.1E-01	1.6E-02
13	*	3.2E+00	2.6E-02	2.7E-02	4.1E-03	1.6E-03	9.0E-04	6.3E-01	2.5E-02
14	*	3.8E+00	3.4E-02	2.6E-02	3.1E-03	4.9E-04	3.2E-04	2.0E+00	4.0E-02
15	*	3.5E+00	4.5E-02	7.9E-02	9.5E-03	1.2E-03	6.6E-04	1.8E+00	4.9E-02
16	*	3.9E+00	4.4E-02	1.6E-02	3.9E-03	3.4E-03	9.1E-04	5.9E-01	1.9E-02
18	*	4.2E+00	5.0E-02	1.3E-02	4.8E-03	8.5E-05	3.9E-04	7.0E-01	2.3E-02
20	*	4.6E+00	2.6E-02	1.9E-02	2.8E-03	1.9E-03	6.4E-04	5.8E-01	1.6E-02
24	*	5.9E+00	6.4E-02	1.6E-02	4.1E-03	3.0E-04	3.5E-04	6.4E-01	1.4E-02
30	*	5.9E+00	2.3E-02	1.4E-02	2.1E-03	1.3E-04	4.5E-04	1.1E+00	1.8E-02
32	*	6.7E+00	3.8E-02	2.0E-02	3.6E-03	7.8E-04	5.1E-04	1.1E+00	1.9E-02

Asterisk denotes 1 cm depth increment, all others 0.5 cm depth increment.

LS96-7		Leachable Solid Phase, all concentrations in μmole / g					
Mean depth, cm		Cu	Std. dev.	Fe	Std. dev.	Mn	Std. dev.
0.24		1.1E+00	7.2E-02	293	5.9E+00	15.3	3.3E-01
1.71		8.2E-01	5.0E-02	219	4.4E+00	11.4	2.4E-01
3.17		1.1E+00	5.7E-02	241	4.9E+00	11.8	2.5E-01
4.63		2.9E-01	2.9E-02	144	2.4E+00	6.2	1.1E-01
6.09		2.9E-01	2.7E-02	182	3.0E+00	8.0	1.3E-01
7.56		2.7E-01	2.6E-02	161	2.7E+00	7.6	1.3E-01
9.02		3.3E-01	2.4E-02	204	3.4E+00	14.5	2.3E-01
10.48		3.3E-01	2.4E-02	204	3.4E+00	15.4	2.5E-01
11.94		4.1E-01	2.5E-02	224	3.7E+00	251.4	3.9E+00
12.92		2.4E-01	1.3E-02	1189	1.8E+01	234.6	3.5E+00
13.41		2.3E-01	4.1E-02	1506	5.9E+01	18.9	7.6E-01
14.14		3.4E-01	2.4E-02	576	8.7E+00	9.7	1.6E-01
15.11		3.0E-01	2.8E-02	125	4.4E+00	2.8	1.1E-01
19.99	*	3.7E-01	3.1E-02	179	6.3E+00	3.0	1.2E-01
22.91	*	3.8E-01	3.3E-02	201	7.0E+00	3.4	1.3E-01
25.84	*	4.7E-01	3.9E-02	231	8.1E+00	3.5	1.4E-01
28.76	*	3.4E-01	2.8E-02	283	4.5E+00	5.0	8.9E-02
31.69	*	3.4E-01	2.7E-02	183	2.9E+00	6.4	1.1E-01
33.64	*	3.1E-01	3.0E-02	194	3.1E+00	11.6	1.9E-01
35.59	*	3.2E-01	2.3E-02	556	8.8E+00	153.2	2.4E+00

LS96-7		Aqueous Phase, all concentrations in ηmole / g					
Mean depth, cm		Cu	Std. dev.	Fe	Std. dev.	Mn	Std. dev.
6	*	4.5E-02	2.5E-03	0.079	1.9E-01	0.024	7.7E-03
10	*	1.4E-02	2.4E-03	0.000	0.0E+00	0.020	2.6E-03
14	*	2.8E-02	1.7E-03	0.210	2.0E-01	15.0	1.6E-01
22	*	3.7E-02	4.3E-03	2.2	3.6E-01	9.2	7.3E-02
24	*	4.0E-02	2.8E-03	2.5	2.2E-01	12.5	7.6E-02
28	*	1.2E-02	2.4E-03	1.2	2.4E-01	8.0	1.0E-01

Asterisk denotes 1 cm depth increment, all others 0.5 cm depth increment.